
**The construction of Molecular Dynamics model
for the response of $\text{Na}_x\text{Cr}_x\text{Ti}_{8-x}\text{O}_{16}$ ($x=1.7$) to
electric fields of up to 100ps duration**

**Thesis submitted for the degree of
Doctor of Philosophy
at the University of Leicester**

By

**Kien Ling Khoo BEng (Hons)
Department of Engineering
University of Leicester**

December 2003

UMI Number: U486992

All rights reserved

INFORMATION TO ALL USERS

The quality of this reproduction is dependent upon the quality of the copy submitted.

In the unlikely event that the author did not send a complete manuscript and there are missing pages, these will be noted. Also, if material had to be removed, a note will indicate the deletion.



UMI U486992

Published by ProQuest LLC 2013. Copyright in the Dissertation held by the Author.
Microform Edition © ProQuest LLC.

All rights reserved. This work is protected against
unauthorized copying under Title 17, United States Code.



ProQuest LLC
789 East Eisenhower Parkway
P.O. Box 1346
Ann Arbor, MI 48106-1346

The construction of Molecular Dynamics model for the response of $\text{Na}_x\text{Cr}_x\text{Ti}_{8-x}\text{O}_{16}$ ($x=1.7$) to electric fields of up to 100ps duration


BY

Kien Ling Khoo

Declaration of Originality

The thesis is submitted in fulfillment of the requirements of Doctor of Philosophy in the Department of Engineering, University of Leicester, United Kingdom. All the work recorded in this thesis is original unless otherwise acknowledge in the text or by references. None of the work has been submitted for any other degree either in the University of Leicester or any other University.

Signed



Kien Ling Khoo

December 2003

ACKNOWLEDGEMENT

This has been the most significant scientific accomplishment in my life and hence I would like to thank many people who have supported and believed in me:

Professor Len Dissado, my research supervisor who has dedicated his time to guide and provide me with valuable suggestions for my research.

Professor John Fothergill, Dr. Richard Cooper, Dr. Simon Gill, Andy Willby and everyone in the high voltage group, who have provided me with much information and help.

My parents Tian Teck and Chor Keng, my brother Kien Kiat for their understanding and support.

Jason and Yee Ping who have been very patient and given me lots of encouragement.

Kai Wu and Yuan Zhao for providing me a nice and comfortable environment to complete my thesis.

Qinetiq and Lee Foundation for their financial support.

Many more that I have not mentioned above.

Kien Ling Khoo

The construction of Molecular Dynamics model for the response of $\text{Na}_x\text{Cr}_x\text{Ti}_{8-x}\text{O}_{16}$ ($x=1.7$) to electric fields of up to 100ps duration

Kien Ling KHOO

ABSTRACT

The hollandite $\text{Na}_x(\text{Ti}_{8-x}\text{Cr}_x)\text{O}_{16}$, ($x = 1.7$) is a non-stoichiometric material that is based on a family of compounds of general formula $\text{A}_x\text{M}_{4-x}\text{N}_y\text{O}_8$. The chromium and sodium ions are randomly placed in unit cells according to the relative proportions of titanium and chromium ions. Charge compensating sodium ions are located in interstitial sites along tunnels. Because of the non-stoichiometric nature, there are vacant sites into which the sodium ions may move.

A molecular dynamics (MD) simulation was used to determine the motion of the sodium ions in the tunnel, when the surrounding ions were held rigid. The dielectric response was calculated from the rate of change of polarisation, dP/dt under the action of a de step-field of 7.43MV/m to 74.3GV/m, at temperature between 200K and 373K.

A resonance behaviour has been observed. The absorption peaks in χ'' at the resonance frequency lie between 4.5×10^{10} and 8.8×10^{10} Hz at 297K which matches very well with the Poley absorption which is typically observed in polar liquids in the $1.2 - 70 \text{ cm}^{-1}$ ($3.6 \times 10^{10} - 2.1 \times 10^{12}$ Hz) region at room temperature. The resonance frequency and the resonance peak height are independent of temperature. The peaks show a non-linear dependence upon electric field. At the very high field of 74.3GV/m, the sodium ions move in collective modes of vibration.

ABSTRACT

1. INTRODUCTION.....	1-1
1.1 Hollandite.....	1-1
1.2 Molecular Dynamics simulation.....	1-4
1.2.1 Overview of simulation work on ionic crystals	
1.3 Thesis overview.....	1-5
2. DIELECTRIC BACKGROUND.....	2-1
2.1. Dielectric Response.....	2-1
2.1.1. Response function	
2.1.2. Frequency-domain response	
2.1.3. Kramers-Kronig Relations	
2.1.4. Correlation functions	
2.1.5. Non-linear response	
2.2. Dielectric relaxation models.....	2-15
2.2.1. Debye, Cole-Cole and Davidson-Cole models	
2.2.2. Universal relaxation law	
2.2.3. Dissado-Hill Theory	
2.3. Poley absorption.....	2-23
2.4. Dielectric Analysis of Solids.....	2-26
2.4.1. Ionic conduction	
3. METHOD AND TECHNIQUE USE.....	3-1
3.1. General introduction.....	3-1
3.2. General aspect of constructing a computer model.....	3-2
3.3. Developing the model structure.....	3-3
3.4. Modelling of ion-ion interactions.....	3-3
3.4.1. Lennard-Jones (LJ) potential	
3.4.2. Coulomb potential	
3.4.3. Total potential	
3.4.4. Method for determining the value for lambda	

3.5. Boundary conditions used.....	3-11
3.5.1. Reflective boundary conditions	
3.6. Developing the equations of motion.....	3-12
3.7. Molecular Dynamics (MD) simulation technique.....	3-13
3.7.1. Structure of the tunnel	
3.7.2. Number of the tunnel ions	
3.7.3. Method for positioning the tunnel ions along c-axis	
3.8. Summary of the iterative process.....	3-21
 4. SOFTWARE DESIGN AND DEVELOPMENT.....	 4-1
4.1. General introduction.....	4-1
4.2. Commercial software package used.....	4-2
4.2.1. Microsoft Visual C++	
4.2.2. Matlab	
4.2.3. Origin	
4.3. Implementation.....	4-4
4.3.1. Program code to perform the MD simulation	
4.3.2. Program code to calculate the average position of the sodium ions	
4.3.3. Program code to perform the MD simulation when a dc electric field is added	
4.3.4. Program code to calculate the polarisation	
4.3.5. Program code to calculate the continuous average for the polarisation	
4.4. Testing.....	4-19
4.4.1. Testing to minimise round-off error	
4.4.2. Testing during coding	
4.4.3. Testing for each mathematical formula used	
4.4.4. Testing for the overall sequence	
 5. RIGID LATTICE APPROXIMATION.....	 5-1
5.1. General introduction.....	5-1
5.2. Simulation procedure.....	5-2
5.2.1. Number and position of the ions	
5.2.2. Temperature given to the simulation	
5.2.3. Initial conditions given for each run	

5.2.4. Average obtained over different runs	
5.2.5. DC electric fields added at 5001 th interval	
5.2.6. Calculation of the polarisation	
5.3. Data analysis.....	5-19
5.3.1. “Origin” software for performing data smoothing	
5.3.2. “Origin” software for performing Fast Fourier Transforms (FFT)	
5.3.3. “Origin” software for performing curve fitting	
5.3.3.1. Relaxation response	
5.3.3.2. Resonance response	
5.4. Two testing processes that are carried out.....	5-30
5.4.1. Only one tunnel ion is allowed to move	
5.4.2. Depolarisation	
6. RESULTS	6-1
6.1. Position and trajectories of movement for the sodium ions.....	6-1
6.1.1. Trajectories of movement for sodium ion in three-dimensions	
6.1.2. Position of sodium ions in c-axis without applied field	
6.1.3. Position of sodium ions in c-axis with applied field	
6.2. Results obtained from the data analysis.....	6-5
6.2.1. The polarisation	
6.2.2. The continuous average for the polarisation	
6.2.3. The smoothing of the continuous average for the polarisation	
6.2.4. The polarisation current	
6.2.5. Results of FFT generated from the “Origin” software	
6.2.6. Results showing the curve fitting using “Origin” software	
6.2.6.1. Real part of the susceptibility	
6.2.6.2. Imaginary part of the susceptibility	
6.3. Results for the two testing processes.....	6-14
6.3.1. Only one tunnel ion is allowed to move	
6.3.2. Depolarisation	
6.4. The results obtained at the temperature range of 200K to 373K and with electric fields in the range of 7.43MV/m to 74.3GV/m.....	6-19

7. DISCUSSION.....	7-1
7.1. Position and trajectories of movement for the sodium ions.....	7-1
7.2. Frequency dependence of χ' and χ''	7-4
7.3. Correlation function	7-6
7.4. Temperature dependence.....	7-8
7.5. Non-linear response	7-10
7.6. Poley absorption	7-11
7.7. Group oscillation at very high field	7-14
7.8. Very short pulse excitation.....	7-16
 8. CONCLUSIONS AND FURTHER WORK.....	 8-1

REFERENCES

APPENDIX

- A1 Positions for the titanium ions and the oxygen ions
- A2 Calculation of the actual mass for the ions
- A3 Results for the curve fitting in the electric field range between 7.43MV/m and 74.3GV/m and at temperature range between 200K and 373K

PUBLICATION

Addenda consisting of a CD-ROM, which contains the program code for the C++ program.

1 INTRODUCTION

1.1 Hollandite

There is a large class of materials, which conduct mainly by motion of ions, so-called fast ion conductors. Fast ion conductors are characterised by having ‘easy’ pathways for ionic transport, so that the activation energy for ionic-mobility is small [1]. Hollandites are ionic crystals of a rather unusual kind, in which the ions of one type are in a disordered and highly mobile state [2]. Such materials often have rather special crystal structures in that there are open tunnels or layers through which the mobile ions may move [3]. Some examples are β -Alumina, Hollandite, AgI and Ag^+ ion solid electrolytes.

Hollandite is our main interest in this research. The aim is to use a hollandite to describe a “simple fluid” and to determine the response of the tunnel ions to an applied field. Hollandite is the name for a family of compounds of general formula $\text{A}_x\text{M}_{4-x}\text{N}_y\text{O}_8$. The basic formula of the Hollandite structure used in the research is $\text{Na}_x(\text{Ti}_{8-x}\text{Cr}_x)\text{O}_{16}$, ($x = 1.7$) [4,5]. The main interest of this Na-priderite is its structure as a promising 1-D Na ion conductor [6]. Priderites, titania-based hollandites, are typical one-dimensional (1-D) ion conductors in which the 1-D tunnels are available for transport of cations in the tunnel (hereafter the “tunnel ion”) [5]. Priderites are generally represented by $\text{A}_x\text{M}_y\text{Ti}_{8-y}\text{O}_{16}$, where A is the alkali or alkaline earth ions and M, di- or trivalent cations [6, 7].

The host structure for the hollandite being used mainly consists of titanium ions and oxygen ions. These titanium ions are each octahedrally bonded to six oxygen ions. Two such octahedra are joined by sharing an edge, and these doubled groups share further edges above and below to form extended double strings parallel to the growth axis. Four such double strings are joined by corner sharing to form a unit tunnel. The sodium ions are situated in the tunnels, and each is ionically bonded to eight oxygen ions of the host structure at the corners of a slightly distorted cube. A typical hollandite is shown in figure 1.1.

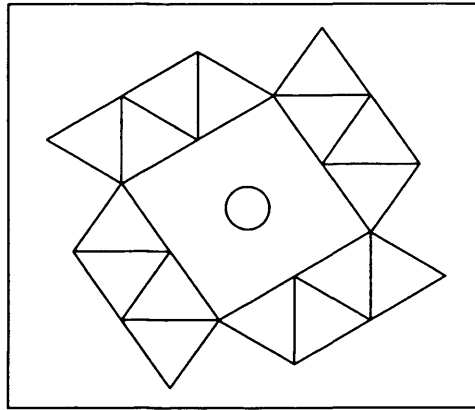


Figure 1.1: A typical hollandite structure. Projected along the c-axis. The square indicates the tunnel and the circle represents the tunnel ion, Sodium ion.

Behaviour of the tunnel ion is usually complicated because it interacts not only with the ions in the lattice sites but also with the other tunnel ions. The main two interactions are Lennard-Jones potential for the short range and Coulomb potential for the long range. Although the ions at the lattice sites give a potential surface for the tunnel ions, which the Sodium ions move on, the interactions with other Sodium ions in the tunnel is a many body problem like a liquid. Another similarity to a liquid is the alternative position that the sodium ions can move to. Hence, it will be quite interesting to investigate the response of the sodium ions under the effect of electric field. The objective of this research is to develop an atomistic model for the dynamics of the sodium ions in the hollandite structure.

The dielectric behaviour of the hollandites is typically studied in the low frequency region [10^2 - 10^9]. Dryden and Wadsley [8], in the first publication on the structure and electrical properties of a hollandite, reported the existence of a dielectric relaxation in several BaMg hollandites, which had a maximum absorption at room temperature in the radio frequency region of the spectrum (10^5 - 10^8 Hz). They reported that the dielectric absorption was only detected when the electric field was in the direction of the tunnel. The activation energy for the peak frequency representing the energy barrier to be overcome for ion displacement was found to be 0.17eV.

Cheary and Dryden [9] reported that the mobility of the tunnel ion in Ba hollandite is very low except in limited regions and the activation energy that they obtained is 0.24eV. Activation energies of the order 0.05eV claimed by others was only detected in some samples with the present of impurity TiO_2 as a second phase. Since then there have been further experimental work on the dielectric properties of hollandites published by Singer et al [10]. Yoshikado et al [11] emphasize the loss factor (ϵ'') at low frequencies which increases with decreasing frequency and usually depends on frequency as f^n where $n < 1$. Jonscher [12] concluded that the response of fast ion conductors follow the “universal law” for the charge carriers. He showed that strong low-frequency dispersion occurs in high temperature, 373K, in the hollandite ($\text{K}_{1.8}\text{Mg}_{0.9}\text{Ti}_{7.1}\text{O}_{16}$).

The behaviour in the high frequency region is not well understood. Michiue and Watanabe [13] reported that the strong response observed for the imaginary part of dielectric constant for K-hollandites around $100\text{-}300\text{ cm}^{-1}$ ($3 \times 10^{12} - 9 \times 10^{12}\text{ Hz}$) is due to the vibration of the framework structure. Not much work has been done in investigation for the frequency range around $1.2\text{-}70\text{ cm}^{-1}$ ($3.6 \times 10^{10} - 2.1 \times 10^{12}\text{ Hz}$).

Hill and Dissado [14] predicted that particles moving in a flexible local environment experienced a cooperative interaction between the particle and their environment leading to a specific form of dielectric response, the constant phase angle response $C''(f) \propto C'''(f) \propto f^{-p}$. Dissado and Allison [15] showed that this form of response included a Poley absorption peak in the far infra-red region of the spectrum. This form of absorption peak was observed by Poley [16], Davies [17] and some others [18, 19] in both liquids and solids and was named after Poley. The “liquid-like” hollandite structure is similar in form to the materials in which the Poley peak is observed, and hence such a peak can be expected. The theories [15, 16] suggest that this peak will be caused by the cooperative librations of the dipole produced by the sodium ions and their environmental counter-charges as the sodium ions displace under the many-body interactions of one another. It is the intention here to use molecular dynamics simulations to see if the predicted Poley absorption will be produced by such motions even in the absence of vibrations and flexible

displacement in the surrounding crystal. Secondly, the effect of high electric fields will be simulated to try to gain some idea of how the Poley absorption will behave in a non-linear region of behaviour.

1.2 Molecular Dynamics (MD) simulation

Molecular dynamics (MD) simulations technique has been used in this research to perform the atomistic calculations, of frequency dependent electrical conductivity in $\text{Na}_x(\text{Ti}_{8-x}\text{Cr}_x)\text{O}_{16}$, ($x = 1.7$). MD simulation is generally carried out to compute the motions of individual molecules in model of solids, liquids and gases. The key idea is motion, which describes how positions, velocities, and orientation change with time [20]. The MD simulation method is carried out in such a way that atoms are represented by point particles and the classical (Newton) equations of motion, “force equals mass times acceleration or $F = ma$ ” are integrated numerically. The motions of these large numbers of atoms are governed by their mutual interatomic interaction. MD simulations are limited largely by the speed and storage constraints of available computers. Hence, simulations are usually done on system containing 100-1000 particles, with a time step of 1×10^{-15} s.

This technique for simulating the motions of a system of particles when applied to biological macromolecules gives the fluctuations in the relative positions of the atoms in a protein or in DNA as a function of time. Knowledge of these motions provides insights into biological phenomena. MD is also being used to determine protein structure from NMR, to refine protein X-ray crystal structures faster from poorer starting models, and to calculate the free energy changes resulting from mutation in proteins [21].

1.2.1 Overview of simulation work on ionic crystals

The first computer simulation study of any fast ion conductor was made by Rahman [22] on CaF_2 using the molecular dynamics method. He shows that molecular

dynamics calculations can be of considerable value in the understanding of the dynamical events on motion of ions in fast ion conductor. Gilan [23] has performed three different simulation techniques on the fast ion conductors, the static energy-minimisation method, Monte Carlo method and molecular dynamics method. He showed that the molecular dynamics method is the most powerful of the three as it gives the largest amount of useful information starting from the smallest number of assumptions.

Beckers et al [24] have carried out Molecular Dynamics simulations on the fast ion conductor Na^+ - β -alumina and shows that the diffusion coefficients and conductivities as a function of temperature display close to Arrhenius behaviour. Results are in agreement with experiment for the temperature range 300-900 K.

Lots of works has been carried out by substituting ions into a structure or introducing an impurity into a structure. Cormack et al [25] have done some work in introducing Sc^{3+} into CeO_2 , a fluorite structure host. The computer simulation shows that there is a stable low symmetry dipolar structure for the position of the Sc impurity, in which the surrounding cage of eight oxygen ions is distorted more so than the position of the Sc ion itself.

Michiue and Watanabe [4, 5, 6] have carried out lots of simulations on the positions of the tunnel ions for the K-hollandites and Na-hollandites. They reported that the distribution of the tunnel ions has a good agreement with the x-ray analysis.

1.3 Thesis overview

Chapter 2 gives a brief discussion of some fundamental concepts relevant to the dielectric response in time domain and frequency domain. The Poley absorption that exists in the far-infrared region is also introduced.

Chapter 3 present the computational methods and techniques used. The development of the hollandite model structure, ion-ion interactions and the way in which the Molecular Dynamics simulation is carried out will be explained.

Chapter 4 then explains the software design and development. The coding for the various tasks will be stated and the flow charts are drawn to give a better understanding of the flow of the program code written.

The presentation of the Rigid Lattice approximation is then given in Chapter 5. The procedures of the work carried out are listed there. The "Origin" software used to perform Fourier transform on the results obtained thus making it easier to interpret is described.

Chapter 6 includes the graphs plotted in Origin and the final results. The results are then commented and analysed.

Chapter 7 discusses the results obtained. The limitation in the methodology is also explained.

Chapter 8 gives the conclusion of the thesis and suggests some further work that can be carried out in the future.

2 DIELECTRIC BACKGROUND

2.1 Dielectric response

Dielectric response is the response of a material to the application of electric field. Polarisation arises when positive charge and negative charge move small distance in opposite directions when an electric field is applied. This produces a dipole moment. If the distribution of ionic charges is considered as in our case, the polarisation becomes the dipole moment per unit volume and is the summation of the individual dipole moments.

The general relation between the polarisation P and the field E can be written as:

$$P = \epsilon_0 \chi E + \text{higher term in } E \quad 2.1$$

The first term proportional to the field is of dominant importance in most system, ϵ_0 is the permittivity of free space and χ is the linear susceptibility. The higher terms give rise to phenomena known as hyperpolarisation where non-linearity of the dielectric response arises.

Consider now a capacitor consisting of two parallel metallic plates of the thickness l with the dielectric medium filling the space between these plates. The area of the plates A would be much greater than l^2 to prevent the fringing effect. If a voltage V is applied between the plates, assuming that the plates make an intimate contact with the material, the electric field is

$$E = V / l \quad 2.2$$

The dielectric induction D (represent the total charge density induced on the plates by a field E) becomes

$$D = \frac{Q}{A} = \epsilon_0 E + P \quad 2.3$$

The response of free space is instantaneous and hence the induced charge $\epsilon_0 E$ follows the field instantaneously and P arises from the delayed generation of the material polarisation. Q is the charge on the plate, ϵ_0 is the permittivity of free space.

The relationship between D and E is

$$D = \epsilon_0 \epsilon_r E, \quad 2.4$$

where ϵ_r is the relative dielectric permittivity

substituting equation 2.1 into equation 2.3 gives

$$D = \epsilon_0 \epsilon_r E = \epsilon_0 E + \epsilon_0 \chi E + \text{terms with higher power of } E \quad 2.5$$

In the case of a linear response the expansion is limited to terms proportional to E and hence,

$$\epsilon_0 \epsilon_r = \epsilon_0 + \epsilon_0 \chi = \epsilon_0 (1 + \chi) \quad 2.6$$

Polarisation is directly related to the surface charge that appears on the polarised medium. There are three ways in which polarisation may arise. When an electric field is applied to a material the positive and negative charges move in opposite directions. This can be due to either the relative motion of nuclei and extra-nuclear electron called atomic polarisation or to the relative motion of positive and negative ions as a whole in ionic solids called ionic polarisation. These two ways also occur in non-polar material. A further effect that occurs in the polar material (i.e. materials that contain permanent dipole moments) is in the application of electric field, the dipole moment will tend to turn into the direction of the field and produce an overall polarisation named orientation polarisation. Orientation polarisation is temperature dependent as the randomising effects of thermal agitation on the dipole directions are greater at high temperatures and the polarisation decreases with increasing temperature.

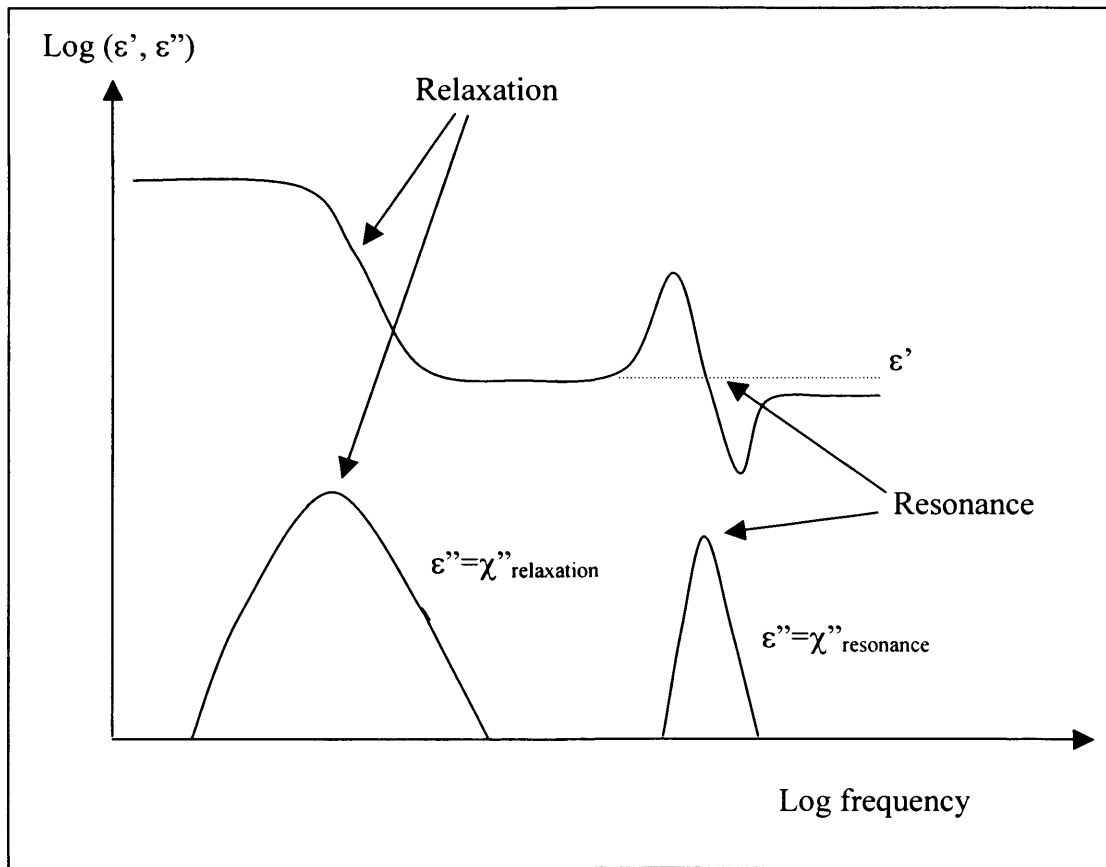


Figure 2.1: A diagram showing the relaxation response and the resonance response.

Atomic polarisation gives rise to resonant response (see figure 2.1) at the frequency of electronic transition in the molecules, i.e. above the frequency of visible light ($\sim 10^{14}$ Hz and above). Nuclear polarisation also produces resonant responses at the vibration (and rotation) frequencies, i.e. IR to far IR (10^{11} to 10^{14} Hz). Orientation polarisation and ionic displacements between sites give relaxation responses (frequency \leq THz).

In a capacitor, the capacitance $C = \frac{Q}{V}$ (Q is the charge on the plate and V is the applied voltage) and hence is proportional to ϵ' (see equation 2.3 and 2.4). Dielectric used in capacitors should therefore have as large a value ϵ' as possible consistent with an ability to survive the applied voltage. The imaginary component, ϵ'' , relates to the electric currents that occur when the charges are moved into position to give the polarisation. Its value therefore determines the amount of

electrical energy that is dissipated as heat in the dielectric. Consequently dielectrics used as insulators in ac fields (e.g. power transmission insulation) should have as low a value of ϵ'' as possible at the transmission frequency.

Polarisation happens in the Hollandite structure when the tunnel ions (sodium ions) move along the tunnel. When the sodium ion moves, it form a dipole having the negative part not moving as the rigid lattice sites contribute to the negative part of the dipole and the positive part from the sodium ion. The sodium ions may also allow the transport of disturbances over long range, which could act as a dc current given suitable electrodes (i.e. ion exchange materials).

The measurement of dielectric responses is useful to provide a diagnostic of the behaviour of dielectric materials used as capacitors and insulators. Because it is non-invasive it can be used as a diagnostic technique for a wide range of materials such as pharmaceuticals and food [1]. It is also useful for studying the dynamics and structures of a wide range of bulk materials.

2.1.1 Response function

The response of a system to a field is important in both the time domain and frequency domain as they represent the most basic form of information about the dielectric properties of a system and they form the basis of most interpretation analysis on experimental data.

The polarisation at a time, t , $P(t)$, is the sum of contributions of responses to the electric field at every time in the past (from $t = -\infty$). This is known as superposition of responses.

$$P(t) = \int_{-\infty}^t \phi(t - \tau) E(\tau) d\tau \quad 2.7$$

where $\phi(t)$ is the dielectric response function.

If $E(\tau)$ follows a step-change (i.e. switch on at $t=0$)

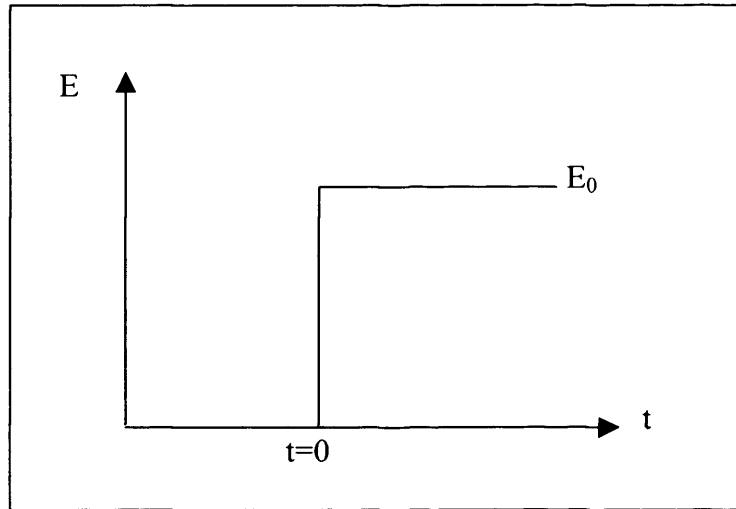


Figure 2.2: A graph showing the step-field E_0 , switch on at $t=0$.

Then

$$\begin{aligned}
 P(t) &= \int_0^t \phi(t-\tau) E_0 d\tau \\
 &= E_0 \int_0^t \phi(t-\tau) d\tau \\
 &= -E_0 \int_t^0 \phi(z) dz \\
 &= E_0 \int_0^t \phi(z) dz
 \end{aligned} \tag{2.8}$$

This gives

$$E_0 \phi(t) = \frac{dP(t)}{dt} \tag{2.9}$$

for this situation. If E is switched off at $t=0$, $E_0\phi(t) = -\frac{dP(t)}{dt}$.

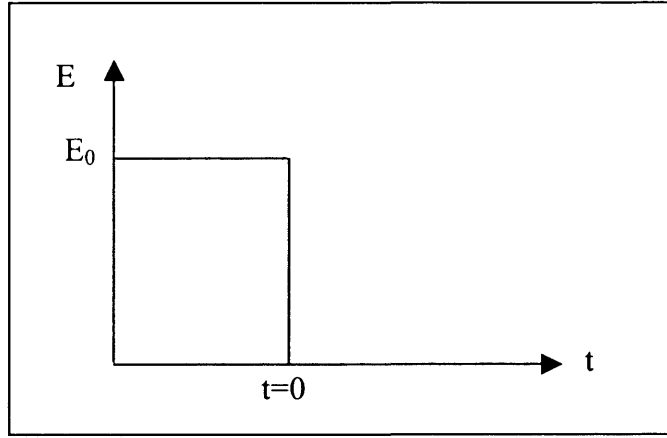


Figure 2.3: A graph showing the step-field E_0 , switch off at $t=0$.

When field is an ac-field, $E(t) = E_0 e^{i\omega t}$. The polarisation $P(t)$ becomes

$$\begin{aligned}
 P(t) &= \int_{-\infty}^t \phi(t-\tau) E_0 e^{i\omega\tau} d\tau \\
 &= e^{i\omega t} \int_{-\infty}^t \phi(t-\tau) E_0 e^{i\omega(\tau-t)} d\tau \\
 &= E_0 e^{i\omega t} \int_{\infty}^0 \phi(z) e^{-i\omega z} (-dz) \\
 &= E_0 e^{i\omega t} \int_0^{\infty} \phi(z) e^{-i\omega z} dz \\
 &= E_0 e^{i\omega t} \epsilon_0 \chi(\omega)
 \end{aligned} \tag{2.10}$$

hence

$$\epsilon_0 \chi(\omega) = \int_0^{\infty} \phi(z) e^{-i\omega z} dz \tag{2.11}$$

which gives

$$\chi(\omega) = \frac{1}{\epsilon_0} \int_0^{\infty} \phi(z) e^{-i\omega z} dz \tag{2.12}$$

2.1.2 Frequency-domain response

The frequency-domain response is important as many measuring techniques use frequency as a parameter. The mathematical basis for the frequency-dependent susceptibility is defined as the Fourier transform of the response function $\phi(t)$

$$\chi(\omega) = \chi'(\omega) - i\chi''(\omega) = \frac{1}{\varepsilon_0} \int_0^\infty \phi(t) e^{-i\omega t} dt \quad 2.13$$

where $\omega = 2\pi\nu$ is the angular frequency, ν is the circular frequency in Hertz. The susceptibility is a complex function of the frequency, the real part $\chi'(\omega)$ gives the amplitude of polarisation in phase with the field and the imaginary part $\chi''(\omega)$ gives the component in quadrature with the field and usually refer to the dielectric loss.

The real and imaginary component of the susceptibility $\chi(\omega)$ as the cosine and sine transform of $\phi(t)$ are

$$\chi'(\omega) = \int_0^\infty \phi(t) \cos(\omega t) dt \quad 2.14$$

$$\chi''(\omega) = \int_0^\infty \phi(t) \sin(\omega t) dt \quad 2.15$$

The frequency-domain response of the dielectric system can be written in terms of dielectric permittivity $\varepsilon(\omega)$. The relationship between the permittivity and the susceptibility are shown below:

$$\varepsilon(\omega) = \varepsilon'(\omega) - i\varepsilon''(\omega) = \varepsilon_0 [1 + \chi'(\omega) - i\chi''(\omega)] \quad 2.16$$

The real part of the permittivity $\varepsilon'(\omega)$ includes the contribution of free space ε_0 , the imaginary component $\varepsilon''(\omega)$ is entirely due to the material.

2.1.3 Kramers-Kronig Relations

Kramers-Kronig relations are very important in connecting the real and imaginary parts of the complex susceptibility and they only hold if the response is linear. It is important as it can be used to eliminate a contribution to χ'' from a dc conduction. The equation 2.14 and equation 2.15 are derived from the same generating function $\phi(t)$ and thus it is possible to express $\chi'(\omega)$ in terms of $\chi''(\omega)$.

First the following transformation is proved:

$$\int_{-\infty}^{\infty} \frac{\sin xt}{x - \omega} dx = \cos \omega t \int_{-\infty}^{\infty} \frac{\sin(x - \omega)t}{(x - \omega)t} d[(x - \omega)t] + \sin \omega t \int_{-\infty}^{\infty} \frac{\cos(x - \omega)t}{(x - \omega)t} d[(x - \omega)t]$$

where the integral ignores the imaginary contributions arising from integration through the pole $x = \omega$. The first integral is equal to π , the second vanishes so that

$$(1/\pi) \int_{-\infty}^{\infty} \frac{\sin xt}{x - \omega} dx = \cos \omega t \quad 2.17$$

The integral on the left is known as the Hilbert transform of the function $\sin xt$. This is substituted into equation 2.14:

$$\chi'(\omega) = (1/\pi) \int_{-\infty}^{\infty} \phi(t) \int_{-\infty}^{\infty} \frac{\sin xt}{x - \omega} dx dt = (1/\pi) \int_{-\infty}^{\infty} \frac{1}{x - \omega} \int_{-\infty}^{\infty} \phi(t) \sin xtdt dx \quad 2.18$$

The second integral in this expression is equal to $\chi''(\omega)$ in view of equation 2.15. The equations finally becomes

$$\chi'(\omega) = \frac{1}{\pi} \int_{-\infty}^{\infty} \frac{\chi''(x)}{x - \omega} dx \quad 2.19$$

$$\chi''(\omega) = -\frac{1}{\pi} \int_{-\infty}^{\infty} \frac{\chi'(x)}{x - \omega} dx \quad 2.20$$

The range of the integration can be changed to $(0, \infty)$ and thus the one-sided Kramers-Kronig integrals become:

$$\chi'(\omega) = \frac{2}{\pi} \int_0^\infty \frac{x \chi''(x)}{x^2 - \omega^2} dx \quad 2.21$$

$$\chi''(\omega) = \frac{2\omega}{\pi} \int_0^\infty \frac{\chi'(x)}{x^2 - \omega^2} dx \quad 2.22$$

2.1.4 Correlation Functions

The dynamic behaviour of ensemble can be described through two-time correlation functions [2] and these can be used to determine the susceptibility. In the case of a linear dielectric response the most used correlation function is

$$\frac{\varphi_\mu(t)}{\varphi_\mu(0)} = \frac{\langle \mu(0) \cdot \mu(t) \rangle}{\mu^2} \quad 2.23$$

$\varphi_\mu(t)$ is called the relaxation function and μ is the dipole moment. $\langle \mu(0) \cdot \mu(t) \rangle$ is the scalar (dot) product of vector μ at given position at time $t=0$ and its value at time t averaged over all positions and possibilities inherent in the ensemble of dipoles. The response function $\phi(t)$ is given by

$$\frac{\phi(t)}{\phi(0)} = \frac{\langle \mu(0) \cdot \dot{\mu}(t) \rangle}{\langle \mu(0) \cdot \dot{\mu}(0) \rangle} \quad 2.24$$

Here $\langle \mu(0) \cdot \dot{\mu}(t) \rangle$ is the average of the scalar (dot) product of vector μ at given position at time $t=0$ and its time derivative value at time t .

From Kubo [2] the relaxation function is determined by the time integral of response function, $\phi(t)$

$$\varphi(t) = \lim_{\varepsilon \rightarrow 0^+} \int_0^\infty \phi(t') e^{-\varepsilon t'} dt' \quad 2.25$$

The susceptibility can be obtained from either the response function or relaxation function as shown below [2]:

$$\chi(\omega) = \lim_{\varepsilon \rightarrow 0} \int_0^\infty \phi(t) e^{-i\omega t - \varepsilon t} dt \quad 2.26$$

$$\chi(\omega) = \varphi(0) - i\omega \int_0^\infty e^{-i\omega t} \varphi(t) dt \quad 2.27$$

These functions can be obtained from molecular dynamics and either can be used to get the susceptibility. The relaxation function is more commonly used because it does not require a time differential to be calculated, but these functions only give the linear response.

For a linear response [2], the response is determined by time-fluctuation (atomic polarisation, dipole orientation and ion displacement) in the equilibrium system occurring in the absence of an electric field. Under linear response the field only alter the concentration, so that more fluctuation occurs in the direction of the field than against it. Non-linear behaviour requires the calculation of higher order correlation functions specific to the experimental situation.

2.1.5 Non-linear response

The linear response is an approximation. The real response is always non-linear as shown in equation 2.1 and it can be written as

$$P = \varepsilon_0(\chi_1 E + \chi_2 E^2 + \dots) \quad 2.28$$

The way in which the non-linear terms in equation 2.28 affect the dielectric behaviour depends on the form of the electric fields involved, i.e. on the experimental format. For example, if only a dc field is applied the second order term gives a field dependent contribution to the static permittivity, i.e.

$$\varepsilon = \varepsilon_0(\chi_1 + \chi_2 E) \quad 2.29$$

If we apply both a dc electric field and an electromagnetic field, χ_2 leads to a contribution to the square of the refractive index ($n^2 = \varepsilon'$) that is dependent upon the dc field, i.e. the electro-optic Kerr effect. If we have ac electric fields χ_2 produces second harmonic responses and frequency mixing. In general, the higher terms are only significant when strong fields in the range of $10^8 - 10^{12}$ V/m are applied.

In one specific instance an exact form can be obtained for $P(E)$. This is where the dipoles are free to take any orientation. The energy of a dipole in an electric field is $-\mu E$, and hence in this case the probability of a dipole μ at an angle θ to the electric field is given by the Boltzman factor

$$\exp\left\{\frac{\mu E \cos \theta}{k_b T}\right\} \quad 2.30$$

The average of $\cos\theta$, which is proportional to the average dipole component in the direction of the field, i.e. the polarisation is given by [3]

$$\langle \cos\theta \rangle = \frac{\int_0^\pi \cos\theta e^{\frac{\mu E \cos\theta}{k_b T}} \frac{1}{2} \sin\theta d\theta}{\int_0^\pi e^{\frac{\mu E \cos\theta}{k_b T}} \frac{1}{2} \sin\theta d\theta} \quad 2.31$$

Using the abbreviations $\frac{\mu E \cos\theta}{k_b T} = x$ and $\frac{\mu E}{k_b T} = a$, equation 2.31 becomes

$$\begin{aligned} \langle \cos\theta \rangle &= \frac{1}{a} \frac{\int_{-a}^a e^x x dx}{\int_{-a}^a e^x dx} \\ &= \frac{1}{a} \frac{[xe^x - e^x]_{-a}^{+a}}{[e^x]_{-a}^{+a}} \\ &= \frac{e^a + e^{-a}}{e^a - e^{-a}} - \frac{1}{a} = L(a) \end{aligned} \quad 2.32$$

This function, $L(a)$ is called the Langevin Function and has a limiting value of 1, which is the maximum of $\cos\theta$. The Langevin Function is plotted against a in figure 2.4.

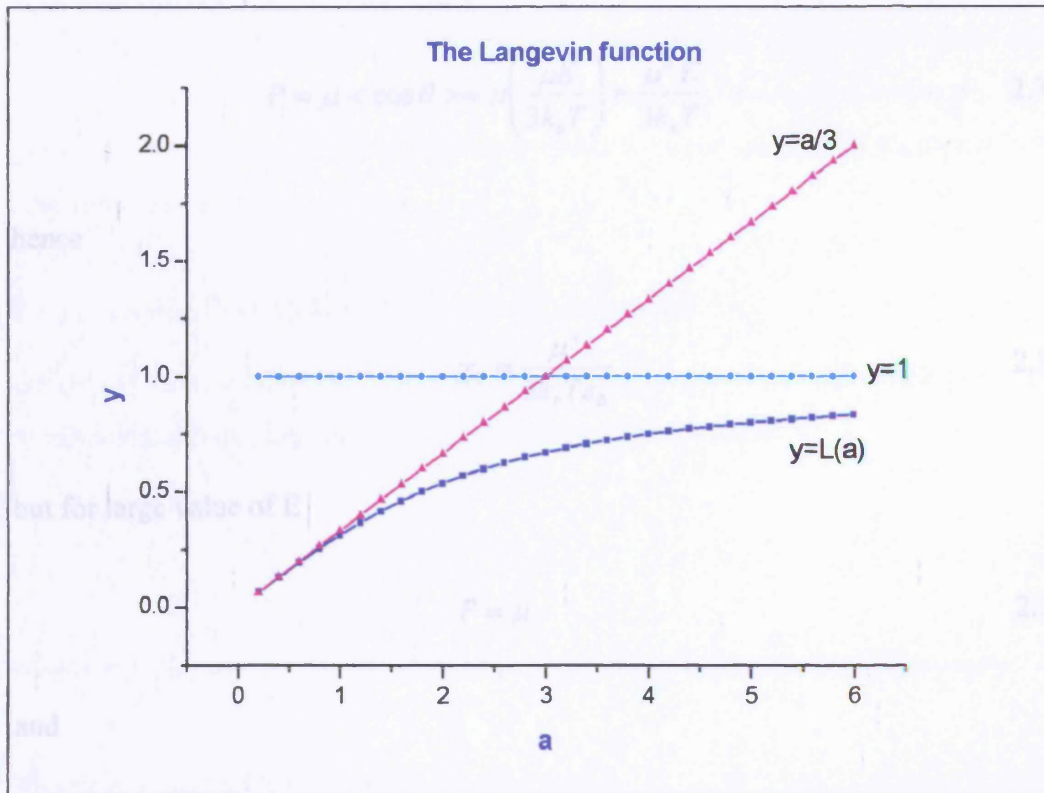


Figure 2.4: The Langevin function.

$L(a)$ can be developed in a series [3]

$$L(a) = \frac{1}{3}a - \frac{1}{45}a^3 + \frac{2}{945}a^5 - \frac{2}{9450}a^7 + \dots \quad 2.33$$

Thus for small value of a , $L(a) = \frac{1}{3}a$.

For small value of E a linear behaviour is found

$$P = \mu \langle \cos \theta \rangle \approx \mu \left(\frac{\mu E}{3k_b T} \right) = \frac{\mu^2 E}{3k_b T} \quad 2.34$$

hence

$$\chi_1 \approx \frac{\mu^2}{3k_b T \epsilon_0} \quad 2.35$$

but for large value of E

$$P = \mu \quad 2.36$$

and

$$\frac{dP}{dE} \approx \frac{1}{E^2} \quad 2.37$$

That is all the dipoles are aligned with the electric field. This result is expected to apply to low concentrations of dipolar molecules in liquid solvents and some experimental work has been carried out to find the magnitude of the χ_2 term and compare it to the prediction [4].

2.2 Dielectric relaxation models

The dynamic behaviour of resonating oscillator is well know and hence their dielectric responses are relatively easy to interpret [3]. Relaxation responses have dynamics that are not localised and have given rise to a number of theoretical and empirical descriptions.

2.2.1 Debye, Cole-Cole and Davidson-Cole models

Debye [5] assumed that the response came from dipoles re-orienting independently in viscous medium. This gives $\phi(t)$ follows an exponential decay

$$\phi(t) \propto e^{-t/\tau_p} \quad 2.38$$

where $\tau_p = 2\pi / \omega_p$, is the re-orientation time and ω_p is the loss peak frequency.

The Debye susceptibility function has the form

$$\chi(\omega) = \frac{\chi(0)}{1 + i(\omega / \omega_p)} \quad 2.39$$

$\chi(0)$ is the average number of dipoles that can be affected by the electric field and is temperature dependent. If the re-orientation involves activation over a potential barrier $\chi(\omega)$ becomes,

$$\chi(\omega) \propto \frac{1}{1 + i\omega\tau_\infty \exp(W / k_b T)} \quad 2.40$$

where τ_∞ is a suitable pre-exponential factor and W is the activation energy.

The real and imaginary components can be written as

$$\chi'(\omega) = \frac{\chi(0)}{1 + (\omega / \omega_p)^2} \quad 2.41$$

$$\chi''(\omega) = \frac{\chi(0)(\omega / \omega_p)}{1 + (\omega / \omega_p)^2} \quad 2.42$$

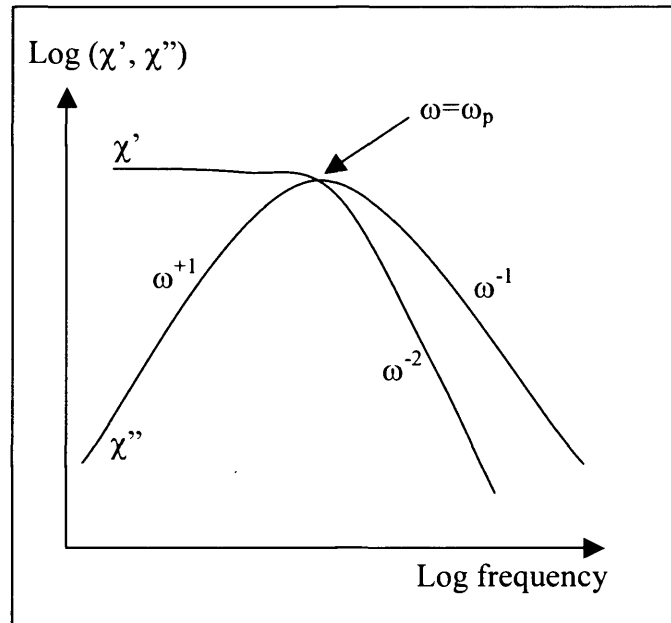


Figure 2.5: Debye model of relaxation.

The Debye susceptibility function represent a symmetrical loss peak around ω_p , the low frequency region has a $\chi''(\omega) \propto \omega^{+1}$ behaviour, and the high frequency region has a $\chi''(\omega) \propto \omega^{-1}$ and $\chi'(\omega) \propto \omega^{-2}$ behaviour.

The Debye model [1] is rarely observed; it is not applicable to condensed phase materials due to its assumption of the non-interacting dipoles but may be observed in gasses. In some cases however, such as water, the response is close to Debye. In actual case, the neighbouring dipoles will be exerting forces on each other.

Cole-Cole function [6] has the form

$$\chi(\omega) = \frac{\chi(0)}{1 + (i\omega / \omega_p)^{1-\alpha}} \quad 2.43$$

where α parameter in the range of (0,1), giving a broader (still symmetrical) loss peak than the Debye function.

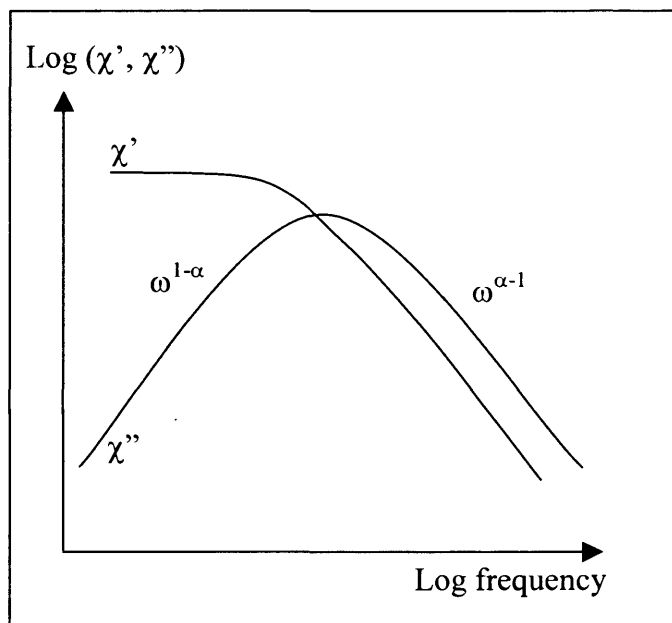


Figure 2.6: Cole-Cole model.

The Cole-Cole susceptibility function represents a broader loss peak around ω_p , the low frequency region has a $\chi''(\omega) \propto \omega^{1-\alpha}$ behaviour and the high frequency region has a $\chi'(\omega) \propto \chi''(\omega) \propto \omega^{\alpha-1}$ behaviour.

The Davidson-Cole function [7] has the form

$$\chi(\omega) = \frac{\chi(0)}{[1 + (i\omega / \omega_p)]^\beta} \quad 2.44$$

where β parameter in the range of (0,1), giving asymmetrical loss peak.

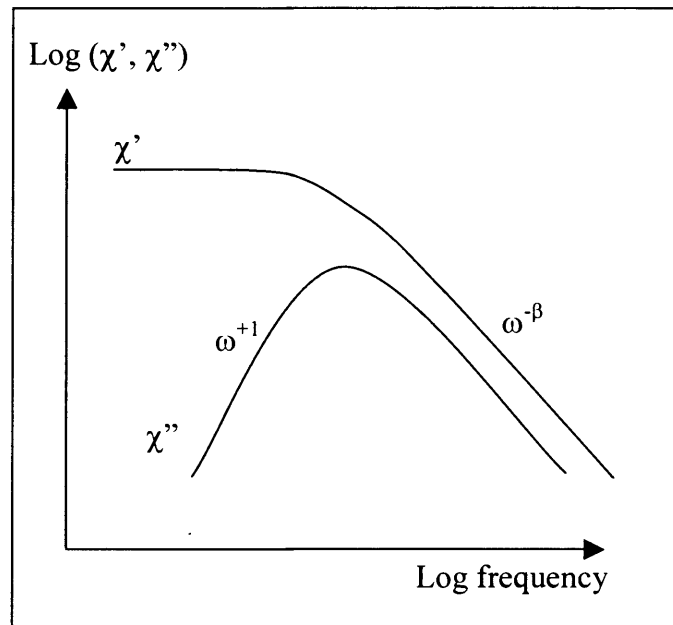


Figure 2.7: Davidson-Cole model.

The Davidson-Cole susceptibility function represents asymmetrical loss peak around ω_p , the low frequency region has a $\chi''(\omega) \propto \omega^{+1}$ behaviour and the high frequency region has a $\chi'(\omega) \propto \chi''(\omega) \propto \omega^{-\beta}$ behaviour.

The above models have none or only one adjustable parameter in the susceptibility function, i.e. none for the Debye model, one for the Cole-Cole and Davidson-Cole models. For this reason, further investigation has been done and it is explained in the following section.

2.2.2 Universal relaxation law

Two-parameter equation for the susceptibility function has been proposed by Jonscher [8]. He takes into account many-body interactions, which are present in a condensed matter. This is the first complete classification of all experimentally observed types of dielectric response in the range below microwave region of the spectrum [8]. According to the universal law, the behaviour of dipolar materials can be characterised by two fractional power laws one below and one above the loss peak frequency ω_p .

$$\chi''(\omega) \propto \frac{1}{(\omega / \omega_p)^{-m} + (\omega / \omega_p)^{1-n}} \quad 2.45$$

in which the exponent m and n are in the range of $(0,1)$.

The universal law takes into account both the dipolar response and the charge carrier responses of hopping electronic and ionic nature [8]. The charge carrier response follow the same law of frequency dependence as the dipolar materials above the loss peak frequency. Hence, above the loss peak frequency, all dielectric system obeys the universal law [8]:

$$\chi'(\omega) \propto \chi''(\omega) \propto \omega^{n-1} \quad 2.46$$

For the charge carrier n is replaced by n_1 to distinguish it from the exponent for the low frequency behaviour. The exponents n and n_1 are in the range of $(0,1)$, and in the power law region, equation 2.46 real and imaginary parts of the susceptibility are in a frequency-independent ratio:

$$\chi''(\omega) / \chi'(\omega) = \cot(n\pi / 2) \quad 2.47$$

Below the loss peak frequency, the real and imaginary parts of the susceptibility have this relation:

$$\chi''(\omega) \propto \omega^m \quad 2.48$$

in which the exponent m is in the range of $(0,1)$.

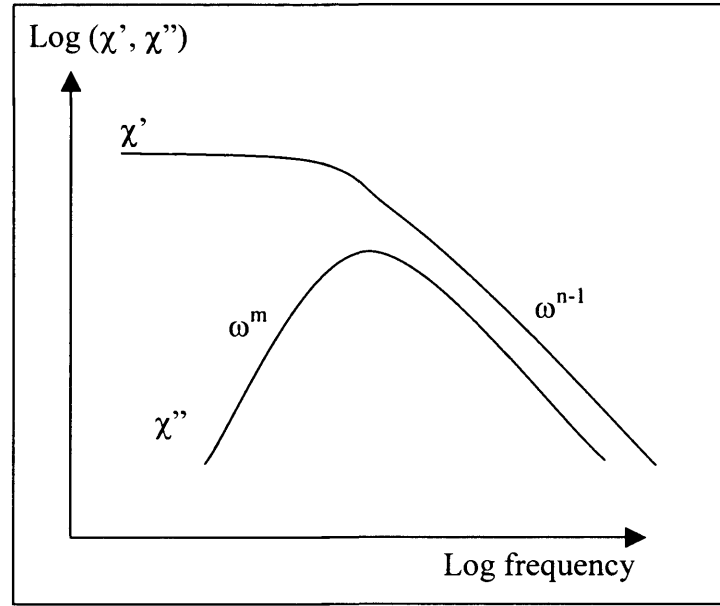


Figure 2.8: Frequency dependencies of universal dielectric response for dipolar materials.

Below the low peak frequency, charge carrier system has another form of behaviour known as low frequency dispersion (LFD) or quasi-dc process (QDC). The real and imaginary components of $\chi(\omega)$ rise steadily towards low frequency without any saturation and are parallel to each other in the log-log plot. It is also shown that since the $\chi''(\omega) > \chi'(\omega)$, the system is highly lossy [8]. The real and imaginary parts of the susceptibility have this relation:

$$\chi'(\omega) \propto \chi''(\omega) \propto \omega^{n_2-1}; \quad \omega \rightarrow 0 \quad 2.49$$

in which the exponent n_2 is in the range of $(0,1)$.

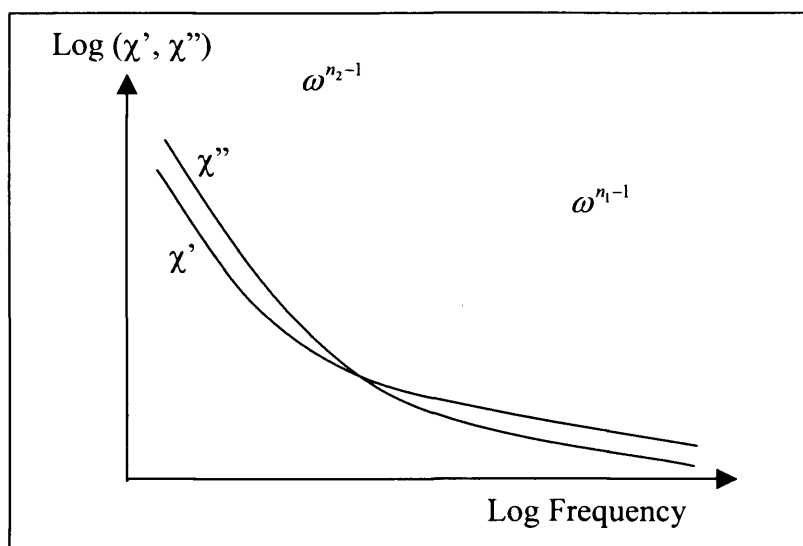


Figure 2.9: Frequency dependencies of universal dielectric response for Low frequency dispersion (LFD) or quasi-dc (QDC) process.

2.2.3 Dissado-Hill theory

The essential features of the Dissado and Hill [9,10,11] theory are a physical approach to the theory of dielectric relaxation. They suggested two theories, which are similar to Jonscher, one for dipolar relaxation and other for the LFD process. For the dipolar case, the dipoles are seen as connected with other dipole through the structure rather than acting independently as in the Debye model. The model assumed that the structure of condensed matter is composed of clusters. Intra-cluster motions and the inter-cluster exchange are observed.

Dissado and Hill proposed three exponents, m , n and p between (0,1); exponent m is referred to degree of structural order for intra-cluster motion and exponent n and p for the inter-cluster exchange mechanism. Each of this process will give its own characteristic contribution to the final form of the susceptibility function.

For the dipolar relaxation, It has been proposed [11] that the total dynamic susceptibility function is given by the single cluster response (intra-cluster motion) averaged over the distribution of clusters (inter-cluster exchange). In the inter-cluster motion, when a dipole is first to relax, it would affect the neighbouring dipoles in the same cluster. These other dipoles come to relax would again affect the

first dipole and so on. The intra-cluster exchange is due to the dipoles near the edge of the cluster interconnecting a neighbouring cluster. The relaxation behaviour of these clusters will affect the overall shape of the response and also the absolute values at any particular frequency. The asymptotic limits of the Dissado-Hill susceptibility function are the “universal” relaxation law as proposed by Jonscher [8].

For the LFD or QDC process, the model divides the response into high frequency behaviour occurring above ω_c (intra-cluster motion) and low frequency region below ω_c (inter-cluster exchange). For the intra-cluster motion, charge hopping between sites within a certain length gives the same form for the susceptibility functions for the dipole model, which is ω^{n-1} behaviour, n in the range of (0,1). In the inter-cluster exchange, charges are physically exchanged between clusters. For this situation the susceptibility function is shown to be a fractional power law of the form ω^{-p} , with p between (0,1). Small value of p indicates a set of clusters that are almost identical to each other. The asymptotic values for the Dissado-Hill QDC model are the same as Jonscher model for QDC with the different notations, $n = n_1$ and $p = 1 - n_2$.

2.3 Poley absorption

Poley [12] did measurements on six mono-substituted benzenes (dipolar liquids) and reported that the difference between the high frequency permittivity ϵ_∞ and refractive index n_{ir}^2 is nearly proportional to the square of molecule's dipole moment, μ . He concluded that a further absorption was found in the $1.2\text{-}70\text{ cm}^{-1}$ ($3.6 \times 10^{10}\text{ Hz}$ to $2.1 \times 10^{12}\text{ Hz}$) region. Davies [13] named this absorption in this far-infrared region 'Poley absorption'.

The far-infrared absorption has been generally thought to be due to the inertial effects during the small angle oscillation of a dipole. Fröhlich [14] suggested that this absorption is of resonance character and is due to the displacement of the dipole from temporary equilibrium positions to which it is bound by the inter molecular forces due to its neighbours.

Many workers [12, 13, 15, 16, 17] have predicted the existence of Poley absorption in the far-infrared region in the polar liquids. It is generally accepted that the Poley absorption originates with the librational motion undergone when a dipolar molecule trapped in a potential well collide with other molecules in its environment. Dissado and Alison [15] in their cluster model predicted the existence of a Poley absorption where fractional power law behaviour occurs in the dielectric response. Its magnitude was connected with the value of their exponent n and was shown to decrease as n decreased, i.e. the larger n , the fraction of the dipole energy involved in cooperative motions, the larger the Poley peak predicted.

Johari [16] reported that the far-infrared absorption spectra of the crystalline structures of ice clathrates contain a broad Poley absorption peak. He showed that the peak frequency decreases with increases in temperature and peak height. Nousekova et al [18] used the model of restricted rotator and obtained a good fit to the experimental results of few polar liquids and he stated that as the temperature increased, the amplitude of the absorption reduces and shifted towards the low frequency.

A number of models have been produced to support the assumption of the existence of Poley absorption. In the Periodic Potential model [19, 20], it is assumed that libration of the polar molecule about a minimum in the potential yields a Poley absorption while incoherent transfer between minima gives the associated relaxation peak. In the Itinerant Oscillator (IO) model [21], it is said that the friction between the disc and annulus damps the libration leading to Poley absorption, while the rotational diffusion generates the relaxation peak. These two models are not completely physically realistic as they neglect the effect of molecular translations upon the potentials and forces controlling the motion. Therefore Molecular Dynamics simulations have been shown to be important [22].

The Poley absorption in the Cluster Model [15] has been shown to be related to the Non-Debye response of the high frequency side of the associated relaxation peak, namely the Constant Phase Angle, CPA power law behaviour $\varepsilon''(\omega) \propto \omega^{n-1}$. The exponent n ($0 < n < 1$) defines the amount of binding between a moving dipole and its surroundings. In the limit where $n=0$, the absorption spectrum would therefore show a Debye relaxation due to rotational diffusion, but no Poley absorption. The other limit of $n=1$, the absorption spectra would show a Poley absorption as the dipole librations were driven against the restraining forces of the complex, but no relaxation peak since the dipole can never be freed to re-orientate independently of its surroundings. This is clearly shown in the figure 2.1.

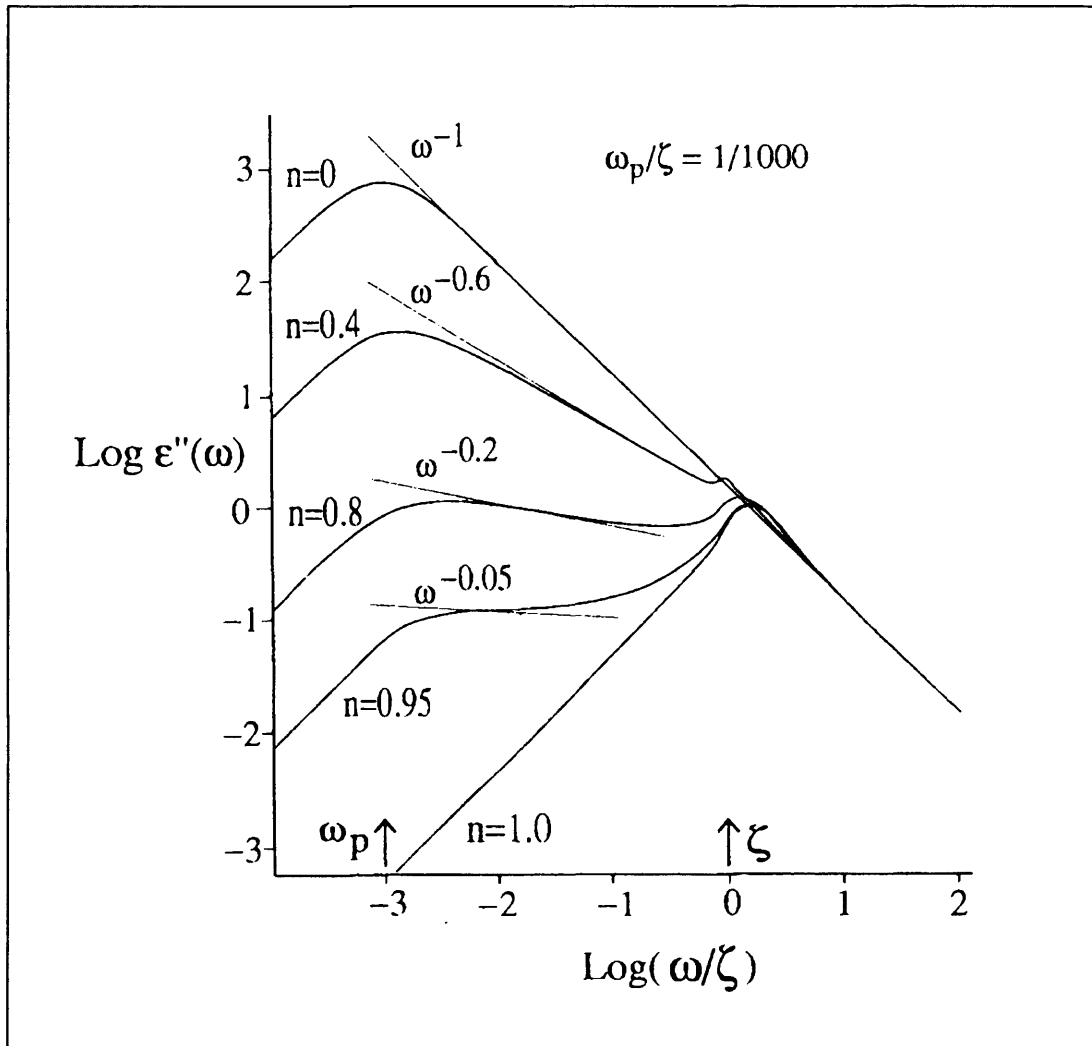


Figure 2.10: Dielectric loss, $\epsilon''(\omega)$ curves computed from the exact form of the Cluster Model response function. The effect upon the shape produced by varying n for a fixed ω_p/ζ ratio is shown. ζ is the frequency of the bare (disconnected) dipole in the potential existing immediately following re-orientation. Note the development of the relaxation loss peak as n is reduced from unity and its non-Debye shape for $0 < n < 1$. (Adapted with permission from Dissado, Figure 2, Ref [15].)

This model is a better approach as it gives a picture of a dipole partially bound by its environment and partially free to rotate. This has a great similarity to our hollandite model. The strength of the loss is divided between the Poley peak and the relaxation peak in proportion to the value of n .

2.4 Dielectric Analysis of Solids

One of the major applications of dielectric analysis is in the study of solids, particularly insulators and semiconductors. One of the difficulties is the lack of a generally agreed interpretive model [1]. In the solid phase the dipoles are more likely to be of the interactive type and not independent.

The Debye model [1] is not applicable to solids due to its assumption in the non-interacting dipoles in gasses and dilutes liquids. In actual case, the neighbouring dipoles will be exerting forces on each other. Cole-Cole [6], Davidson-Cole [7] and the universal functional power law [8] have been used for fitting observed dielectric data of relaxation process in solids. The above models, however, do not provide a physical interpretation of the properties of solids. Further progress has been made by the quantum-mechanical model by Dissado and Hill [9, 10, 11].

The dielectric response could be represented in time domain and frequency domain, where it was shown that the time dependence of current in response to a step function field and the frequency dependence of the dielectric susceptibility in response to sinusoidal excitation were connected by the Fourier transform. This is explained in section 2.1.2. There is no difference between the two types of measurements so far as linear dielectric systems are concerned.

2.4.1 Ionic conduction

The original theory of ionic conduction is based on the movement of ions and vacancies through an ionic crystal and considered both the concentration of carriers and their mobility as functions of temperature. The ionic conduction also depends upon the formation of lattice defects under the action of thermal excitation, thus creating vacancies through which ionic motion may proceed under the action of external electric field [23]. Later the theory has been used to describe the conduction in polymers [24]. Dissado and Fothergill [24] have illustrated the theory by considering a cubic crystal structure with a missing central cation and the net probability of vacancy movement in the direction of the field is defined.

In the case of hollandites, it has the property of having “redundant” lattice vacancies occurring not from lattice defects but as a property of their structure. This eases the ionic movement even without thermal excitation.

AC conductivity, $\sigma_{ac}(\omega)$ can be expressed as two independent terms

$$\sigma_{ac}(\omega) = \sigma_{dc} + \sigma'(\omega) \quad 2.50$$

where σ_{dc} represent the part of $\sigma_{ac}(\omega)$ that is frequency independent. It can be defined as the low frequency limit of the frequency dispersion, $\sigma_{ac}(\omega)$, such that

$$\sigma_{dc} = \lim_{\omega \rightarrow 0} \sigma_{ac}(\omega) \quad 2.51$$

$$\sigma_{ac}(\omega) - \sigma_{dc} = \sigma'(\omega) = \omega \chi''(\omega) \epsilon_0 \quad 2.52$$

where ϵ_0 is the permittivity of free space. $\sigma'(\omega)$ is the frequency dependent term and it results from the contribution of localised ionic hops or dipolar reorientation process [25]. Henn [25] explained that the term localised in this representation means that the ion hop is confined in a double well so that the application of an electric field creates a polarisation. In that case the dc conductivity cannot be the zero frequency limit of the dipolar effect.

3 METHOD AND TECHNIQUE USED

3.1 General introduction

The construction of the molecular dynamics model involved mainly model development and the use of the Molecular Dynamics simulation technique to solve the equation of motion iteratively, see section 3.2. In model development, firstly the interaction between ions and the interaction between ion and environment have to be defined. The interaction between ions comprises three components: Lennard-Jones potential, Coulomb potential and Van der Waals' attraction. The rigid lattice approximation is being used in the simulation. This describes the interaction between the ions and the environment. In the rigid lattice approximation only the tunnel ions are allowed to displace from their equilibrium position. The environment ions still give an interaction with the tunnel ions, i.e. they produce a constant potential surface for the tunnel ions. The tunnel ions interact with one another and are allowed to displace. After this has been done, the equations of motion are developed.

The second part of the chapter describe the Molecular Dynamics (MD) simulation technique. The initial positions for all the lattice ions of the hollandite model in a, b and c-axis are determined. A program, Gretep [1] is used to generate the positions of all the ions by keying in parameters such as space group, unit cell dimensions, atomic parameters and etc. Then titanium ions are replaced by chromium ions randomly placed in unit cells along the tunnel according to the relative proportions of titanium and chromium. A tunnel ion, which is the sodium ion, is added to the model structure for every chromium ion, in order to preserve charge neutrality. These will be explained in more detail in the section 3.7.

3.2 General aspect of constructing a computer model

There are two main tasks in constructing a computer model to solve the dynamic modelling problem: developing a suitable model for the problem at hand and applying molecular dynamics to that model [2]. The figure 3.1 shows how the major tasks are being carried out.

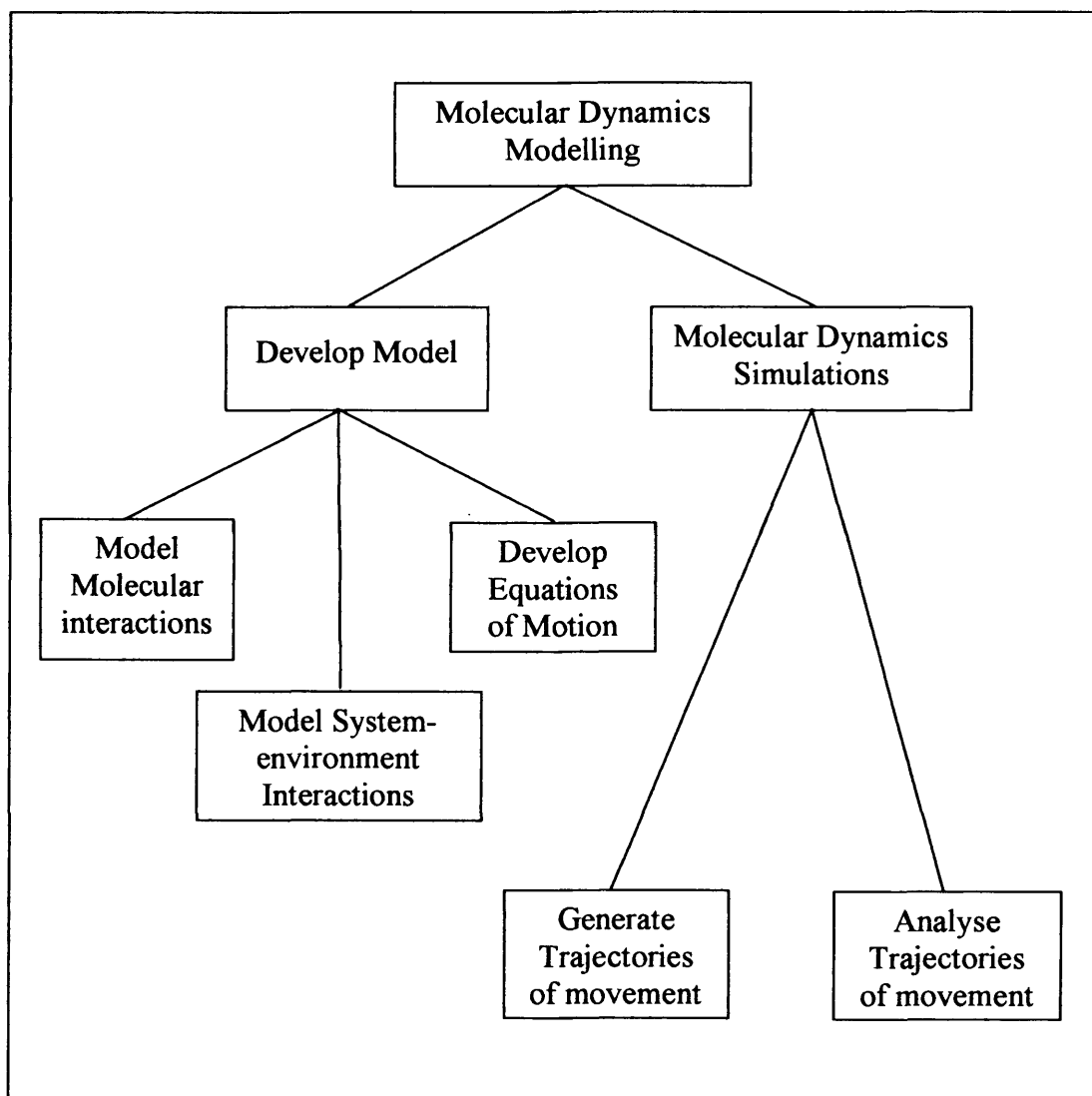


Figure 3.1: Hierarchy of the principal steps in molecular dynamics modelling. The two main tasks are the development of the model structure and the molecular dynamics simulation.

3.3 Developing the model structure

The simulation model is actually a composite of two interactions: one for interactions among the ions making up the system and another for interactions between the ions and their environment [2]. This is shown in figure 3.2. This simulated model is important because it is applied to a precisely defined model for the material of interest, which is hollandite in this research.

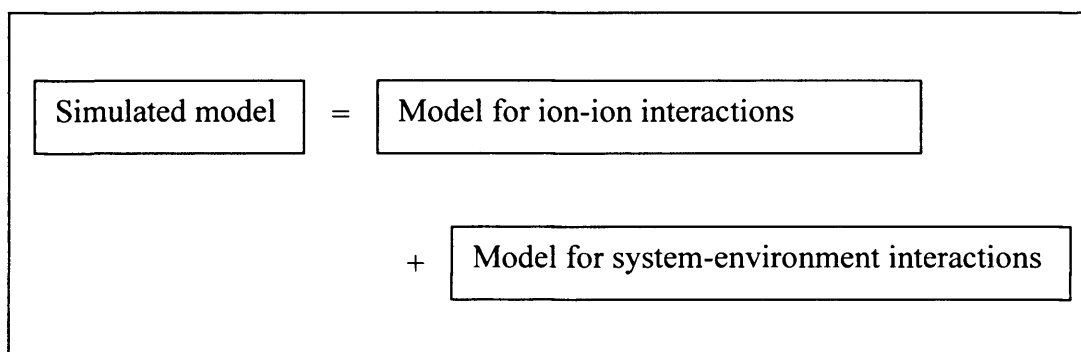


Figure 3.2: Schematic for the simulation model, which consists of the interaction between the ions and the interactions between the ions with their surroundings.

The equations of motion are worked out from the interaction between the ions. The MD simulation is then constructed based on the equations of motion obtained and the boundary conditions set.

3.4 Modelling of ion-ion interactions

The molecular interactions are based on the intermolecular potential energy function. This consists the Lennard-Jones (LJ) potential, and the Coulomb potential.

3.4.1 Lennard-Jones (LJ) potential

Lennard-Jones potential has an attractive tail at large r , r being the distance between two ions; at shorter distance it passes through zero and becomes strongly repulsive. In order to pull the ions apart to infinity, the attractive force would have to be overcome. If the two ions are squashed, together a little more the potential rises steeply. In other word the repulsive force, increase greatly [3].

The most common form of this potential is the 6-12 potential:

$$V(r) = 4\epsilon \left[\left(\frac{\sigma}{r} \right)^{12} - \left(\frac{\sigma}{r} \right)^6 \right] \quad 3.1$$

ϵ is the depth of the minimum potential energy, σ is the intermolecular distance at which $V(r) = 0$ and r is the distance between ions. The r^6 term describes the Van der Waals' attraction, while the r^{-12} term describe short-range repulsion. A typical plot of this 6-12 potential is shown below:

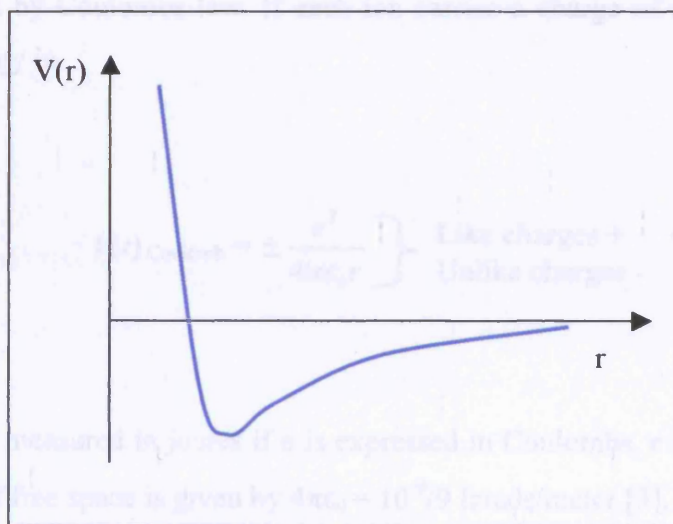


Figure 3.3: Lennard-Jones potential. LJ is a potential that is strongly repulsive at very short interatomic distances, attractive forces at large distances, and weak attractive forces at very large distance.

Van der Waals' attraction is negligible compared to Coulomb potential in the case of hollandite; therefore, it is not taken into account. The LJ potential used in this work becomes [3], :

$$V(r) = \frac{\lambda}{r^p} \quad 3.2$$

where p has a value of 10. This potential is used in ionic crystals [3] and is used in this research, hence it is denoted as the 6-p potential rather than a 6-12 potential. The method for determining the value for lambda will be explained in section 3.4.4.

3.4.2 Coulomb potential

Lattices like those of Sodium Chloride and Lithium Chloride consists of arrays of ions each positively or negatively charged. This electrostatic attraction or repulsion force is given by Coulombs law. If each ion carries a charge of magnitude e, the potential energy is

$$V(r)_{\text{Coulomb}} = \pm \frac{e^2}{4\pi\epsilon_0 r} \left. \begin{array}{l} \text{Like charges +} \\ \text{Unlike charges -} \end{array} \right\} \quad 3.2$$

The energy is measured in joules if e is expressed in Coulombs, r in meters and ϵ_0 , permittivity of free space is given by $4\pi\epsilon_0 = 10^{-9}/9$ farads/meter [3].

The Coulomb potential is shown in the figure 3.4 below:

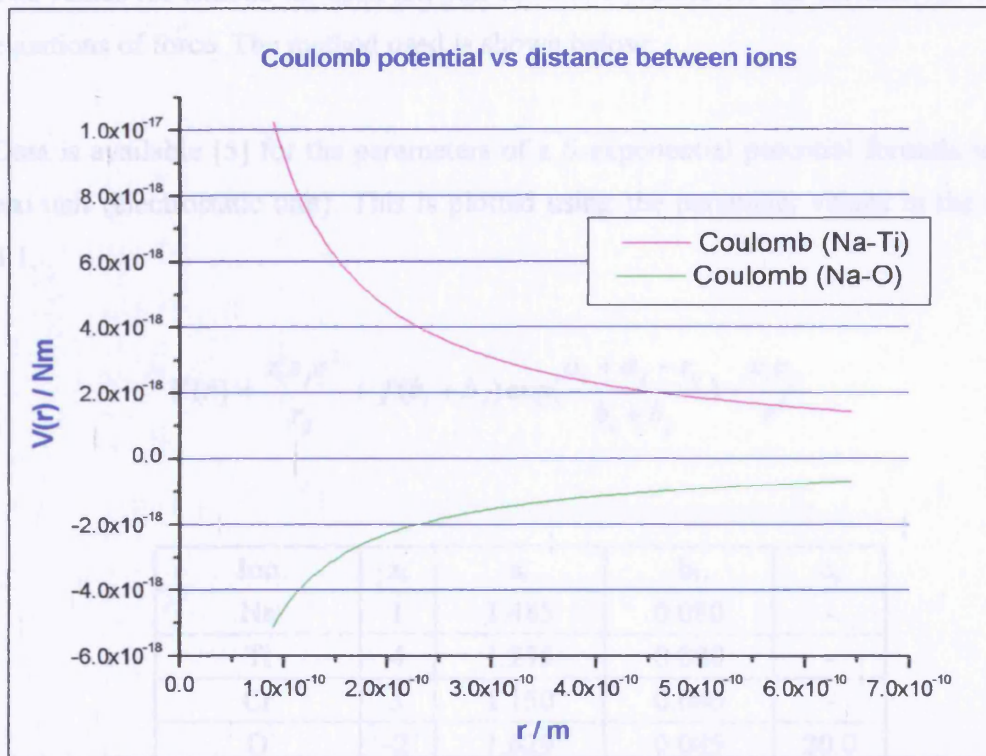


Figure 3.4: The Coulomb potential between two ions based on the equation used. This shows the general graph between like ions and unlike ions. The bottom curve represents the interaction between sodium and oxygen ions, two ions of opposite charge (unlike ions); the top curve represents the interaction of sodium and titanium ions, (like ions).

3.4.3 Total potential

The total potential energy between two ions is the total of force due to Lennard-Jones potential and Coulomb force [4],

$$V(r) = \frac{\lambda}{r^p} \pm \frac{e^2}{4\pi\epsilon_0 r} \quad 3.3$$

where p is about 10 and the values for λ are different for different ion-pairs, e is the electron charge and r is the distance between two ions. Value for λ will be different for different ion-pairs. This will be explained in the next section.

3.4.4 Method for determining the value for lambda

The values for lambda for each ion-pair have to be found for the calculations of the equations of force. The method used is shown below:

Data is available [5] for the parameters of a 6-exponential potential formula in the esu unit (electrostatic unit). This is plotted using the parameter values in the table 3.1.

$$V(r) = \frac{z_i z_j e^2}{r_{ij}} + f(b_i + b_j) \exp\left(\frac{a_i + a_j - r_{ij}}{b_i + b_j}\right) - \frac{c_i c_j}{r^6} \quad 3.4$$

Ion	z_i	a_i	b_i	c_i
Na	1	1.485	0.080	-
Ti	4	1.235	0.080	-
Cr	3	1.150	0.080	-
O	-2	1.629	0.085	20.0

Table 3.1: The constant used for the 6-exponential potential formula [5]. z , a_i , b_i , c_i are parameters corresponding to polarity of the charge, size, softness and polarizability of the ion respectively.

If the softness of the ion is low, the repulsion would be bigger when the two ions get closer to each other and the slope of the graph of potential versus distance will be steeper (in short distance) compared to the ion which has a higher softness. The formula we intend to use is a 6-p potential expression as shown in equation 3.3 because we think that it will describe the repulsions better at short distance. Lambda is chosen such that equation 3.3 is as close to equation 3.4 as possible. Particular care will be taken to match as closely as possible the regions of the potential where repulsions become important. This gives the value of lambda to be used. Graph of comparing 6-exponential potential and 6-p potential for $\text{Na}^+ - \text{Ti}^{4+}$ is shown in figure 3.5.

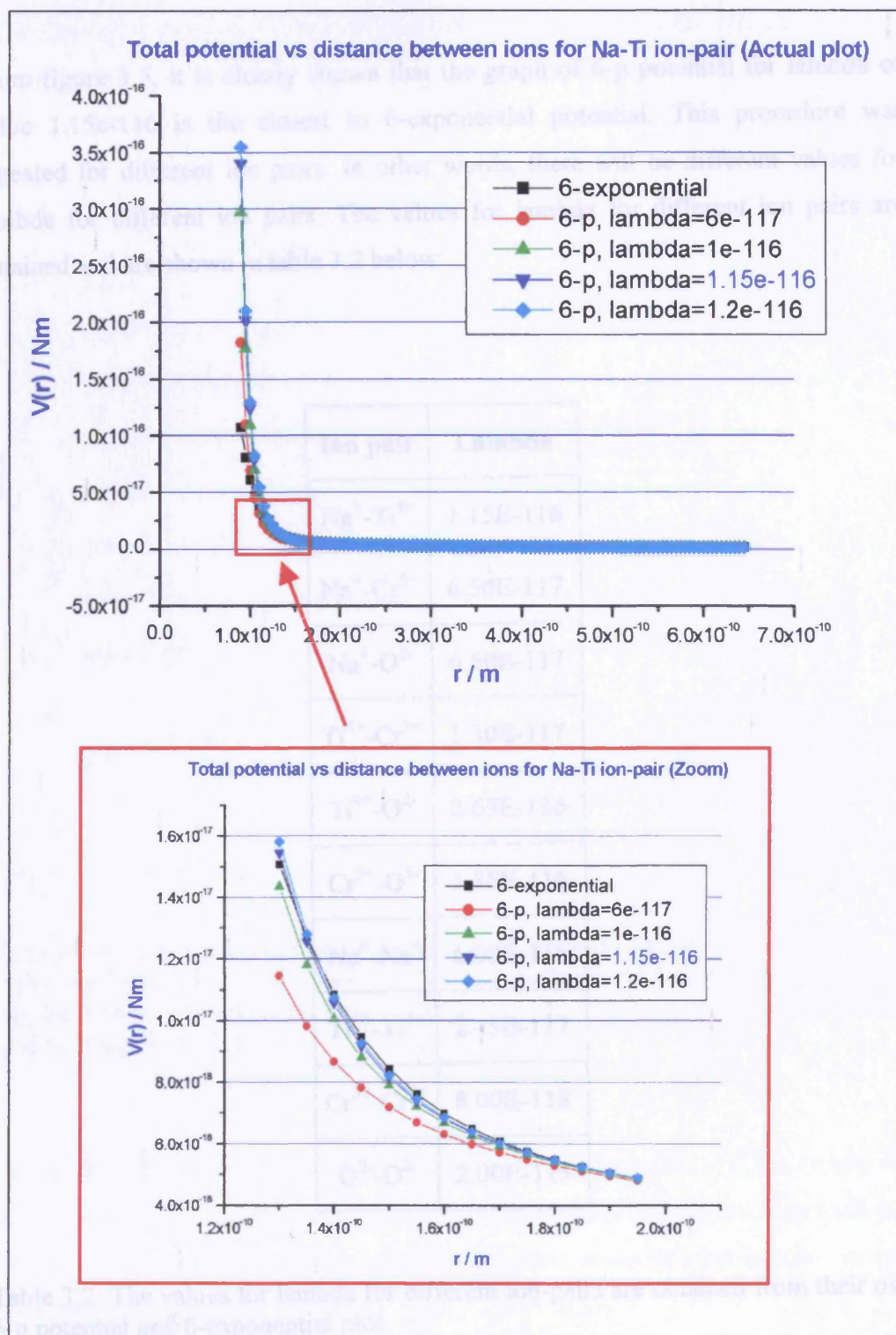


Figure 3.5: Graph of comparing 6-exponential potential & 6-p potential for $\text{Na}^+ - \text{Ti}^{4+}$.
(a) actual plot; (b) small red box shown by the arrow.

From figure 3.5, it is clearly shown that the graph of 6-p potential for lambda of value 1.15e-116 is the closest to 6-exponential potential. This procedure was repeated for different ion pairs. In other words, there will be different values for lambda for different ion pairs. The values for lambda for different ion pairs are obtained and are shown in table 3.2 below:

Ion pair	Lambda
$\text{Na}^+ - \text{Ti}^{4+}$	1.15E-116
$\text{Na}^+ - \text{Cr}^{3+}$	6.50E-117
$\text{Na}^+ - \text{O}^{2-}$	6.50E-117
$\text{Ti}^{4+} - \text{Cr}^{3+}$	1.30E-117
$\text{Ti}^{4+} - \text{O}^{2-}$	2.65E-116
$\text{Cr}^{3+} - \text{O}^{2-}$	1.55E-116
$\text{Na}^+ - \text{Na}^+$	6.00E-116
$\text{Ti}^{4+} - \text{Ti}^{4+}$	2.45E-117
$\text{Cr}^{3+} - \text{Cr}^{3+}$	8.00E-118
$\text{O}^{2-} - \text{O}^{2-}$	2.00E-115

Table 3.2: The values for lambda for different ion-pairs are obtained from their own 6-p potential and 6-exponential plot.

The figure 3.6 shows the graph of total potential energy between two ions based on the equation used. This will show the general graph between ions of the same polarity and of opposite polarity.

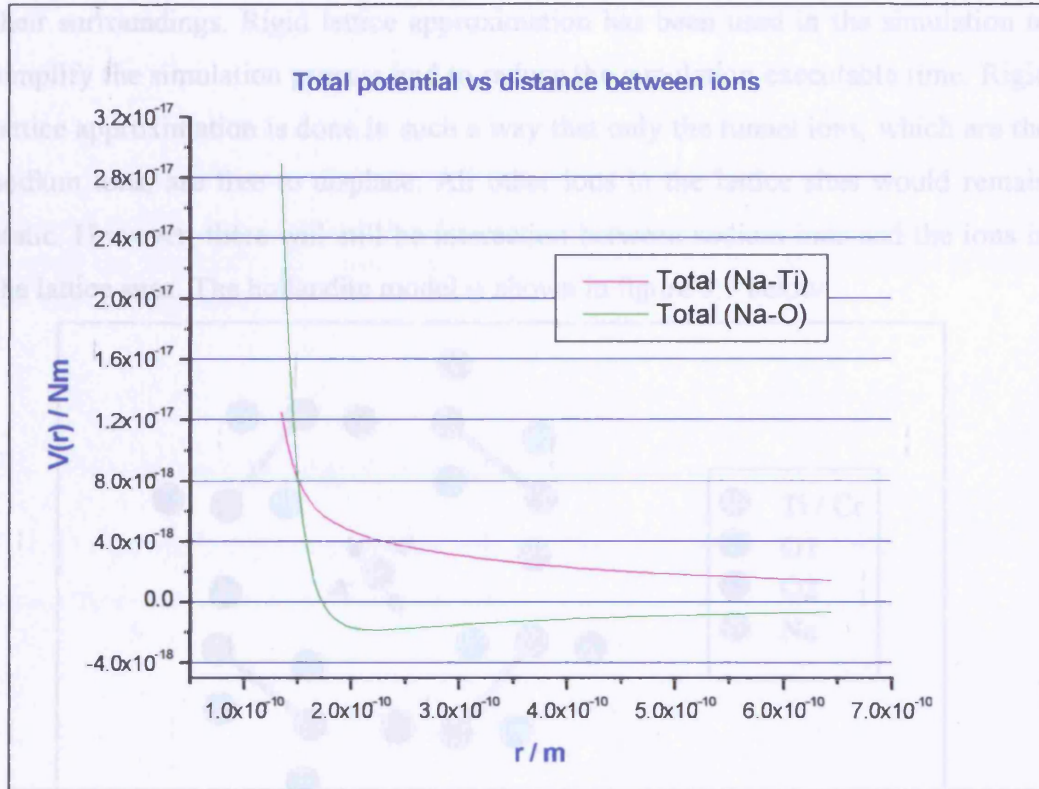


Figure 3.6: The total potential between two ions based on the equation used. The green curve represents the interaction between sodium and oxygen ions, two ions of opposite charge (unlike ions); the pink curve represents the interaction of sodium and titanium ions, (like ions).

It is clearly shown that the total potential for the like ions ($\text{Na}^+ - \text{Ti}^{4+}$) is repulsive at all distances. For the unlike ions ($\text{Na}^+ - \text{O}^{2-}$), the two ions tend to attract to each other at bigger distance; the two ions repulse each other at the smaller distance to avoid them to squash together.

3.5 Boundary conditions used

The relationship between the tunnel system and its surroundings is defined by using boundary conditions. These describe the interactions between the molecules with their surroundings. Rigid lattice approximation has been used in the simulation to simplify the simulation process and to reduce the simulation executable time. Rigid lattice approximation is done in such a way that only the tunnel ions, which are the sodium ions, are free to displace. All other ions in the lattice sites would remain static. However, there will still be interaction between sodium ions and the ions in the lattice sites. The hollandite model is shown in figure 3.7 below:

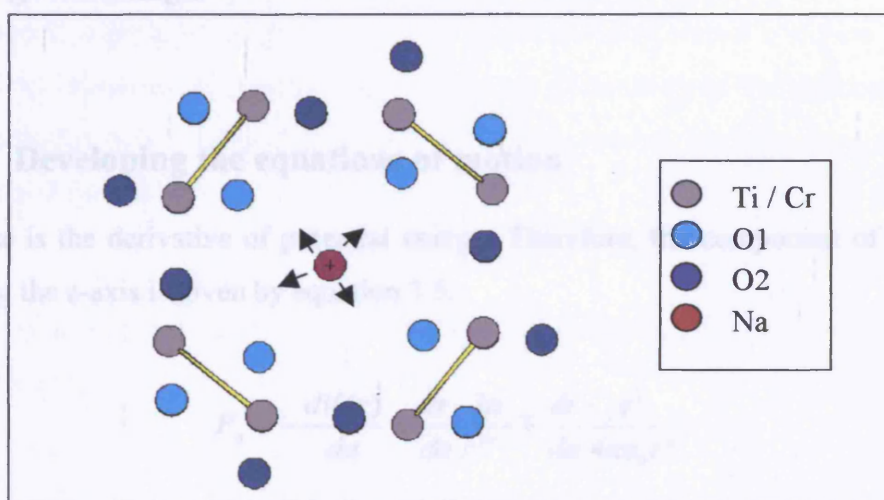


Figure 3.7: The hollandite model. Rigid lattice approximation is done in such a way that only the sodium ion is free to displace, the ions in the lattice site remain stationary.

3.5.1 Reflective boundary conditions

Reflective boundary conditions are used at the two ends of the tunnel. Rebound is a special type of collision involving a direction change; the result of the direction change is a large velocity change. Collisions in which particles rebound with the same speed are known as elastic collisions. Thus, the velocity of the ion that bounds back from the boundary should have the opposite sign and equal in magnitude with that velocity of ion which hits the boundary. The angle of the velocity hitting the boundary is the same as the angle leaving the boundary as shown in figure 3.8.

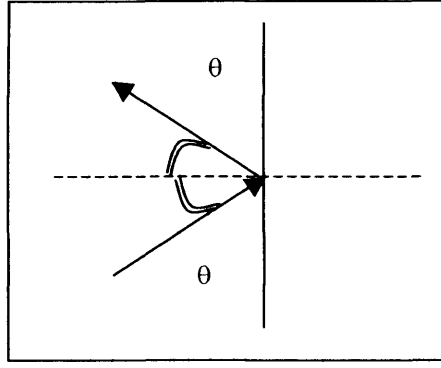


Figure 3.8: The angle of the velocity hitting the boundary is the same as the angle leaving the boundary. The magnitude of the velocity will remain the same whereas the sign will change.

3.6 Developing the equations of motion

Force is the derivative of potential energy. Therefore, the component of the force along the a-axis is given by equation 3.5.

$$F_a = -\frac{dV(r)}{da} = \frac{dr}{da} \frac{\lambda p}{r^{p+1}} \mp \frac{dr}{da} \frac{e^2}{4\pi\epsilon_0 r^2} \quad 3.5$$

and

$$r = \sqrt{(Aion1 - Aion2)^2 + (Bion1 - Bion2)^2 + (Cion1 - Cion2)^2} \quad 3.6$$

and

$$\frac{dr}{da} = \frac{|Aion1 - Aion2|}{r} \quad 3.7$$

where $|Aion1 - Aion2|$ is the absolute value of the displacement in a-axis for ion1 and ion2 and r is the distance between ion1 and ion2. The expressions for the component of forces in the b and c-axis are equivalent in form.

3.7 Molecular Dynamics (MD) simulation technique

In order to construct a MD simulation, it is necessary to visualize the structure of the hollandite in 3-dimensional form and to obtain the initial positions of the ions. It is difficult to get a clear picture from journal papers due to the 2-dimensional structure shown. Java program and Gretep [1] are used to generate the visual display of the hollandite model. In the visual display a hollandite structure of formula $\text{Ba}_x(\text{Ti}_{8-x}\text{Mg}_x)\text{O}_{16}$ [6] is used. All the hollandite structures of different formula will give a similar three-dimensional pattern.

Gretep is a program to generate visual display of any crystal structure by keying unit cell dimensions, space group, and atomic parameters of the structure [1]. The coordinates and the bonding between each ion needed for Java program can be obtained from it.

The parameters for the hollandite structure of formula $\text{Ba}_x(\text{Ti}_{8-x}\text{Mg}_x)\text{O}_{16}$ are given as follows [6]:

- Tetragonal ($a = b$, $\alpha = \beta = \gamma = 90^\circ$)
- Unit cell dimensions: $a = 10.11 \text{ \AA}$, $c = 2.986 \text{ \AA}$ (± 0.005)
- Space group: $I4/m$
- Atomic parameters are shown in table 3.3 below:

	x	y	z
Ba	0	0	0.5
(Ti, Mg)	0.167	0.348	0
O₁	0.208	0.152	0
O₂	0.152	0.542	0

Table 3.3: Atomic parameter for hollandite structure of formula $\text{Ba}_x(\text{Ti}_{8-x}\text{Mg}_x)\text{O}_{16}$.

In order to construct a hollandite model where the structure can be accessible anywhere, anytime, an html file has to be written. Some help has been given by Dr. Simon Gill on writing html code as he had created some movable structures on the University of Leicester Material's web page. The html file for the Java program created is then modified with permission by keying the coordinates of each ion, adding the bondings for each ion-pair manually and so on. Finally, the 3D movable hollandite model is developed and is placed on the University of Leicester Engineering's web page shown below:

(<http://www.le.ac.uk/engineering/research/groups/power/highvolt/hollandite/Hollandite.html>).

A copy of the hollandite model is shown in figure 3.9. The model can be rotated by using the mouse and it can be observed from the required directions.

You can play with the hollandite molecule below by dragging it with your mouse. The ions are represented as follows: Red = Barium, Green = Titanium, Blue = Oxygen

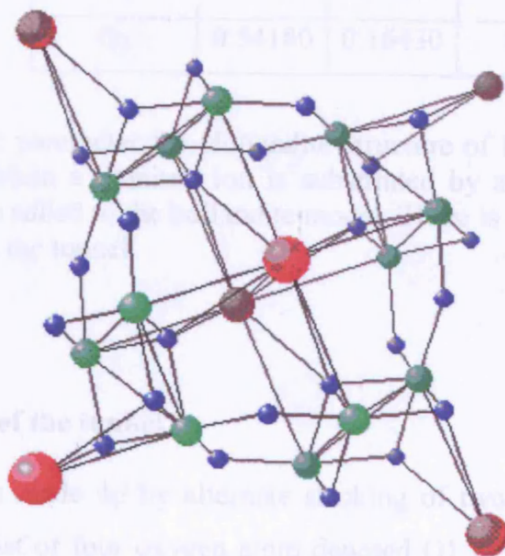


Figure 3.9: The hollandite structure of formula $\text{Ba}_x(\text{Ti}_{8-x}\text{Mg}_x)\text{O}_{16}$. This is a copy obtained from the web page shown above. The structure can be rotate by using the mouse.

In this work, the hollandite of formula $\text{Na}_x(\text{Ti}_{8-x}\text{Cr}_x)\text{O}_{16}$, ($x = 1.7$) [7,8] has been used instead because more information on the structure can be obtained and most importantly it is obtained from a more recently published paper. Gretep is again used to obtain the initial positions of all the lattice-ions. The parameters shown below are needed:

- Tetragonal ($a = b$, $\alpha = \beta = \gamma = 90^\circ$)
- Unit cell dimensions: $a = 10.0990 \text{ \AA}$, $c = 2.971 \text{ \AA}$
- Space group: $I4/m$
- Atomic parameters are shown in table 3.4 below:

	x	y	z
Na1	0.071	0.014	0.5
Na2	0	0	0.2
Na3	0	0	0
(Ti, Cr)	0.35112	0.16793	0
O₁	0.15440	0.20240	0
O₂	0.54180	0.16430	0

Table 3.4: Atomic parameter for Hollandite structure of formula $\text{Na}_x(\text{Ti}_{8-x}\text{Cr}_x)\text{O}_{16}$, ($x = 1.7$) [8,9]. When a titanium ion is substituted by a chromium ion only one sodium ion will be added to the hollandite model. There is a specific pattern to place the sodium ions in the tunnel.

3.7.1 Structure of the tunnel

The tunnel wall is made up by alternate stacking of two different oxygen-square layers which consist of four oxygen atom denoted O1 at $z = 0$ (square-plane) and four oxygen atom denoted O2 at $z = 0.5$ (cavity) [8]. These two layers are illustrated in figure 3.10 on the following page. It shows a bottleneck shape, where the cavity is bigger than the square-plane. The hollandite structure that is used here would not have the bottleneck effect in term of size (as the Na^+ ion is much smaller than the

bottleneck) but the smaller region will also generate a potential barrier for the transfer of a sodium ion along the tunnel.

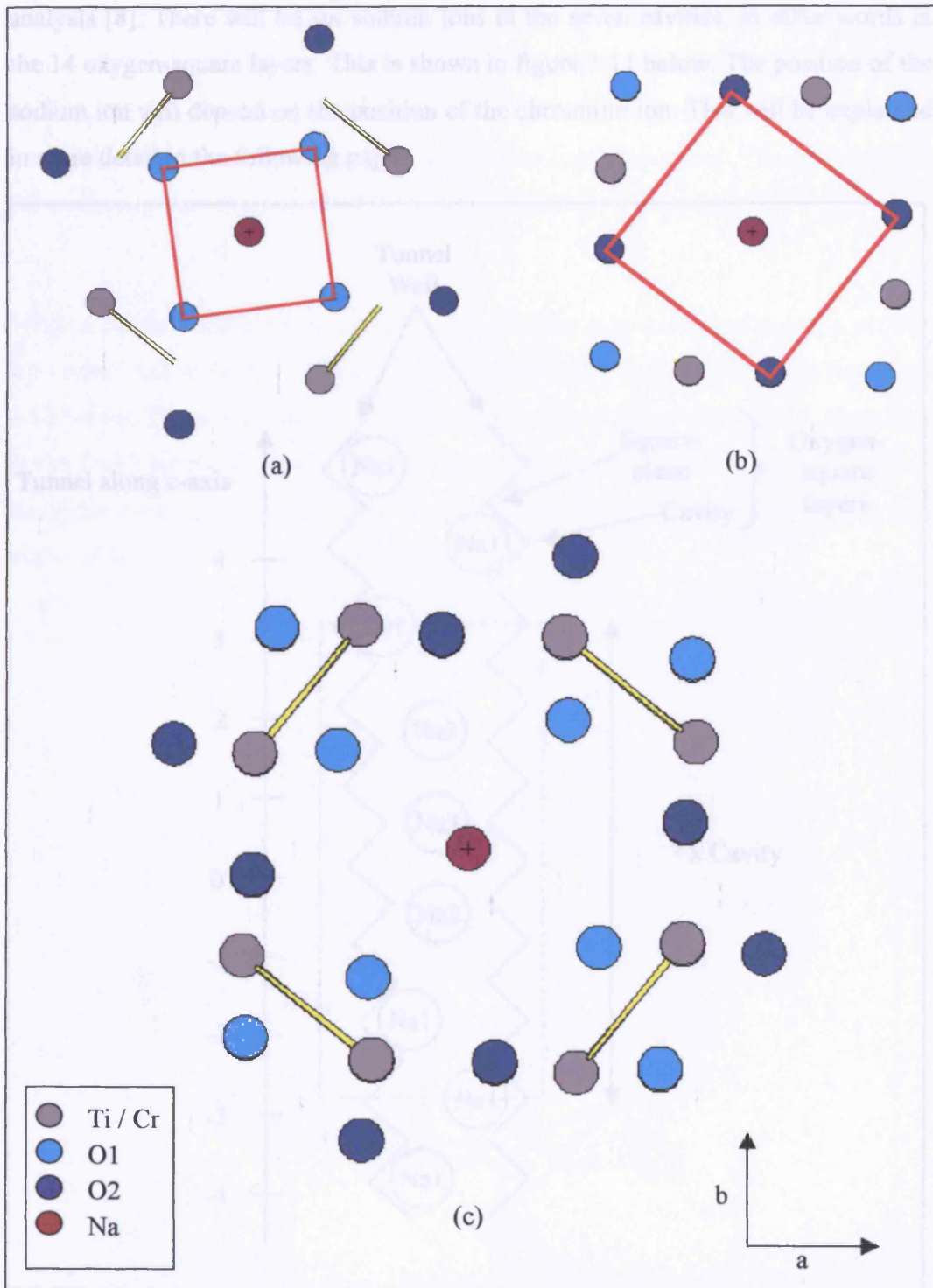


Figure 3.10: Hollandite model projected along the c-axis. The tunnel wall is made up by alternate stacking of two different oxygen-square layers (a) Square plane which consists of four O1 at $z = 0$, (b) Cavity that comprises four O2 at $z = 0.5$ (c) Overview of the tunnel wall when two oxygen-square layers are stacked together.

3.7.2 Number and position of the basic tunnel ions

The number and the positions of the basic tunnel ions are obtained from the x-ray analysis [8]. There will be six sodium ions in the seven cavities, in other words in the 14 oxygen-square layers. This is shown in figure 3.11 below. The position of the sodium ion will depend on the position of the chromium ion. This will be explained in more detail in the following pages.

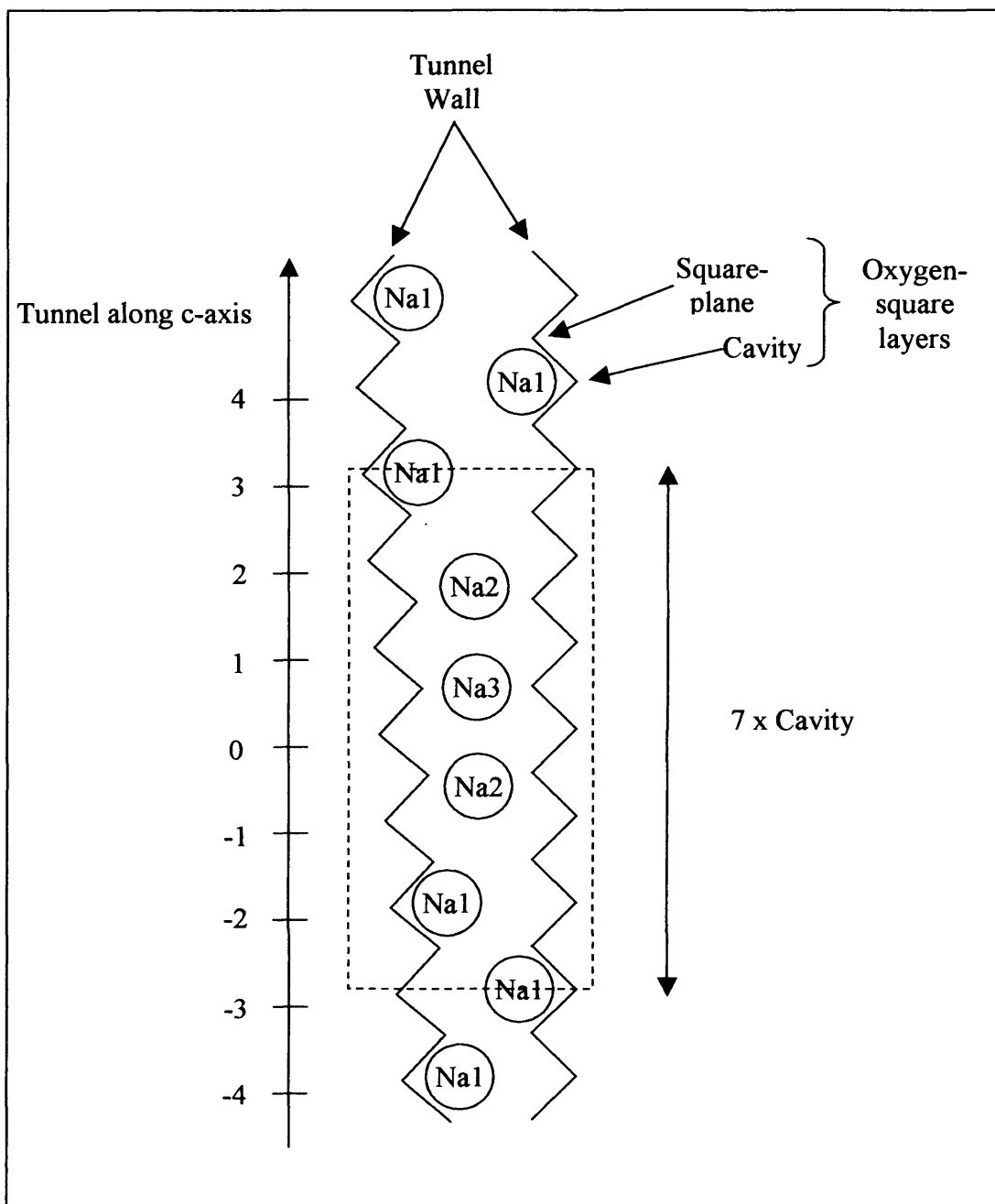


Figure 3.11: Schematic representation of a probable local arrangement for sodium ions in the tunnel of $\text{Na}_x\text{Cr}_x\text{Ti}_{8-x}\text{O}_{16}$. In the 7 x Cavity (indicated by the rectangular box), there are six sodium ions.

3.7.3 Method for positioning the tunnel ions along c-axis

From figure 3.11, it is clearly shown that there are three possible equilibrium positions for the sodium ions. The most likely structure in which the ions are located at each of these three positions Na1 (0.072,00014,0.5), Na2 (0,0,0.2) and Na3 (0,0,0) [8]. The three positions are very close to each other and therefore it is impossible for Na ions to occupy these positions simultaneously. The positions for the sodium ion are dependent on the position of the chromium ion.

When a titanium ion in the square-plane is substituted by a chromium ion, a sodium ion (either Na2 or Na3) will be placed in the hollandite model as shown in the figure 3.12 below. The site of the chromium ion is chosen randomly from the titanium ions in the four corners, A, B, C or D. The Na2 and Na3 differ slightly in their position along the c-axis. The atomic parameters for Na2 and Na3 in c-axis or z-axis shown in the table 3.4 are 0.2 and 0 respectively.

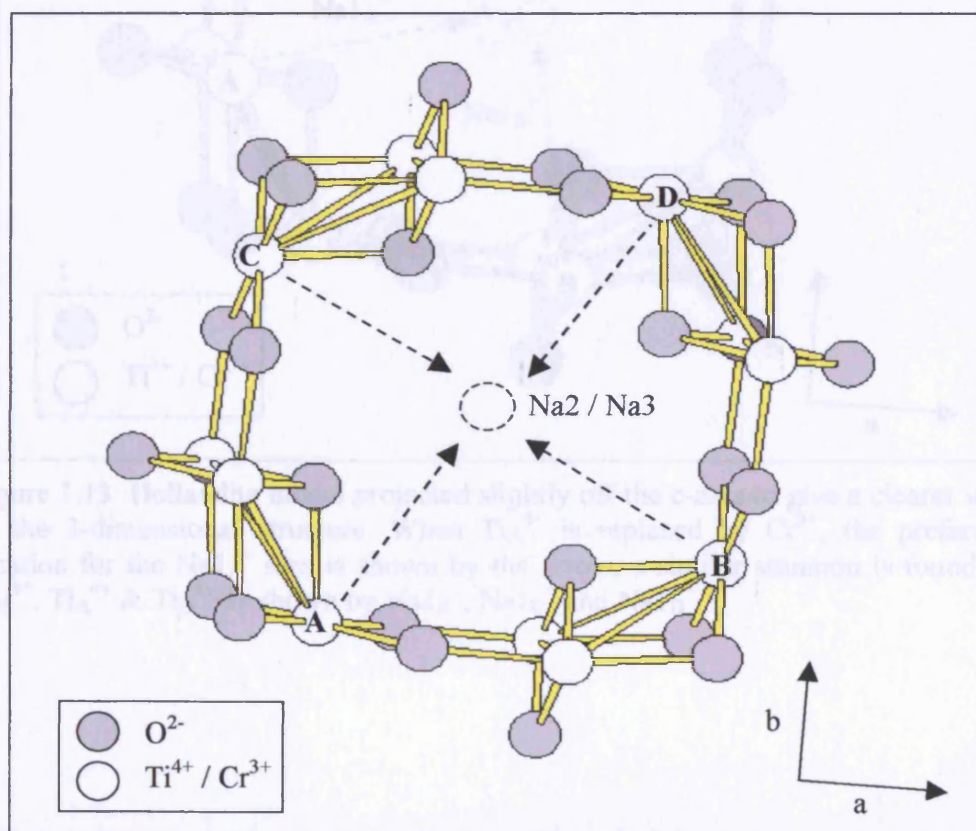


Figure 3.12: Hollandite model projected slightly off the c-axis to give a clearer view of the 3-dimensional structure.

When a titanium ion in the cavity is substituted by a chromium ion, there will be four possible positions for the sodium ion (Na1). The chromium ion is chosen randomly from the titanium ions in the four corners, A, B, C or D. The sodium ion preferably resides at an interstitial site within the same unit cell that contains a chromium ion [7] shown by the arrow in figure 3.13 below:

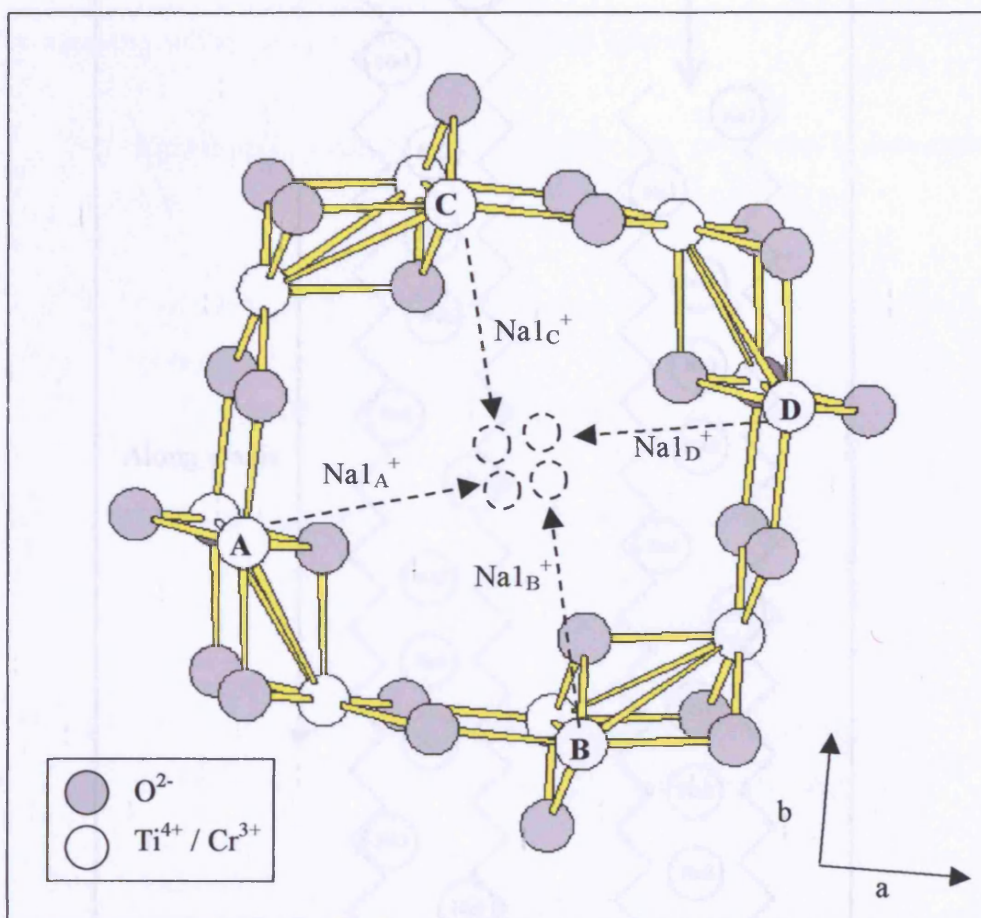


Figure 3.13: Hollandite model projected slightly off the c-axis to give a clearer view of the 3-dimensional structure. When Ti_A^{4+} is replaced by Cr^{3+} , the preferable location for the Na_A^{1+} ions is shown by the arrow, a similar situation is found for Ti_B^{4+} , Ti_C^{4+} & Ti_D^{4+} as shown by Na_B^{1+} , Na_C^{1+} and Na_D^{1+} .

Figure 3.14: The positions for the 24 sodium ions used in the hollandite model along the c-axis. It will be marked on top of 3 to show the whole tunnel

In this work, 24 sodium ions have been considered. Therefore, four sets of the six sodium ions shown in figure 3.11 are stacked up together to form a longer tunnel. This is illustrated below:

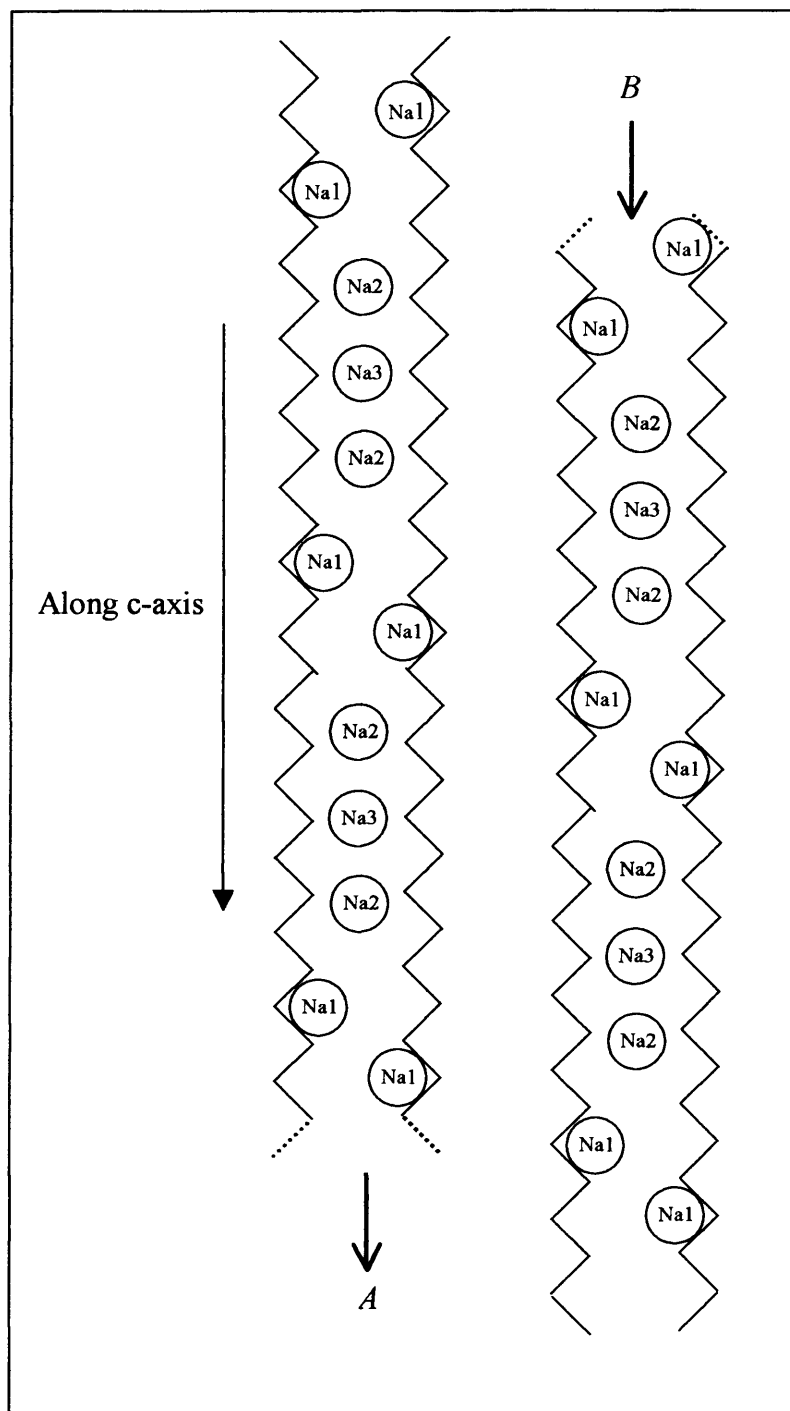


Figure 3.14: The positions for the 24 sodium ions used in the hollandite model along the c-axis. *A* will be stacked on top of *B* to show the whole tunnel.

3.8 Summary of the Iterative Procedure

The force is used to calculate the change in velocity; velocity is then used to calculate the change in position for the required number of intervals. This sequence is used to obtain a set of coordinates to show the trajectories of movement for each ion in the structure and further calculations are carried out with these results.

The summary of the iterative procedure is shown below:

1. First the positions and velocities of the ions are defined at time interval, $t=0$.
2. The initial positions and velocities are used to calculate the new position.
→ **New position = Old position + Old velocity x Time step**
3. The new positions are used to calculate the forces.
→ **New Force = (New Position)**
This is explained in more detail in the following chapter.
4. The new forces are then used to calculate the new velocities.
→ **New velocity = Old velocity + (Force/Mass) x Time step**
5. The cycle is repeated for next time interval.

4 SOFTWARE DESIGN AND DEVELOPMENT

4.1 General introduction

In order to design our software, we follow a series of steps referred as the ‘waterfall model’ implemented by Pont [1] for software engineers as follows:

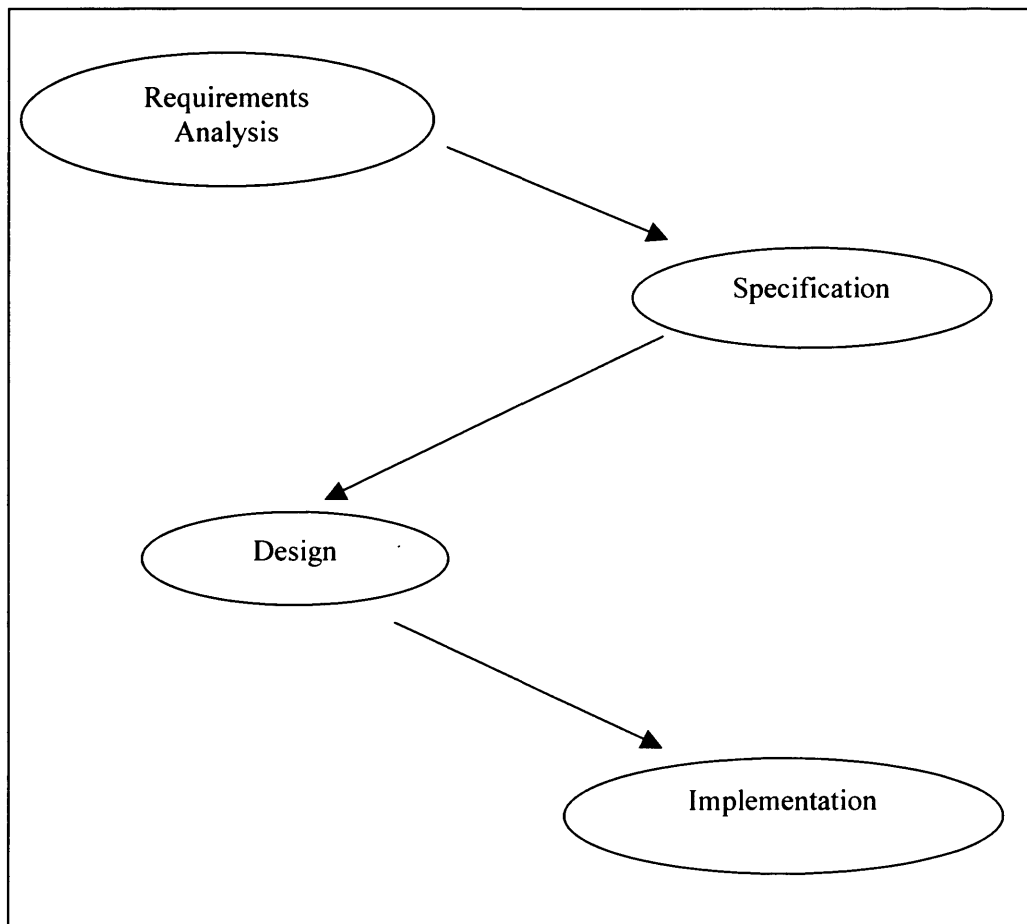


Figure 4.1: An overview of the software engineering process, referred as the ‘waterfall model’.

The process begins with the discussion of the requirement for the system. Next is to draw the specifications of the problem, such as what the proposed software must do, the agreed time scale and the budget details. Then, the design of the system is carried out based on the specifications given. Finally, the design has to be translated into a working product using commercial software packages. In my research, the

commercial software packages used are Microsoft Visual C++, Matlab and Origin. Microsoft Visual C++ is used to perform the complicated calculations and to carry out the molecular dynamics simulation; whereas Matlab and Origin are used to plot the graphs and to show the results required. Matlab is useful in showing the animation of the trajectories of movement, and Origin is good for plotting graphs with more than 100 000 points. In other words, it is excellent in reading large text files.

4.2 Commercial software package used

4.2.1 Microsoft Visual C++

Why is C++ chosen? First of all, this is the programming language supported throughout the university and moreover, it is a flexible language which is available for all major computer systems on the market. More importantly, C++ can be viewed as a modern, block-structure, high-level language, with excellent support for writing even the largest program. It can provide an efficient solution to virtually any programming task [1]. Microsoft Visual C++ is the software package available in the university, therefore it is preferred.

The program code is written in Microsoft Visual C++ using object-oriented Programming techniques, OOP. OOP is a popular, recent way of thinking about program organization. The difference between the object technique and the modules technique is: the emphasis of objects technique is on data whereas the emphasis of modules technique is on procedures. Modules are verbs followed by nouns: Push(S,x), while objects are nouns followed by verbs: S.Push(x) [2]. One of the advantages in using object-oriented technique is allows code to be reused through inheritance relationships, class libraries and templates. Furthermore the coding is more simplified.

4.2.2 Matlab

Matlab - Matrix Laboratory is a high-performance language for technical computing. Typical uses include mathematics and computational, modelling, simulation, data analysis, visualization and etc [3]. It works exceptionally well in displaying information graphically.

In this research, M-file has been written in order to read data from the text file generated from C++ to give a visual output in Matlab. Two forms of results can be obtained. One is to show the trajectories of movement, by using the command “plot3”. The other command used is “comet3”. Replacing this with the previous command will show you the animated version of the trajectories of movement. This is useful as the motion of the ions is shown and the starting and the ending points can be determined. This is very useful to understand the trajectories of movement in three-dimensions.

4.2.3 Origin

Origin is an all-in-one scientific graphing software and analysis software that is fast, flexible, user friendly and powerful [4]. It can also import data files and exports graphs as EPS, JPEG, TIFF, PDF and many more. Besides that it can also perform signal processing such as Fourier Transform, curve fitting and so on.

Origin is very powerful, it can plot graphs as easily as it can import a text file directly, which is fundamentally useful to this research as all the results are stored in text files. There is no problem in importing big text files as 100000 intervals have been used in the simulation. It has sufficient columns and rows to store the data, which Microsoft Excel does not have. Another advantage of this software is that no coding is needed. It is preferred in comparison to Matlab for performing Fourier Transforms, since writing a program code in Matlab is more time consuming.

4.3 Implementation

C++ is used as a tool to carry out the molecular dynamics simulation, to perform the complicated calculations and to store the required results in the specified text files. A total of five C++ programs has been written. A flow chart of the five programs used is shown in figure 4.2.

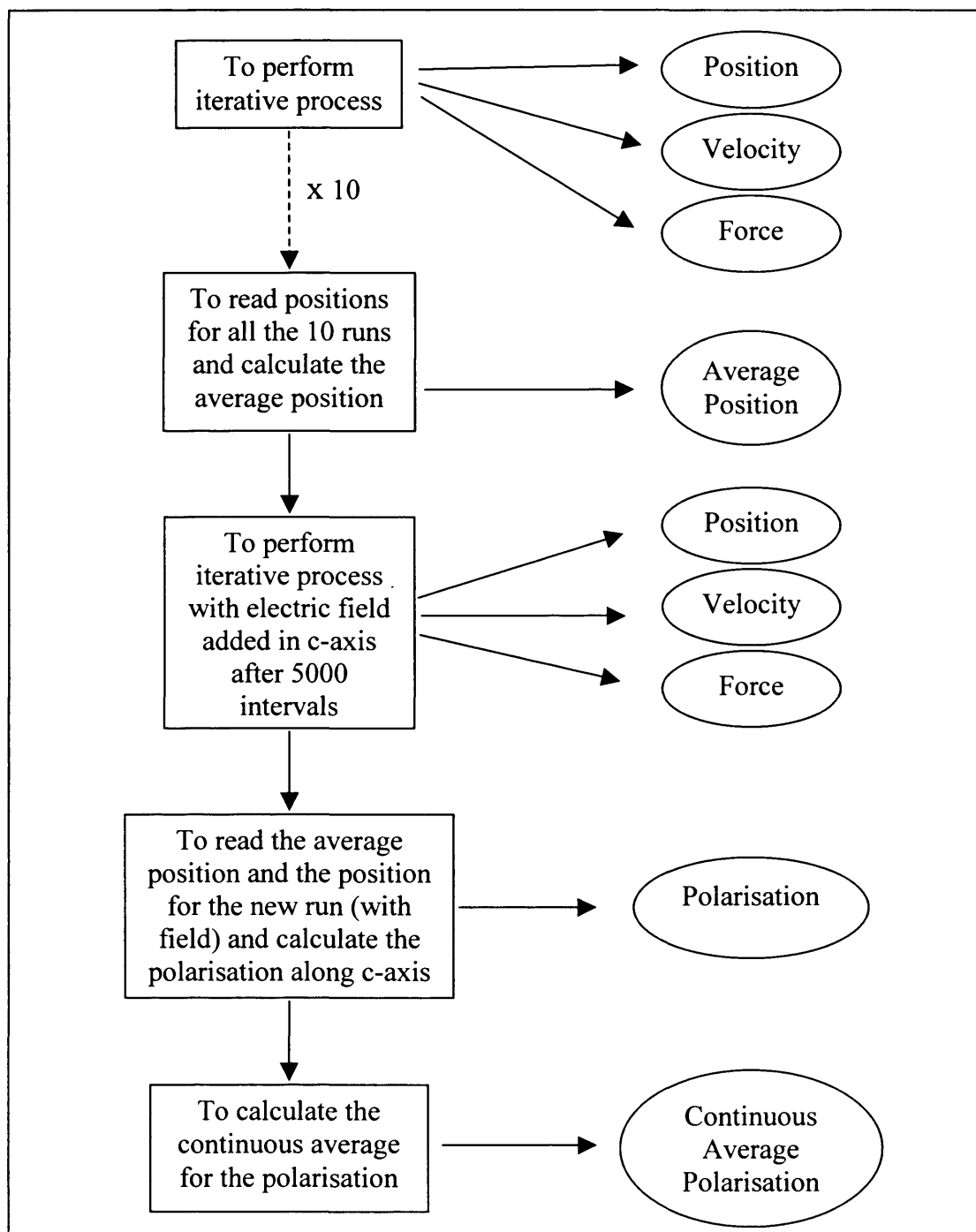


Figure 4.2: Flow chart showing the five program codes written to perform the MD simulation, to carry out the complicated calculations and to generate the data required in text files.

4.3.1 Program code to perform the MD simulation

The first program, which is also the main program, is to perform the iterative process and to generate the positions, forces and velocities of the sodium ions for each interval in three different text files. To start off, the initial conditions for the hollandite model are defined. The initial positions for each ion are given as the position in a, b and c-axis, the temperature is set as required

One tunnel consists of 60 layers with 24 sodium ions are being considered in the simulation. There are a total of 744 ions including the ions that form the lattice sites and the tunnel ions. The ion type for each ion has to be specified for the tunnel ions and the ions in the lattice sites. The time step used is $1\text{e-}15\text{s}$. The sequence of the program is shown in the figure 4.3.

The user has to key in the number of intervals required. 100000 intervals has been use in the simulation. The time scale used is 100ps. The program will go through the iterative process 100000 times. The iterative process includes three main functions, calculate new position, calculate new force, and calculate new velocity. There is an output text file for each function used. The flow chart of each function used is not shown due to the complexity of the program code. However, the calculations performed by each function will be explained.

This procedure is repeated for ten times by varying the direction and magnitude of the velocity for each sodium ion. This is done because there are numerous possibilities for the initial velocity given to each sodium ion. After the results of the ten runs have been collected, the second program has been carried out. This is explained in the next section.

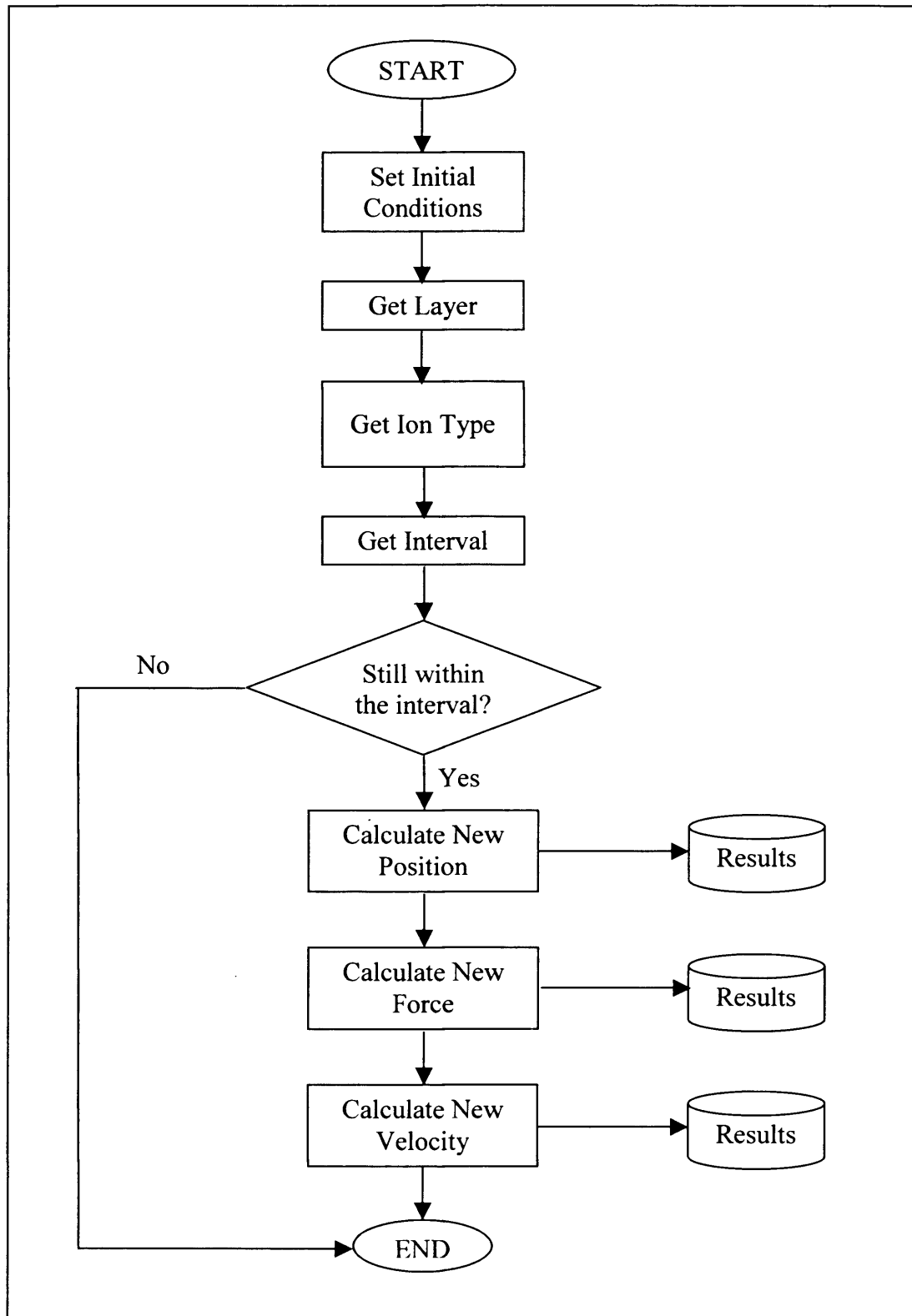


Figure 4.3: Flow chart for the program code to perform the MD simulation. Results in .txt format are generated in each function. The iterative process will be repeated Nth intervals required. In the simulation, 100000 intervals have been set.

In the function <Set Initial Conditions> which has a different filename called CIon.h, the initial positions, velocities, temperature, time step and all the constants used in the calculations will be defined. The velocities, positions and forces are initialised to Zero. This is done to avoid an unnecessary calculation error occurring at a later stage.

For the function <Get Layer>, the number of layers is input to the simulation. In this work, it is preset to 60 layers. This has been altered to perform some check on the calculations whenever it is required. In the function <Get Ion Type>, the ion type is specified. The exact positions of any specific ions can be obtained by looking at the outputs from this function. Ion type defined here is also the polarity of the ions, sodium ion is +1, chromium ion is +3, titanium ion is +4 and oxygen ions is -2. This ion type has been used in the function <Calculate New Force> to calculate the interaction forces.

In the function <Get Interval>, the user will be prompted: "Please key in the number of intervals required?". 100 000 intervals have been used throughout the calculations, whereas a smaller number of intervals is used either when errors have been detected in the program or to perform a check on the flow of the program. The next three functions are performed if it is still within the required number of intervals, else the program will be terminated.

<Calculate New Position>, <Calculate New Force> and <Calculate New Velocity> are the three main functions used to perform the iterative process. In the <Calculate New Position>, the new position is given by the summation of the old position and the change in position. The Old position and the Old velocity which are also the initial position and velocity defined in the function <Set Initial Conditions> are used to calculate the New position. The calculation for the new position in a-axis is shown as follows:

$$\text{New position}_a = \text{Old position}_a + \text{Old velocity}_a \times \text{Time step}$$

The calculations of the new position in b and c-axis is similar. These positions in a, b and c-axis for each intervals are stored in a text file. These new calculated positions are then used in function <Calculate New Force> for calculating the force. The constants used for calculation and the value for lambda for different ion pairs are defined before these calculations have been carried out. The method of determining the values for lambda has been explained in section 3.4.4. Force acting on each sodium ion by other ions consists of the force due to Lennard-Jone potential and Coulomb force.

$$\text{Force}_a = \text{Force (Lennard-Jones)}_a + \text{Force (Coulomb)}_a$$

The force acting in b and c-axis is calculated similarly. The total force acting on an ion along the a-axis is the summation of all the forces acting on that ion by other ions in the same axis. In the research, there are 720 ions in the hollandite model. It would be easier to explain with just ten ions, 1st to 10th ion. Total force acting on the 1st ion will be as shown below:

$$\begin{aligned} &\text{Total force}_a \text{ (acting on 1}^{\text{st}} \text{ ion)} \\ &= \text{Force}_a \text{ (acting on 1}^{\text{st}} \text{ ion by 2}^{\text{nd}} \text{ ion)} \\ &+ \text{Force}_a \text{ (acting on 1}^{\text{st}} \text{ ion by 3}^{\text{rd}} \text{ ion)} \\ &+ \text{Force}_a \text{ (acting on 1}^{\text{st}} \text{ ion by 4}^{\text{th}} \text{ ion)} \\ &+ \dots \\ &+ \text{Force}_a \text{ (acting on 1}^{\text{st}} \text{ ion by 10}^{\text{th}} \text{ ion)} \end{aligned}$$

Hence total force acting on the 2nd ion will be the summation of the force acting on 2nd ion by 1st ion, by 3rd ion and so on. It would not consist of only the force acting by the same ion (which is the 2nd ion) as an ion can not exert a force on itself. There is a check in the program code that prevents this from happening. The calculations for the total force in b and c-axis are similar.

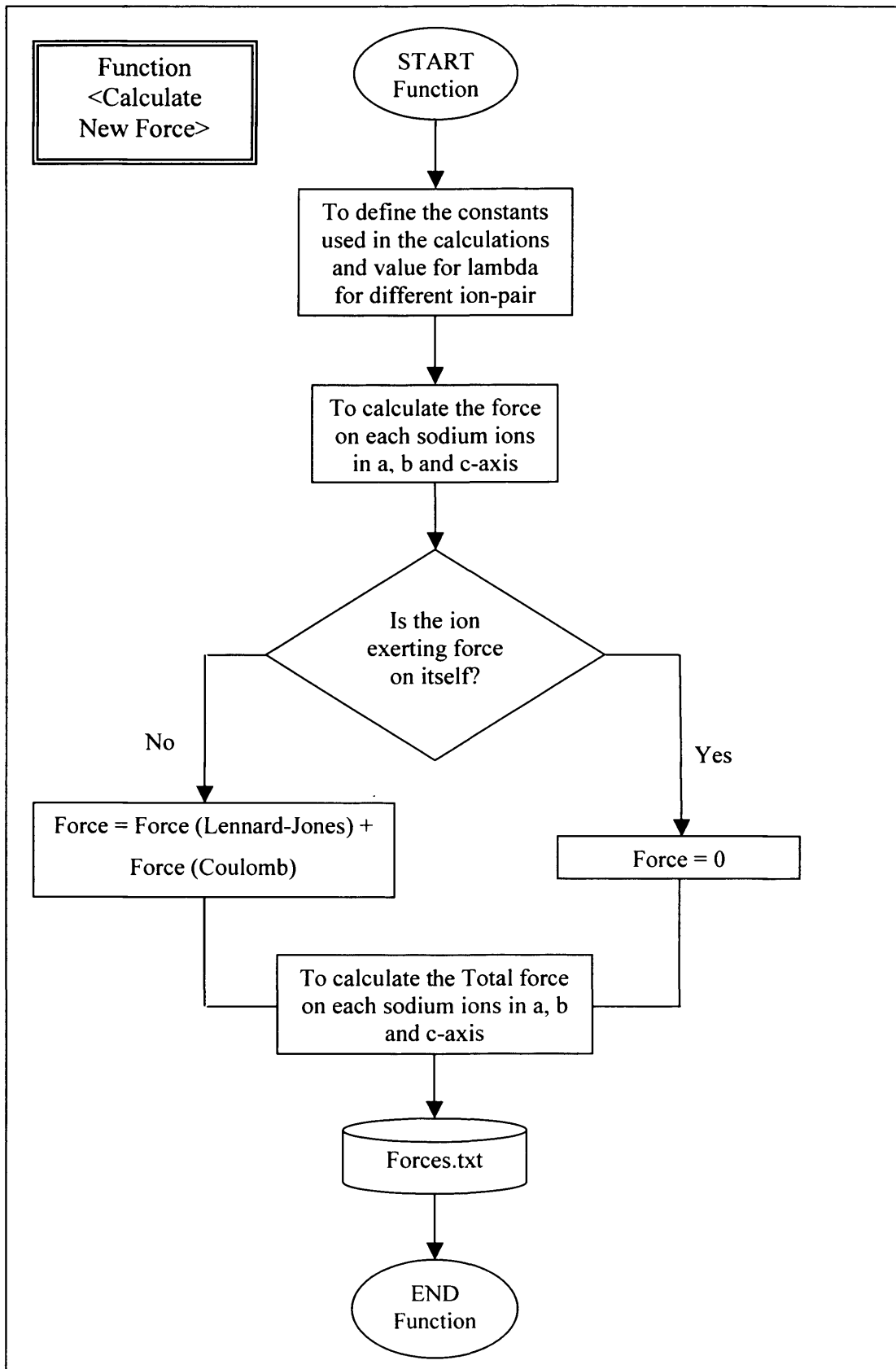


Figure 4.4: The flow chart showing the program code in function `<Calculate New Force>`.

These forces in a, b and c-axis for each intervals are stored in a text file. These new calculated forces are then used in function <Calculate New Velocity> for calculating the velocities for each sodium ions. The mass of the sodium ion and the boundary conditions at the two ends of the tunnels are defined. The calculations for the new velocity in a-axis is shown as follows:

$$\text{New velocity}_a = \text{Old velocity}_a + (\text{Force}_a / \text{Mass}_{\text{Na}}) \times \text{Time step}$$

The calculations for the new velocity in b and c-axis is similar. The reflective boundary conditions are taken into account at the two ends of the c-axis, one end being BoundCStart and the other end is BoundCEnd. A check is performed to make sure that the sodium ions would stay within the tunnel. A reflective boundary condition has been used as described in section 3.5.1. If the position of the sodium ion in c-axis is greater than BoundCEnd or smaller than BoundCStart the new calculated velocity would be acting in the opposite direction. This is clearly shown in figure 4.5:

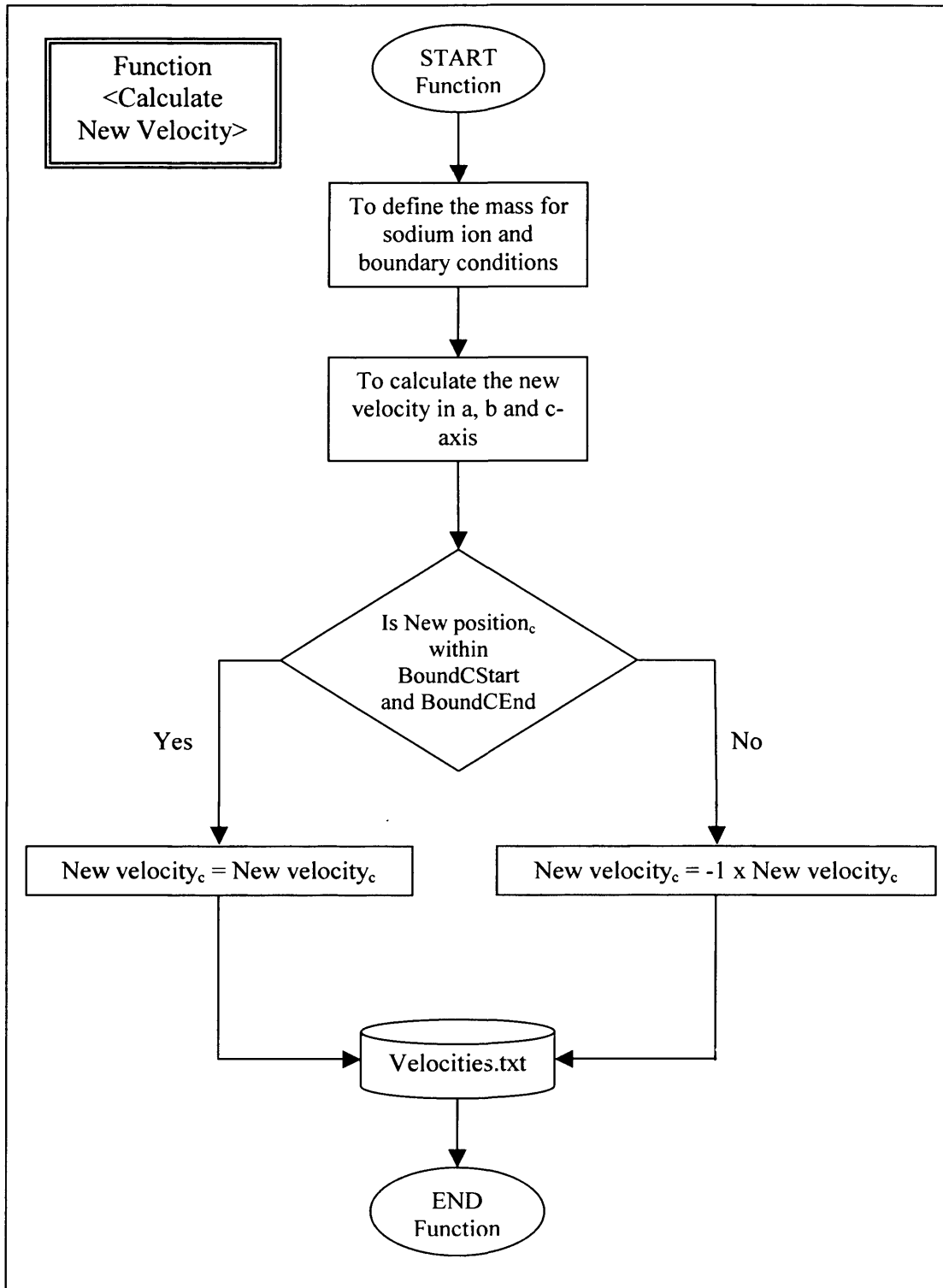


Figure 4.5: The flow chart showing the program code in function <Calculate New Velocity>.

4.3.2 Program code to calculate the average position of the sodium ions

In the second program, the ten text files for the positions generated by the first program with different initial conditions are read and input into the program. Each file comprises the positions of all the 24 tunnel ions in a, b & c-axis over 100000 intervals. The average positions in c-axis for each tunnel ion are then calculated. The flow chart for the program code is shown in figure 4.6.

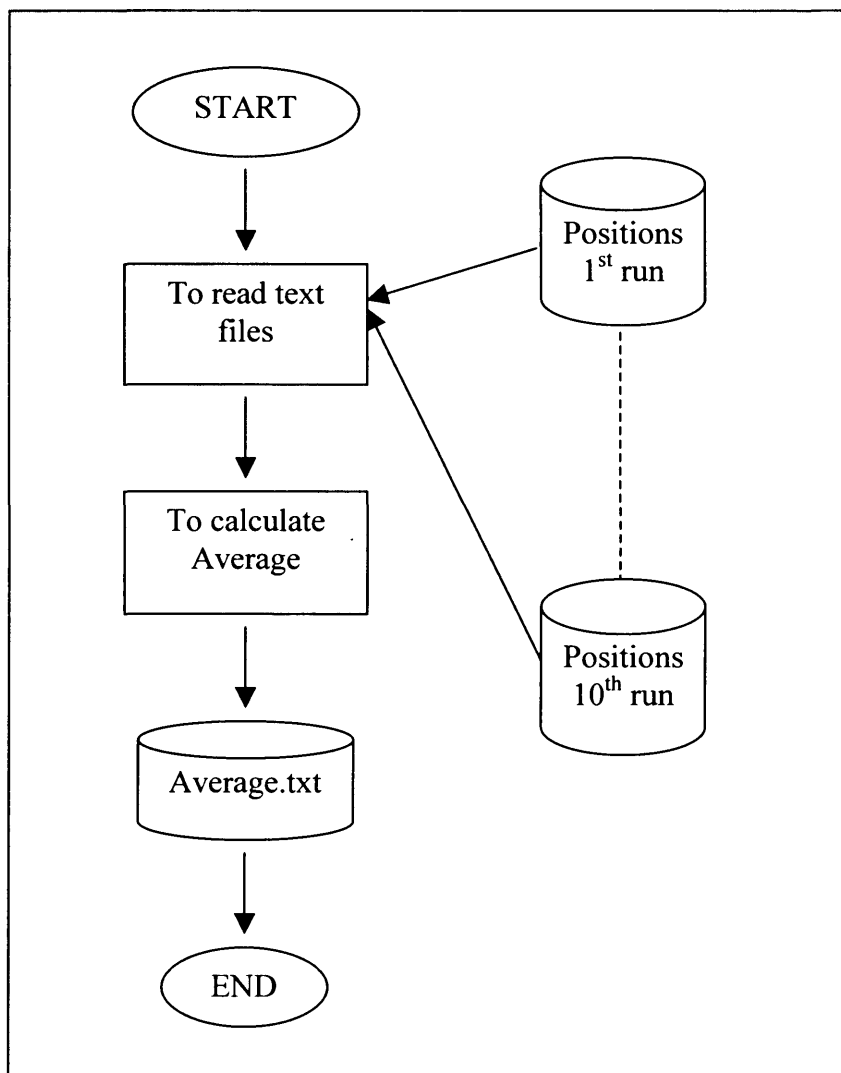


Figure 4.6: Flow chart for the program code to calculate the average positions of the sodium ions. All the ten sets of positions for the sodium ions generated by the previous program are being input to this program and the average positions of each sodium ion are being stored in a new text file.

The average positions in c-axis for each tunnel ion are stored in a new text file name Average.txt. Only the average position in c-axis has been calculated here because the motion along c-axis is the main interest.

4.3.3 Program code to perform the MD simulation when a dc electric field is added

The third program, figure 4.7 is very similar to the first program as shown in figure 4.4. The electric field is given by adding an additional force in c-axis at the 5001th intervals. (The initial 5000 intervals are to allow the sodium ions to reach their equilibrium positions.) This program also performs the iterative process and to generate the positions, forces and velocities of the sodium ions. The only difference between this program and the first program is the difference in <Calculate New Force>. For the first 5000 intervals the calculations for the total force is the same as described in section 4.3.1. Starting from the 5001th interval the total force acting on each sodium ion in a and b-axis is remain the same. In c-axis, the force due to the dc-field is added to the total force acting on the sodium ion

For example, there are only ten ions in the hollandite model, 1st to 10th ion. Total force acting on the 1st ion will be as shown below:

$$\begin{aligned} &\text{Total force}_c \text{ (acting on 1}^{\text{st}} \text{ ion)} \\ &= \text{Force}_c \text{ (acting on 1}^{\text{st}} \text{ ion by 2}^{\text{nd}} \text{ ion)} \\ &+ \text{Force}_c \text{ (acting on 1}^{\text{st}} \text{ ion by 3}^{\text{rd}} \text{ ion)} \\ &+ \text{Force}_c \text{ (acting on 1}^{\text{st}} \text{ ion by 4}^{\text{th}} \text{ ion)} \\ &+ \dots \\ &+ \text{Force}_c \text{ (acting on 1}^{\text{st}} \text{ ion by 10}^{\text{th}} \text{ ion)} \\ &+ \text{Force}_c \text{ (dc-field)} \end{aligned}$$

Hence total force acting on the 2nd ion will be the summation of the force acting on 2nd ion by 1st ion, by 3rd ion until the 10th ion and the force due to dc-field. It would not consist of the force acting by the same ion (which is the 2nd ion) as an ion cannot exert a force on itself. There is a check in the program code that prevents this from happening.

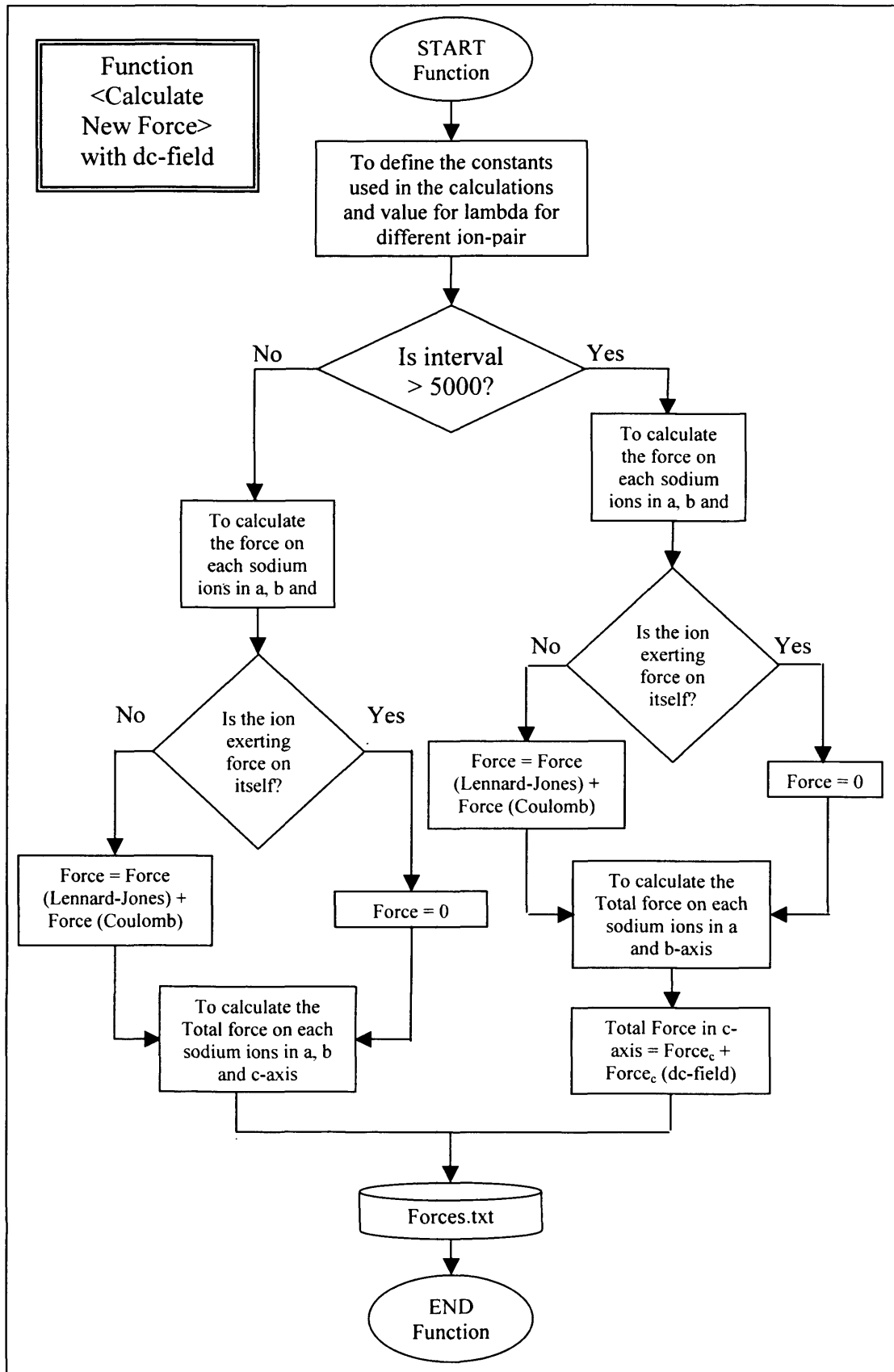


Figure 4.7: The flow chart showing the program code in function <Calculate New Force> with dc electric field added to the force at 5001th interval.

4.3.4 Program code to calculate the polarisation

This program is to calculate the polarisation for the sodium ions in the c-axis by reading the average positions (section 4.3.2, when no field is applied) and the new positions generated by the program in section 4.3.3. The value for volume and the constants used in the calculations are defined. The polarisation is the dipole moment per unit volume. In this simulation, there are a total of 24 sodium ions. The dipole moment is:

Dipole moment

$$\begin{aligned} &= (+1)e \times [\text{Position}_c \text{ (for 1}^{\text{st}} \text{ ion)} - \text{Average position}_c \text{ (for 1}^{\text{st}} \text{ ion)} \\ &\quad + \text{Position}_c \text{ (for 2}^{\text{nd}} \text{ ion)} - \text{Average position}_c \text{ (for 2}^{\text{nd}} \text{ ion)} \\ &\quad + \text{Position}_c \text{ (for 3}^{\text{rd}} \text{ ion)} - \text{Average position}_c \text{ (for 3}^{\text{rd}} \text{ ion)} \\ &\quad + \dots \\ &\quad + \text{Position}_c \text{ (for 24}^{\text{th}} \text{ ion)} - \text{Average position}_c \text{ (for 24}^{\text{th}} \text{ ion)}] \end{aligned}$$

e is the electron charge and +1 is the polarity of sodium ion.

$$\text{Polarisation} = \text{Dipole moment} / \text{Volume}$$

A flow chart of this program code is shown in the figure 4.8.

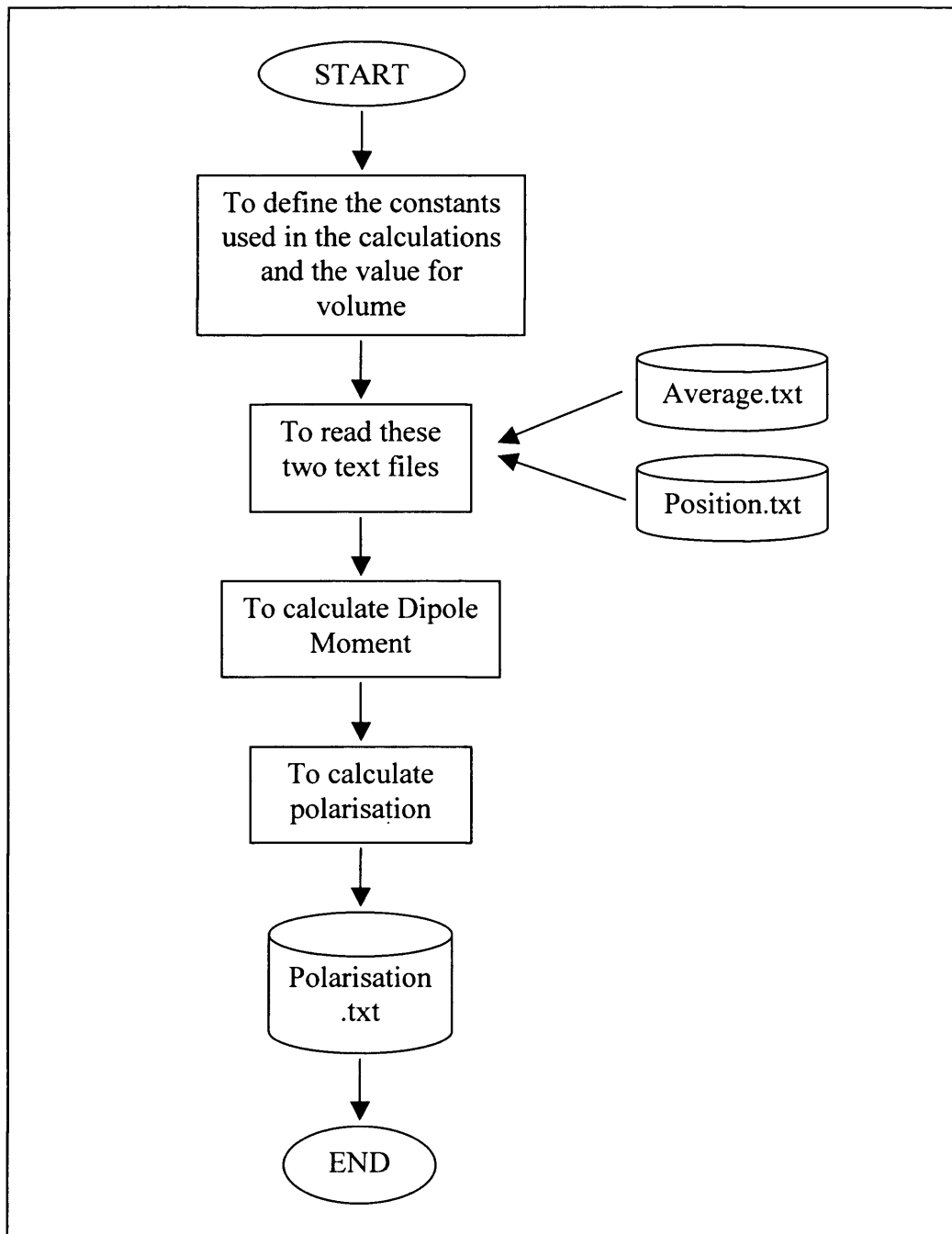
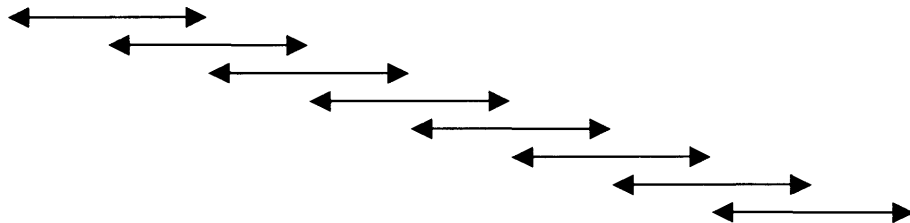


Figure 4.8: The flow chart for the program code to calculate the polarisation. Two text files are input to the program; calculation for the polarisation is carried out and stored in polarisation.txt file.

4.3.5 Program code to calculate the continuous average for the polarisation

This program is to calculate the continuous average for the polarisation. In this work the polarisations of every 100 intervals are averaged in the 100000 intervals. In order to show how does this continuous average work, an example of a total of 10 intervals with continuous averaging of three intervals is explained here. The value for each intervals are shown below:

Intervals:	1 st	2 nd	3 rd	4 th	5 th	6 th	7 th	8 th	9 th	10 th
Polarisation:	10	11	15	20	14	13	21	8	16	20



Polarisation of every 3 intervals is averaged and saved. Only eight data will be saved for this example against the middle of the three intervals that is taken into account. The data saved for this example will be shown below:

Intervals:	2 nd	3 rd	4 th	5 th	6 th	7 th	8 th	9 th
Polarisation:	12	15.333	16.333	15.667	16	14	15	14.667

The results obtained are stored in a text file. The program code is shown in the flow chart figure 4.9:

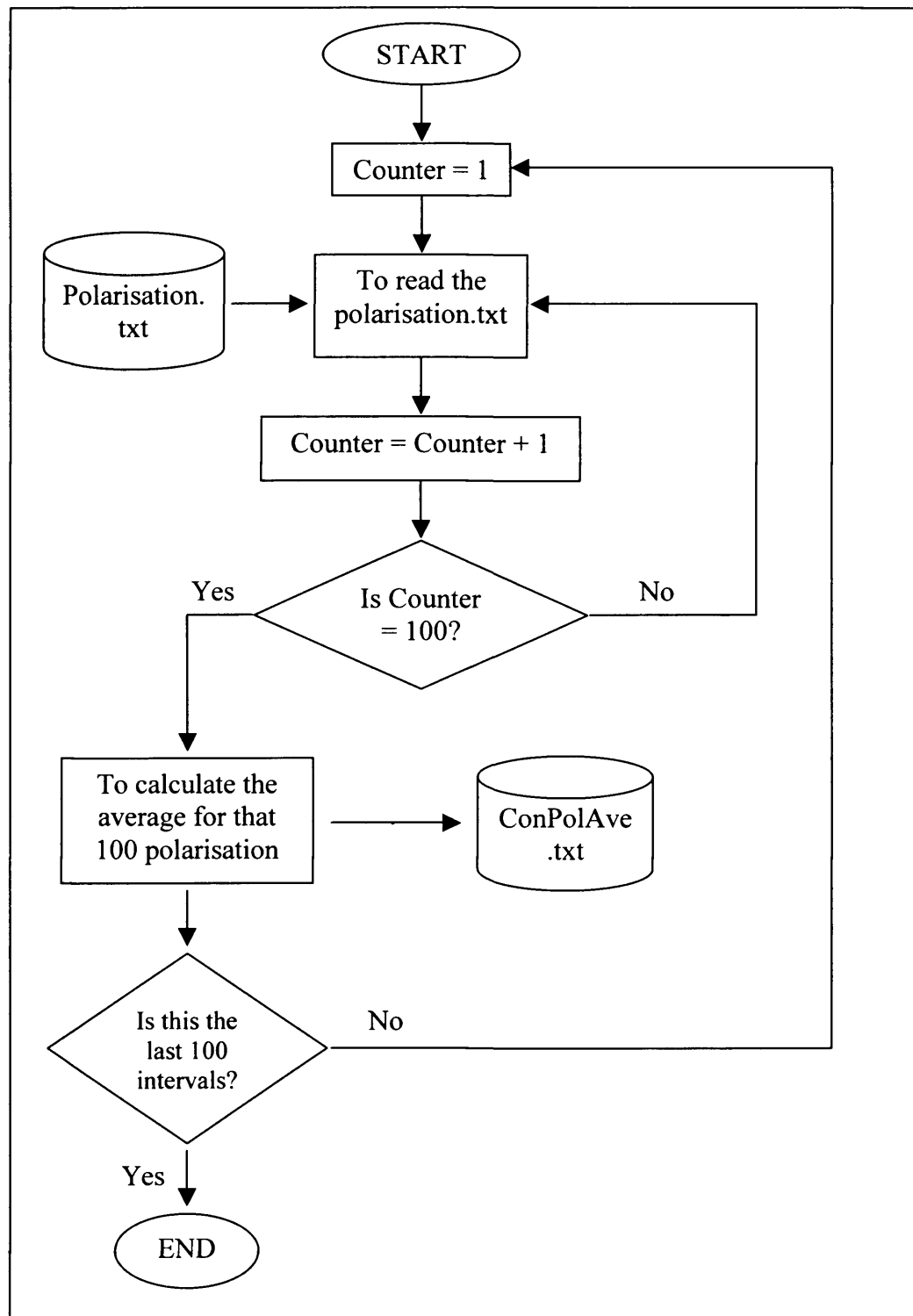


Figure 4.9: The flow chart for the program code to calculate the continuous average for the polarisation. Polarisations for the 100 intervals are read and the average is obtained and stored in ConPolAve.txt. The polarisations for the continuous 100 intervals are read and averaged. This procedure is repeated until the last 100 intervals.

4.4 Testing

As much testing as possible is carried out during the construction of the model. This is to minimise the round-off error, as this error will affect the entire set of calculations. Another phase is the testing of individual functions as they are coded. This is necessary as the model is complicated, the possible errors that would be difficult to locate at a later stage could be identified. The more difficult aspect to test is the introduction of new features when the main structure of the model is completed.

There are two ways to display the test results. First is to print out the results to screen, not much program codes have to be added for this. There is a disadvantage in this as the results cannot be stored for future reference. Second is to store the results in data files (in text files); the results can be retrieved and compared later.

4.4.1 Testing to minimise round-off error

Round-off error is affected by the number of significant figures kept at each stage of the calculation, by the order in which the calculations are actually performed, and by any approximations used in evaluating square roots, exponentials and so on. Round-off error will affect the overall calculations as this error is incurred during each interval and it is then accumulated over the entire calculation. In order to overcome this error, a program code with high precision arithmetic has to be used: double precision rather than single [5].

In this work, long double has been used for most of the parameters. Long double has precision digits of 15 and a maximum exponent of 308 [6]. This would reduce the round-off error to the minimum.

4.4.2 Testing during coding

There are two fundamental approaches to testing throughout the programming phase known as White Box and Black Box testing [1]. Each of these tests is carried out as the program code is written.

In White Box testing, the program code is read line-by-line to detect potential errors. The various possible logical paths in the program code have to be considered. The advantage of this thorough testing is to check whether the approach and implementation is appropriate and efficient.

In Black Box testing, a set of test data is used to determine whether the program or function satisfies the design criteria. In other words, each function is tested separately, providing a range of inputs and checking that the outputs are correct. Both these testing have been carried out to ensure the reliability of the program code and this is very important prior to the checking of the errors generated by the complicated calculations. Modifications are made as required.

4.4.3 Testing for each mathematical formula used

There are two ways to check the accuracy of the calculations generated by the mathematical formula. The first test is by using dummy vectors, to check whether the results obtained are as expected. This test is often used to check whether the mathematical formulas used are correctly performed in the program code. Brackets are always misplaced in the program code, and it will make a very big difference to the results obtained and this is not easily observed with White Box testing.

The other test is to perform the calculations on one or two other software and to compare the results obtained. The number of other software used depends on the complexity of the functions. Matlab and Microsoft Excel have been used. This test is usually used for calculations that involve iteration of more than one formula. The two tests are both useful to make sure that the mathematical formula used is working properly.

4.4.4 Testing for the overall sequence

The best way to perform the test in this phase is going through the Microsoft Visual C++ debugger. It will perform a thorough line-by-line check following the sequence of the program code being implemented. In other word, it will go through every possible logical path. The values of the specific parameters interested can be display and checked in the debugger window. During the debugger session, there is an option of going into each function written or just go through the main program. The debugger can be stopped at any desired moment.

The other way to do this is to draw a flow chart for the program code written including every possible logical path (if-else statement, while loop and etc.) in the program code. The flow of the program will be easily seen. If there is a broken flow in the program code, it will be easily spotted and corrected. However, this is more suitable for checking the flow of the individual functions rather than the whole program code, as it will cause confusion for the whole program code.

5 RIGID LATTICE APPROXIMATION

5.1 General introduction

The rigid lattice approximation has been used in this research for the ions that form the crystal lattice environment of the tunnel, figure 3.7, chapter 3. Only the sodium ions in the tunnel are free to move, all other ions remain fixed in their crystal lattice positions. There will still be interaction between sodium ions and the ions in the lattice sites. The reasons for using this approximation are firstly to simplify the computer simulation process so as to reduce the complexity of the program code for the boundary conditions used and secondly to reduce the executable time. This hollandite model consists of one tunnel extended along the c-axis and 720 ions at the lattice sites, where 480 ions are oxygen ions, 216 ions are titanium ions and 24 ions are chromium ions. The tunnel contains 24 sodium ions.

There are a total of six basic experimental procedures in this research.

1. The initial conditions of all the ions have to be specified.
2. The temperature is set by giving some kinetic energy of k_bT to the sodium ions, where k_b is the boltzmann's constant and T is the temperature in Kelvin.
3. A total of ten runs are carried out. The amount of kinetic energy given to individual sodium ions vary depending on which run is being performed.
4. The kinetic energy of each individual sodium ion in a real crystal will be distributed as well as the direction of the velocity of the ions, in the form of normal modes of vibration [1]. In consequence the calculations will have to be averaged over the ten runs with each run corresponding to one possible mode.
5. After that, a new simulation is carried out in which an electric field is imposed at some specific time.
6. The polarisation is then calculated for that applied field. The calculation of the continuous average of the polarisation is then carried out. The smoothing of the data is performed before the data is analysed to reduce the noise in the data.

The Origin software is used for the data smoothing, the data analysis and the non-linear curve fitting. The Fast Fourier Transform (FFT) is performed in order to investigate the behaviour of the hollandite model in frequency domain.

Two testing process have been carried out. In the first test only one tunnel ion in the hollandite model is allowed to move. In this case, the chosen sodium ion moves in a fixed potential. Its motion will be that appropriate to sodium ion in the absence of the 'fluid-like' interactions of the other sodium ions. In the second test, a constant dc electric field of 10MV/m is added at the start of the simulation and is switched off at 5001th interval. This provides a check on the linearity of the response to the electric field, since for a linear response both polarisation and depolarisation current are identical.

5.2 Simulation procedure

There are a total of six basic experimental procedures that are carried out. To start off, the number and position of the sodium ions are specified. The position of each of the sodium ion depends upon the position of the titanium ion that is substituted by a chromium ion. Temperature is introduced into the simulation by giving each ion some kinetic energy. For the same temperature, the total kinetic energy given to the hollandite model will remain the same for each of the ten runs carried out, whereas the kinetic energy given to each sodium ion is varied in each of the runs according to a range of vibration modes.

After collecting the results, which are the positions for the sodium ions, generated by the different runs, the average of the position in c-axis is calculated over the number of runs. A new simulation is then carried out for a linear superposition of the ten vibration modes previously considered. A dc electric field is introduced at the 5001th interval. The displacement in the average sodium ion position allows the polarisation in the applied field to be calculated. The calculation of the continuous average of the polarisation is then carried out before the data is analysed. These procedures are then repeated with different applied electric field and temperature.

The temperature given to the simulation varied between 200K and 373K. The applied dc electric fields varied between 7.43MV/m and 74.3GV/m. This will be explained in more detail in the subsequent sections below.

5.2.1 Number and position of the ions

The initial conditions of each ion in the hollandite model have to be determined before the simulation work is carried out. The positions in a and b-axis for the ions in the lattice sites are obtained from the “Gretep” program [2] (explained in section 3.7, chapter 3) whereas the positions in c-axis is dependent on the layer the ions belong to. The distance between each layer is 1.486\AA and is denoted G here. The first layer being 0, the second layer being G , the third layer being $2G$ and etc. $2G$ is the c-axis lattice spacing, see figure 5.1.

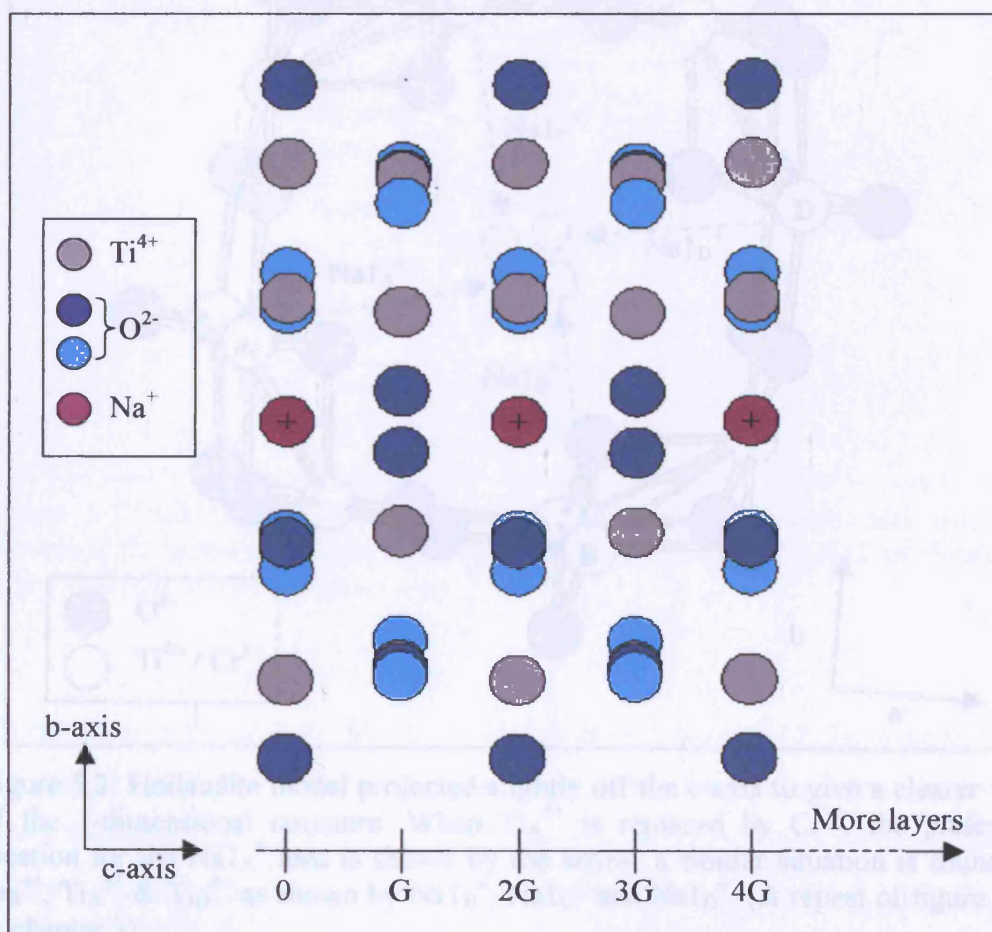


Figure 5.1: Hollandite model showing five layers projected along a-axis. There are a total of 60 layers in the hollandite model in this research.

The positions of the chromium ions in a, b and c-axis are the same as the positions of the titanium ions that are substituted. In this research, 24 sodium ions have been placed in the tunnel. The method for positioning these sodium ions is explained in section 3.7.3, chapter 3 and these positions depend on the positions of the chromium ions. The figure 5.2 below is a repeated figure from chapter 3 (figure 3.13) and is shown here again to give a better understanding of the exact positions for the sodium ion Na_1 . When Ti_A^{4+} is replaced by Cr^{3+} , the preferable location for the Na_1^+ ions is shown by the arrow, a similar situation is found for Ti_B^{4+} , Ti_A^{4+} & Ti_D^{4+} as shown by Na_1^+ , Na_1^+ and Na_1^+ .

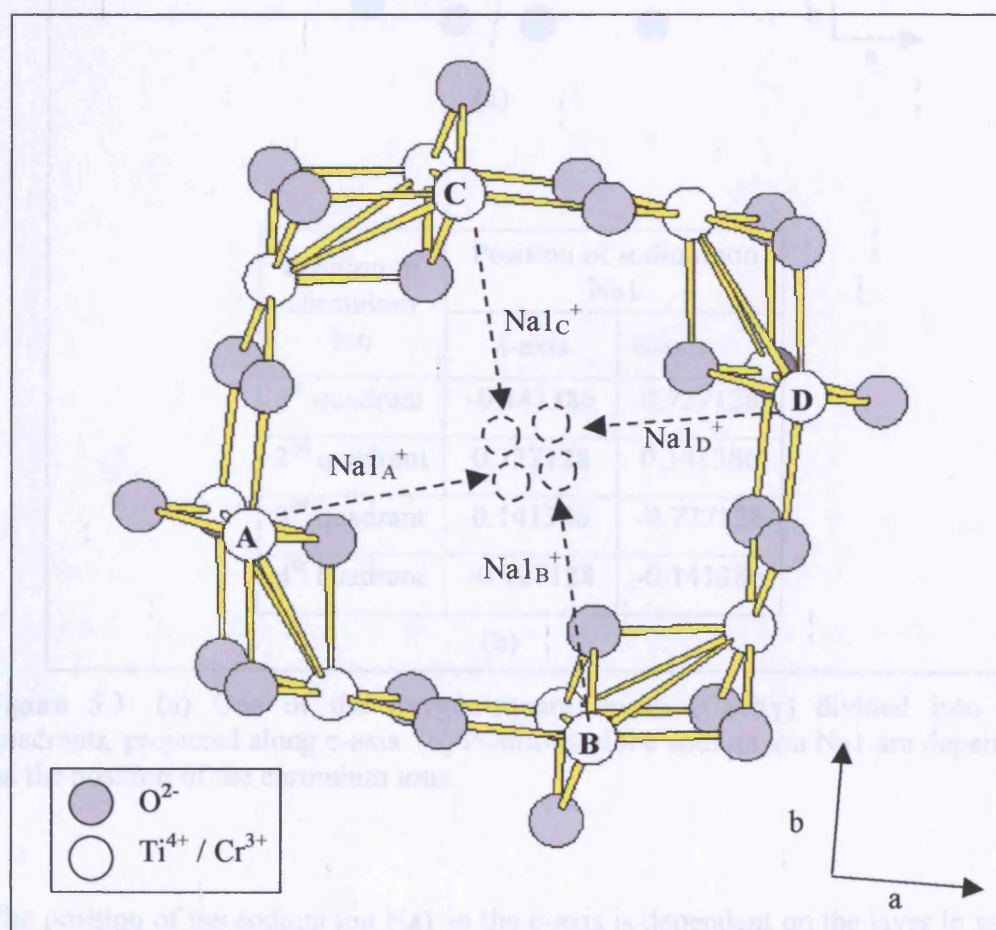


Figure 5.2: Hollandite model projected slightly off the c-axis to give a clearer view of the 3-dimensional structure. When Ti_A^{4+} is replaced by Cr^{3+} , the preferable location for the Na_1^+ ions is shown by the arrow, a similar situation is found for Ti_B^{4+} , Ti_A^{4+} & Ti_D^{4+} as shown by Na_1^+ , Na_1^+ and Na_1^+ . (A repeat of figure 3.13 in chapter 3)

When a sodium ion NaI is placed in the tunnel, its position in a and b-axis is dependent on the positions of the chromium ions in the cavity.

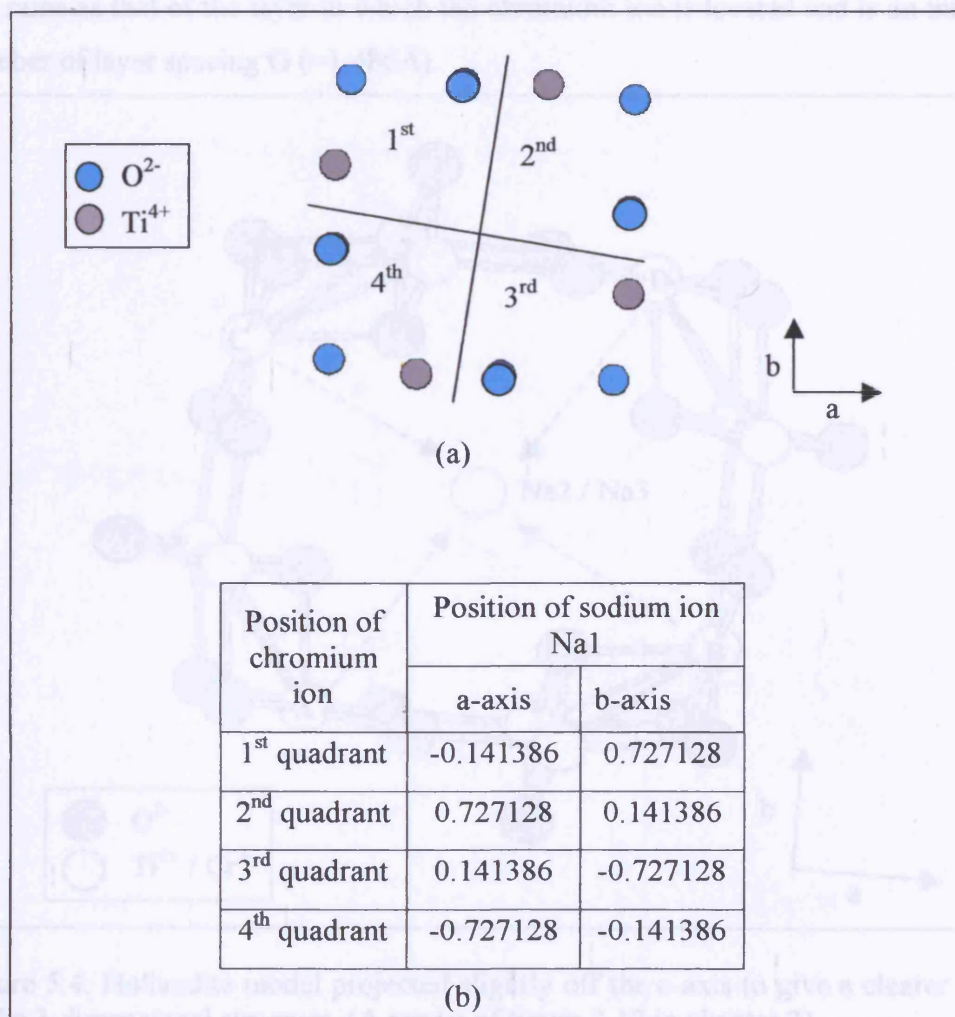


Figure 5.3: (a) One of the oxygen-square layers (Cavity) divided into four quadrants, projected along c-axis. (b) Positions of the sodium ion NaI are dependent on the position of the chromium ions.

The position of the sodium ion NaI in the c-axis is dependent on the layer in which it is placed. This is the same as the position in c-axis for the chromium ions in the lattice layer and is an integral number of layer spacing G ($=1.486\text{\AA}$). For example, if sodium ion NaI is placed in layer 22, the position in c axis is 31.206\AA ($21 \times G$).

Sodium ions Na2 and Na3 appear as odd-number groups between group of Na, see figure 5.5 and table 5.1. These ions are located at the centre of the tunnel, i.e. the a and b coordinate are zero, see figure 5.4 and 5.5. The c -coordinate of a Na3 ion is the same as that of the layer in which the chromium ion is located and is an integral number of layer spacing G ($=1.486\text{\AA}$).

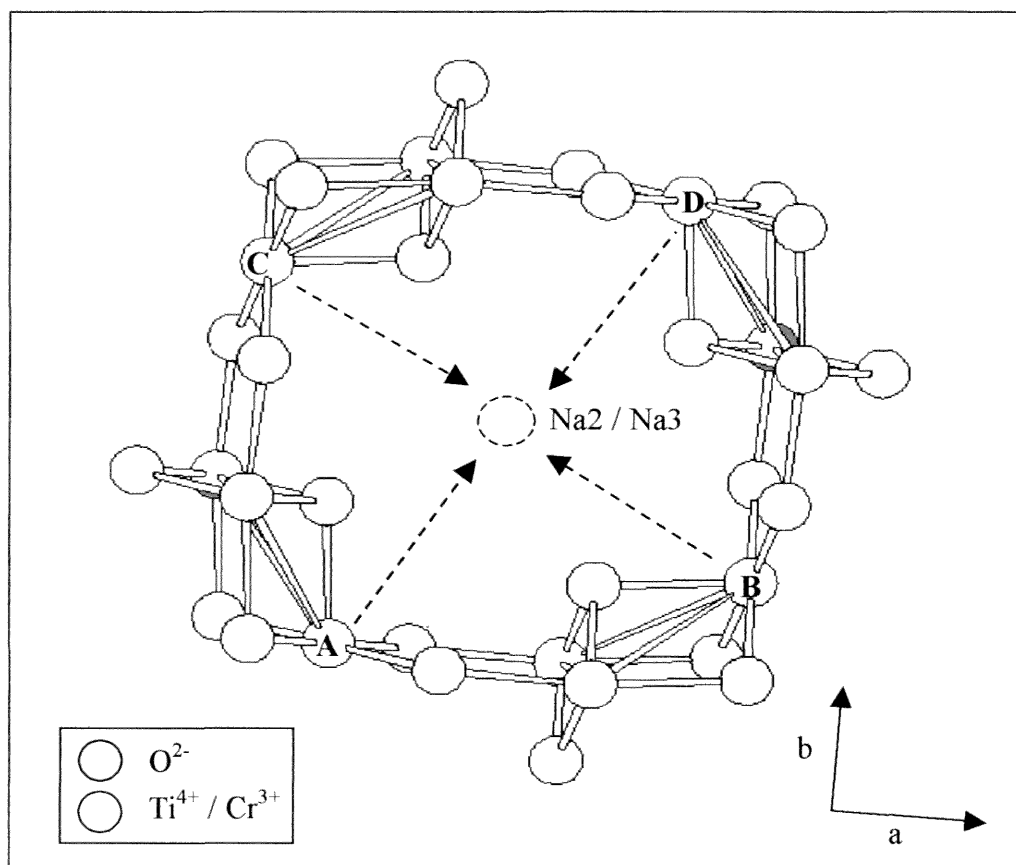


Figure 5.4: Hollandite model projected slightly off the c -axis to give a clearer view of the 3-dimensional structure. (A repeat of figure 3.12 in chapter 3)

In the groupings of sodium ions Na2 and Na3 each Na3 ion is in between two Na2 ions, see figure 5.5 and table 5.1, which are displaced away to either side from an integral number of layer spacing, i.e. it is nearer to the square plane, see figure.5.5. Some sample calculations have been carried out to obtain the exact position for the Na2 ion in the c-axis.

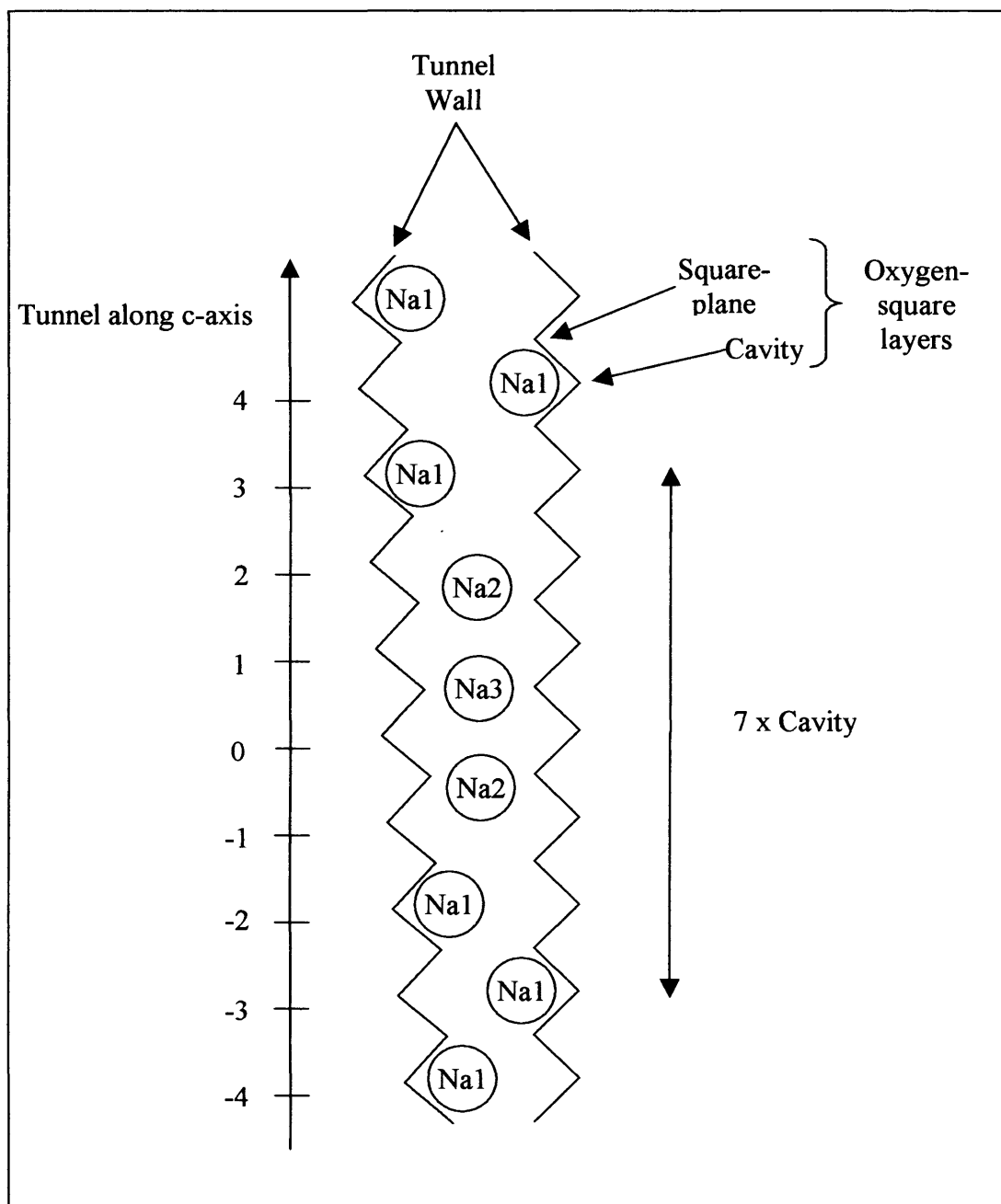


Figure 5.5: Schematic representation of a probable local arrangement for Na⁺ ions in the tunnel of Na_xCr_xTi_{8-x}O₁₆. In the 7 x Cavity, there will be six Na⁺ ions. (A repeat of figure 3.11 in chapter 3)

The coordinates in c-axis obtained from the x-ray analysis [3] for sodium ion Na1, Na2 and Na3 are 0.5, 0.2 and 0 respectively (also shown in table 3.4, chapter 3). Figure 5.6 below shows the possible positions of the sodium ions in c-axis. This is just to give a better understanding of the positions of these sodium ions, Na1, Na2 and Na3. In the model used only one sodium ion is allowed in each layer.

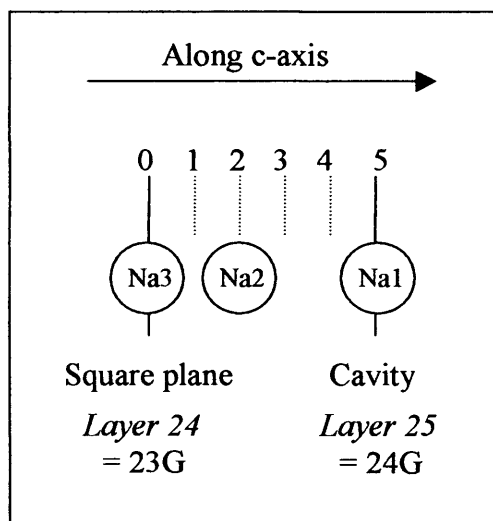


Figure 5.6: The positions of all the three sodium ions Na1, Na2 and Na3 in c-axis for the calculation of the position for sodium ion Na2. The solid line on the left is the Square plane, layer 24 and the solid line on the right is the Cavity, layer 25. The dotted lines are added for the calculation.

Position of the sodium ion Na2 in c-axis is

$$\frac{24G - 23G}{5} \times 2 + 23G = 34.7724 \text{ \AA} \quad 5.1$$

where G is 1.486\AA.

The position of the sodium ion Na2s in c-axis are therefore (N-2)G-0.5944 and (N+2)G+0.5944 when a Na3 ion is at NG.

The positions for the 24 sodium ions and 24 chromium ions are shown in the table 5.1. The value 34.7724Å obtained from the calculation shown above is the position for *Na10* in c-axis.

Ions	Positions /Å			Ions	Positions /Å		
	a-axis	b-axis	c-axis		a-axis	b-axis	c-axis
<i>Cr1</i>	-3.354	1.504	2.972	<i>Na1</i>	-0.141386	0.727128	2.972
<i>Cr2</i>	3.354	-1.504	5.944	<i>Na2</i>	0.141386	-0.727128	5.944
<i>Cr3</i>	-1.696	3.546	10.402	<i>Na3</i>	0	0	9.8076
<i>Cr4</i>	1.696	-3.546	13.374	<i>Na4</i>	0	0	13.374
<i>Cr5</i>	1.696	-3.546	16.346	<i>Na5</i>	0	0	16.9404
<i>Cr6</i>	-3.354	1.504	20.804	<i>Na6</i>	-0.141386	0.727128	20.804
<i>Cr7</i>	-1.504	-3.354	23.776	<i>Na7</i>	-0.727128	-0.141386	23.776
<i>Cr8</i>	3.546	1.696	28.234	<i>Na8</i>	0	0	27.6396
<i>Cr9</i>	-3.546	-1.696	31.206	<i>Na9</i>	0	0	31.206
<i>Cr10</i>	3.546	1.696	34.178	<i>Na10</i>	0	0	34.7724
<i>Cr11</i>	-1.504	-3.354	38.636	<i>Na11</i>	-0.727128	-0.141386	38.636
<i>Cr12</i>	1.504	3.354	41.608	<i>Na12</i>	0.727128	0.141386	41.608
<i>Cr13</i>	-3.354	1.504	44.58	<i>Na13</i>	-0.141386	0.727128	44.58
<i>Cr14</i>	3.354	-1.504	47.552	<i>Na14</i>	0.141386	-0.727128	47.552
<i>Cr15</i>	-1.696	3.546	52.01	<i>Na15</i>	0	0	51.4156
<i>Cr16</i>	1.696	-3.546	54.982	<i>Na16</i>	0	0	54.982
<i>Cr17</i>	-1.696	3.546	57.954	<i>Na17</i>	0	0	58.5484
<i>Cr18</i>	3.354	-1.504	62.412	<i>Na18</i>	0.141386	-0.727128	62.412
<i>Cr19</i>	-1.504	-3.354	65.384	<i>Na19</i>	-0.727128	-0.141386	65.384
<i>Cr20</i>	3.546	1.696	69.842	<i>Na20</i>	0	0	69.2476
<i>Cr21</i>	-3.546	-1.696	72.814	<i>Na21</i>	0	0	72.814
<i>Cr22</i>	3.546	1.696	75.786	<i>Na22</i>	0	0	76.3804
<i>Cr23</i>	-1.504	-3.354	80.244	<i>Na23</i>	-0.727128	-0.141386	80.244
<i>Cr24</i>	1.504	3.354	83.216	<i>Na24</i>	0.727128	0.141386	83.216

Table 5.1: The initial positions for all the 24 sodium ions and 24 chromium ions in a, b and c-axis. The 24 sodium ions and 24 chromium ions are denoted as *Na1* to *Na24* and *Cr1* to *Cr24* respectively.

Na1, *Na2*, *Na6*, *Na7*, *Na11*, *Na12*, *Na13*, *Na14*, *Na18*, *Na19*, *Na23* and *Na24* are sodium ion Na1.

Na3, *Na5*, *Na8*, *Na10*, *Na15*, *Na17*, *Na20* and *Na22* are sodium ion Na2.

Na4, *Na9*, *Na16* and *Na21* are sodium ion Na3.

The positions of the titanium ions and the oxygen ions in a and b-axis are shown in Appendix A1.

5.2.2 Temperature given to the simulation

The temperature is set by giving an initial ($t=0$) average kinetic energy equivalent to $k_b T$ to the sodium ions, where k_b is the boltzmann's constant and T is the temperature in Kelvin.

$$\frac{1}{2} m v_1^2 = k_b T \quad 5.2$$

Here m is the mass¹ for the sodium ion and v_1 is the velocity given to the sodium ion. The velocity, v_1 given to sodium ion becomes

$$v_1 = \sqrt{\frac{2k_b T}{m}} \quad 5.3$$

Ten runs are carried out for the same temperature by changing the direction and magnitude of the velocities given to each sodium ion while keeping the average kinetic energy the same. The total energy given to the hollandite model will remain the same for each run. In some of the runs, the initial kinetic energy of some sodium ions has been doubled to $2k_b T$ while others have zero initial kinetic energy to compensate. The initial velocity for these ions, v_2 is given by

$$v_2 = \sqrt{\frac{4k_b T}{m}} \quad 5.4$$

Five different temperatures are investigated between 200K and 373K, which are 200K, 250K, 273K, 297K and 300K. The velocity given to the sodium ions for each of the 10 runs is described in the following section.

¹ The mass here is the actual mass calculated in unit kg and the calculation is shown in Appendix A2.

5.2.3 Initial conditions given for each run

The direction and the magnitude of the velocities given to the sodium ions for the ten runs are shown below:

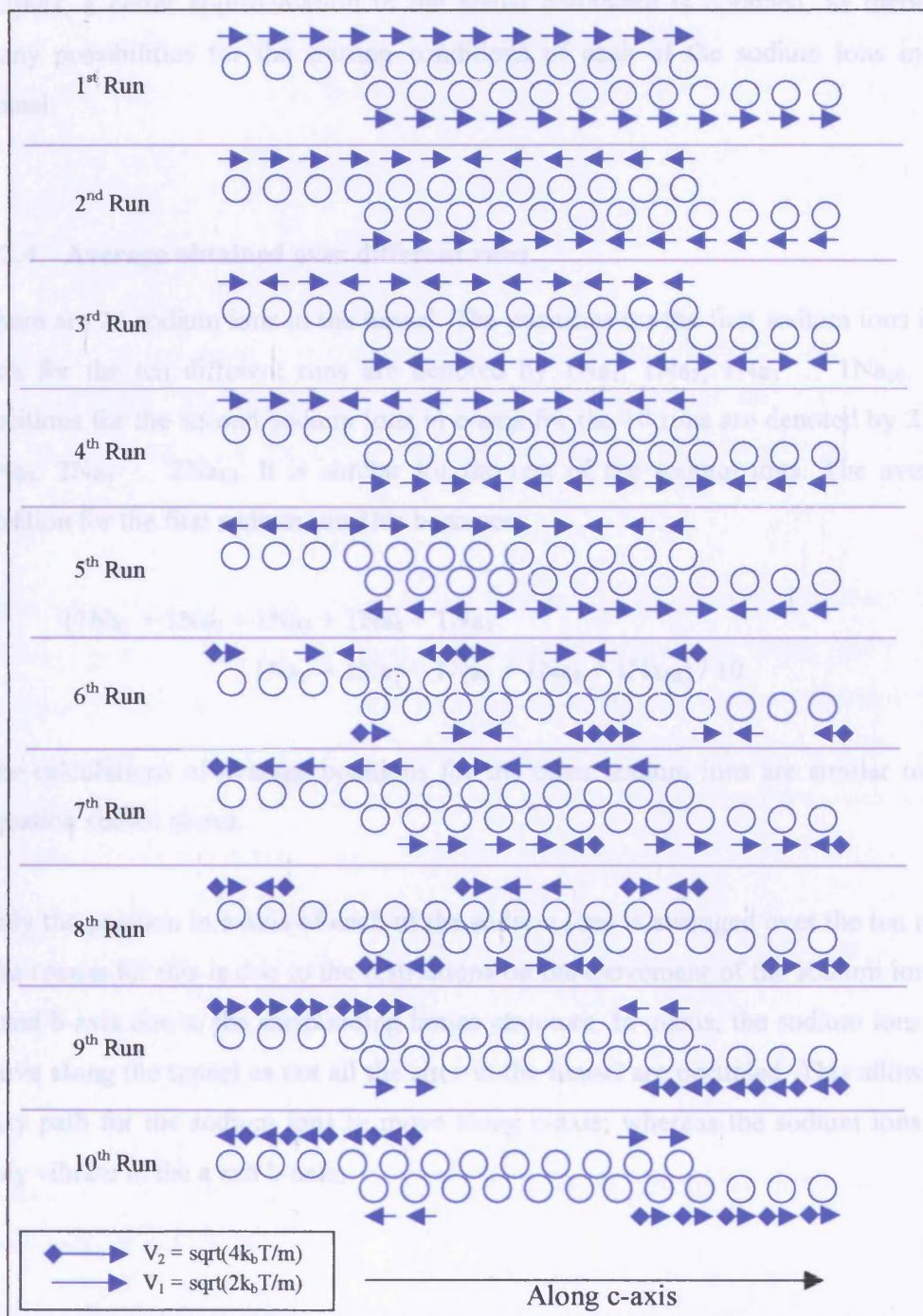


Figure 5.7: The direction and magnitude of velocities given to the sodium ions for the 10 runs. The top row is actually situated on the left of the bottom row to show all the 24 sodium ions along the tunnel (c-axis).

The directions and magnitude of the velocities have the form of normal modes of vibration with the total kinetic energy kept constant. The outputs from the simulations are the positions in c-axis of the 10 different runs. By averaging these outputs, a better approximation to the actual hollandite is obtained, as there are many possibilities for the starting conditions of each of the sodium ions in the tunnel.

5.2.4 Average obtained over different runs

There are 24 sodium ions in the tunnel. The positions for the first sodium ions in c-axis for the ten different runs are denoted by $1Na_1, 1Na_2, 1Na_3 \dots 1Na_{10}$. The positions for the second sodium ions in c-axis for the 10 runs are denoted by $2Na_1, 2Na_2, 2Na_3 \dots 2Na_{10}$. It is similar for the rest of the sodium ions. The average position for the first sodium ion $1Na$ becomes:

$$\begin{aligned} & (1Na_1 + 1Na_2 + 1Na_3 + 1Na_4 + 1Na_5 \\ & + 1Na_6 + 1Na_7 + 1Na_8 + 1Na_9 + 1Na_{10}) / 10 \end{aligned} \quad 5.5$$

The calculations of average positions for the other sodium ions are similar to the equation shown above.

Only the position in c-axis of each of the sodium ions is averaged over the ten runs. The reason for this is due to the restrictions on the movement of the sodium ions in a and b-axis due to the surrounding lattice structure. In c-axis, the sodium ions can move along the tunnel as not all the sites in the tunnel are occupied. This allows an easy path for the sodium ions to move along c-axis; whereas the sodium ions can only vibrate in the a and b-axis.

5.2.5 DC electric fields

In order to calculate the response of the system to an electric field a constant dc field is switched on at the 5001th interval. The initial 5000 intervals are used to allow the sodium ions to get to the equilibrium positions or so-called desired positions. The force that is exerted on the sodium ion due to the dc field is given below:

$$Force_{field} = (+1) \times e \times field \quad 5.6$$

where +1 is the polarity of sodium ion, e is the electron charge and field is the applied field. Six different fields are investigated between 7.43MV/m and 74.3GV/m, which are 7.43MV/m, 74.3MV/m, 371.5MV/m, 743MV/m, 7.43GV/m and 74.3GVMV/m.

The initial velocities given to the sodium ions for this program is determined by the energy given to each of the sodium ion. However, the total energy given to the hollandite model remains the same as the total energy given to the hollandite model for each run shown in figure 5.7. Take the first sodium ion for example; the energy given to it is the total of 1/10 of the energy given to the first sodium ion in each of the ten runs shown below.

$$\begin{aligned} \frac{1}{2}mv_{f1}^2 &= \frac{k_b T}{10} + \frac{k_b T}{10} + \frac{k_b T}{10} + \frac{k_b T}{10} + \frac{k_b T}{10} + \frac{2k_b T}{10} + \frac{2k_b T}{10} + \frac{2k_b T}{10} + \frac{2k_b T}{10} + \frac{2k_b T}{10} \\ &= \frac{15}{10}k_b T = \frac{3}{2}k_b T \end{aligned} \quad 5.7$$

where m is the mass for the sodium ion, k_b is the boltzmann's constant and T is the temperature in Kelvin.

Speed given to the first sodium ion becomes

$$|v_{f1}| = \sqrt{\frac{3}{m}(k_b T)} \quad 5.8$$

A positive velocity shows that the sodium ion is in a positive direction, which is towards the right hand side. The velocity given to the first sodium ion is

$$v_{f1} = \sqrt{\frac{3}{m}(k_b T)} \quad 5.9$$

In this program all sodium ions are given a positive direction of motion to simplify the initial conditions. The initial velocities of the rest of the sodium ions can be determined by using the same method.

The reason for doing this is that the energy given to each of the sodium ion in this program is the average energy given for the sodium ions in the ten runs discussed before (section 5.2.3). This average energy will give an average speed to each of the sodium ion and during the initial 5000 intervals in the simulation, these ions will get to the desired position. These desired positions would be quite similar to the average positions in zero-field equilibrium as shown in the figure 5.8. Only c-axis is shown in the figure because that's the axis for which the calculation of polarisation is carried out. Although there are some big fluctuation at some point but they still go to rather the same position at 5000th interval. Hence the change in the positions from 5001th interval will be due to the field.

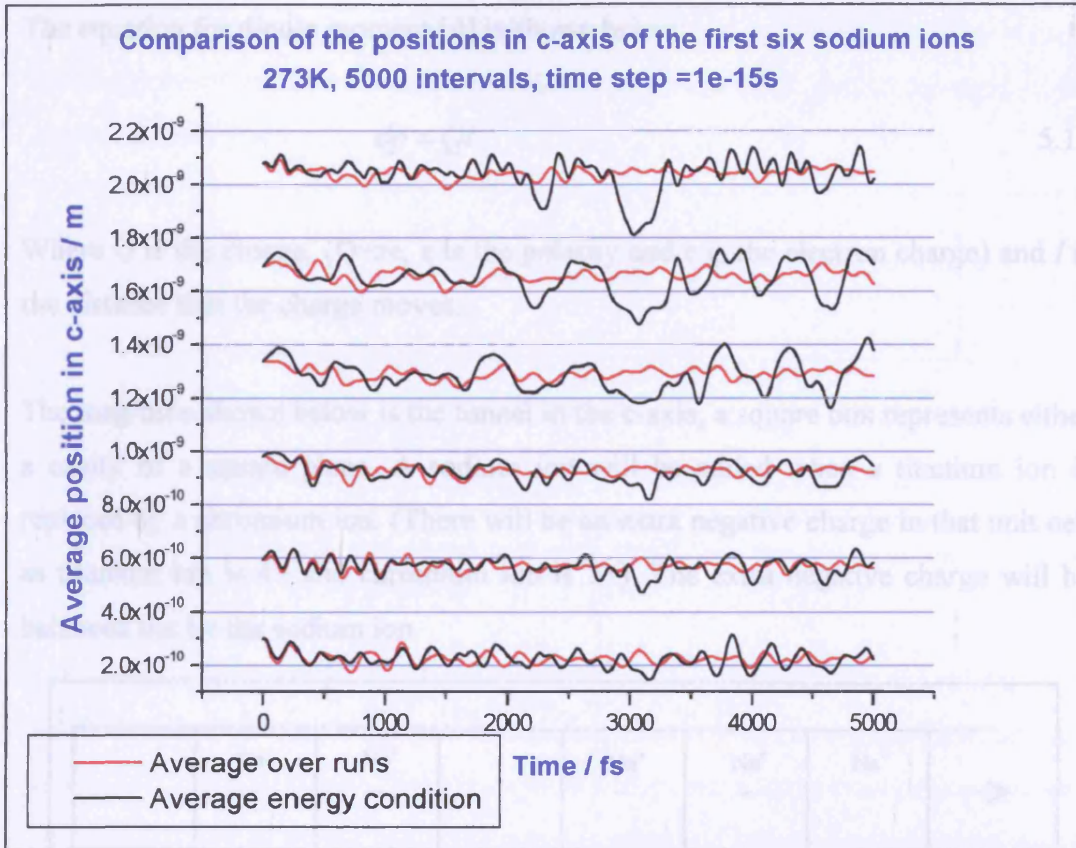


Figure 5.8: A comparison of the position of the first six sodium ions in c-axis for the average positions of the ten runs (red) and the positions generated from the initial condition of average energy (black).

5.2.6 Calculation of the polarisation

In this research, only the polarisation in the c-axis is taken into consideration, as the dc field acts only along the c-axis. The polarisation is defined as the electric dipole moment per unit volume. The formula [4] is shown as follows:

$$dp = Pd\tau \quad 5.10$$

Where dp is the dipole moment and $d\tau$ is the volume.

The equation for dipole moment [4] is shown below:

$$dp = Ql \quad 5.11$$

Where Q is the charge, ($Q=ze$, z is the polarity and e is the electron charge) and l is the distance that the charge moves.

The long tube shown below is the tunnel in the c -axis; a square box represents either a cavity or a square plane. A sodium ion will be added when a titanium ion is replaced by a chromium ion. (There will be an extra negative charge in that unit cell as titanium ion is $4+$ and chromium ion is $3+$). The extra negative charge will be balanced out by the sodium ion.

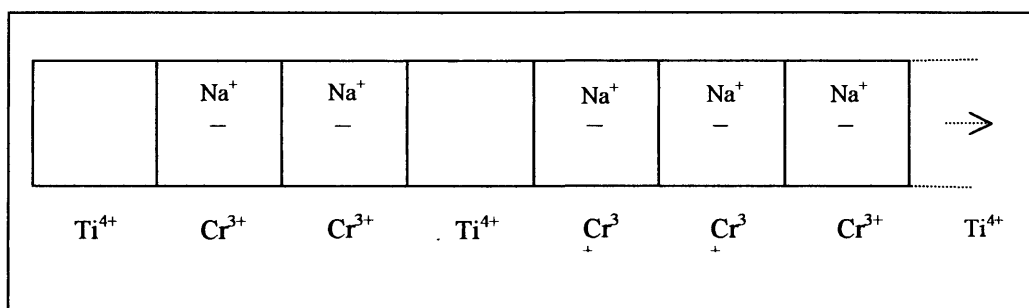


Figure 5.9: The tunnel along c -axis, square box represents either a cavity or a square plane. This is just part of the tunnel.

When a dc-field is added to the structure in the direction shown below, the sodium ions will move along the tunnel in the direction of the applied dc field.

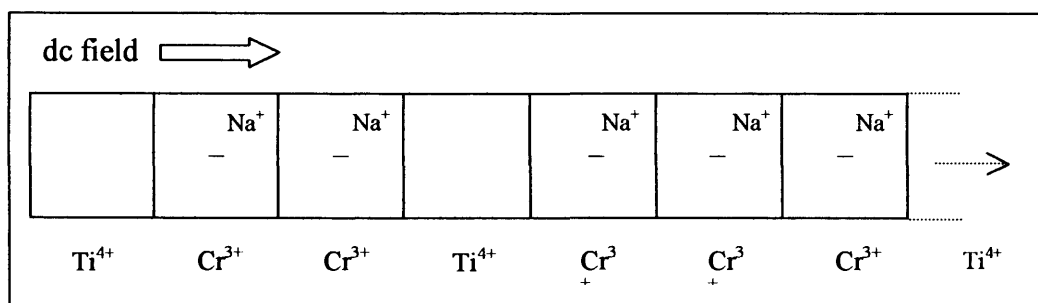


Figure 5.10: The tunnel along c -axis, square box represents either a cavity or a square plane. This is just part of the tunnel. The sodium ions will move along the tunnel in the direction of the applied dc field.

The negative charge is a net charge of the unit cell and would not displace because the positions of the ions in the lattice sites are remain static due to the rigid lattice approximation made.

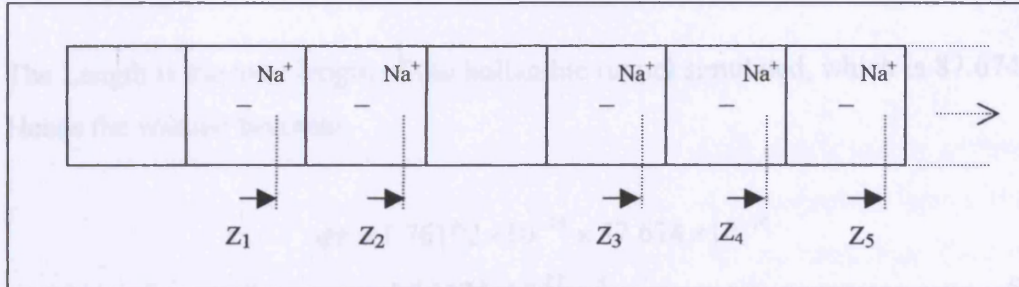


Figure 5.11: The tunnel along c-axis, square box represents either a cavity or a square plane. This is just part of the tunnel. Z and Z' are the distances moved by Na ion and negative charge respectively.

Z is the distances moved by sodium ion when dc field is applied to the model. (The distance moved is the difference in position between the new positions for each sodium ion when an electric field is applied with respect to their average positions.) The distance moved by the negative charge in this rigid lattice approximation would not change. Hence the total dipole moment becomes

$$dp = e\{+Z_1 + Z_2 + Z_3 + Z_4 + Z_5\} \quad 5.12$$

Volume used is Area x Length. The Area is assumed to be the cross-sectional area that the sodium ion is allowed to move in a and b-axis as shown in the diagram below:

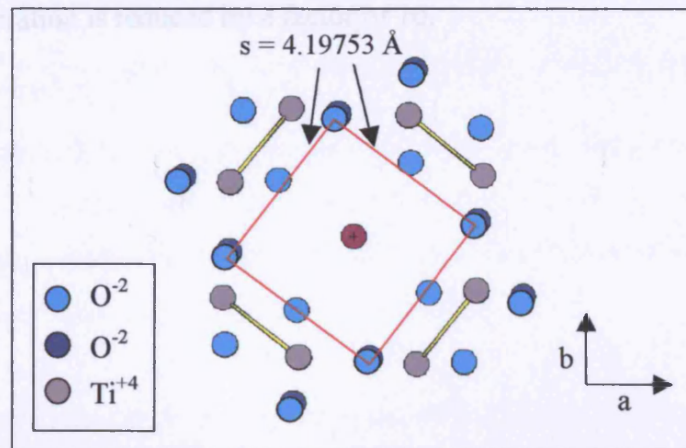


Figure 5.12: The hollandite model projected along c-axis. The square in red is the cross-sectional area that the sodium ion is allowed to move in.

s being the distance between two oxygen ions. The Area is

$$(4.19753 \times 10^{-10})^2 = 1.76192 \times 10^{-19} \text{ m}^2 \quad 5.13$$

The Length is the total length of the hollandite tunnel simulated, which is 87.674 Å. Hence the volume becomes

$$\begin{aligned} d\tau &= 1.76192 \times 10^{-19} \times 87.674 \times 10^{-10} \\ \dots &= 1.54475 \times 10^{-27} \text{ m}^3 \end{aligned} \quad 5.14$$

A more accurate calculation of the volume could be found using the volume of the unit cell and calculating the total number of unit cells in the assembly being considered. This would be considerably more complicated and would only change the value of polarisation by a small factor. The values reported here would all be changed by the same factor and would not change the conclusions.

Polarisation is calculated by substituting the equation 5.12 and the equation 5.14 into the equation 5.10. After this has been done, the continuous average for the polarisation is calculated. The reason for carrying out a continuous average is to reduce the quantum vibration, which has a frequency of about 10^{13} Hz and hence a period of about 10^{-13} s. The time step used in the simulation is 1×10^{-15} s. Hence by averaging the polarisation over 100 intervals, ($100 \times 1 \times 10^{-15} \text{ s} = 10^{-13} \text{ s}$), the quantum vibration is reduced by a factor of 10.

5.3 Data analysis

The Origin software is used for the data smoothing, the data analysis and curve fitting.

5.3.1 “Origin” software for performing data smoothing

“Origin” software had a function to smooth the ‘noisy’ graph and it can be carried out by selecting Analysis:Smoothing:FFT Filter. This menu command opens the Smoothing dialog box. The smoothing is accomplished by removing Fourier components with frequencies higher than: $\frac{1}{n} \text{deltat}$, where n is the number of data points considered at a time, and *deltat* is the time (or more generally the abscissa) spacing between two adjacent data points. The number of points to be considered for smoothing the continuous average of the polarisation is 5000 points.

5.3.2 “Origin” software for performing Fast Fourier Transform (FFT)

The Fast Fourier Transform (FFT) is performed in order to calculate the behaviour of the hollandite model in the frequency domain. The continuous average of the polarisation is imported to “Origin” program. A graph of polarisation versus time is plotted. Only the data between the 5001th and 100000th gives the polarisation since the electric field is switched on at the 5000th interval. The time derivative of the polarisation is then obtained via the program, and is plotted. The one-sided Fourier Transform of $\frac{dP}{dt E \epsilon_0}$ gives the frequency dependent dielectric susceptibility (as shown in equation 2.12) for comparison with experiment. The easier way to carry out the FFT in “Origin” software is by performing FFT on the dP/dt, the results obtained are then divided by electric field, E and permittivity of free space, ϵ_0 to give the real and imaginary parts of the susceptibility.

The FFT is carried out by selecting Analysis: FFT. This menu command opens the FFT tool to prepare the data and allowed the parameters for the calculations to be chosen. For the FFT in this program it is assumed that the independent variable (X

data set) is time and that the dependent variable (Y data set) is some sort of amplitude. The Operation tab is shown as follows:



Figure 5.13: The Operation tab for performing the FFT in “Origin” program.

The Forward radio button is selected to perform a forward FFT and the Amplitude radio button is selected to plot amplitude and phase data.

Next is to select the parameter in the Setting tab as shown below:

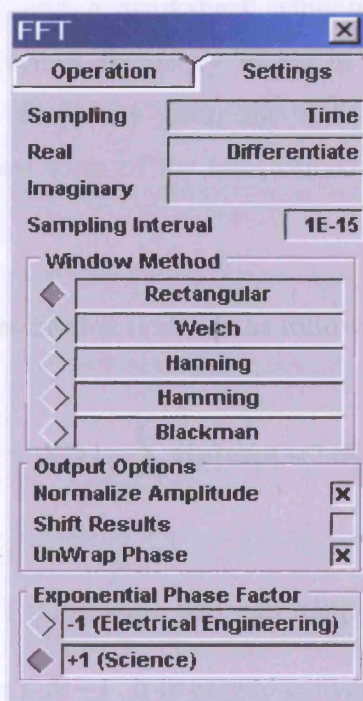


Figure 5.14: The Setting tab for performing the FFT in “Origin” program.

In the Sampling text box, by default the X data set of the active data plot is selected as the sampling data set, which is Time. In the Real text box, by default the Y data

set of the active data plot is selected as the real data set, which is the “Differentiate”. In the imaginary text box, in this case no data set is specified. The time interval used is 1e-15s, hence this is typed in the Sampling interval text box.

The rectangular window method is selected because this is the window method that would lose the least data in comparison to the other window methods although the Blackman method [5] is more popular method to be used in signal processing. In this research, as much data as possible should remain after the transformation of FFT in order to obtain a more accurate susceptibility plot. The Normalization Amplitude box is selected to reveal the true amplitudes in the original data set. The check box for Shift Results is cleared so that the transform is displayed for positive frequencies only. The UnWrap Phase check box is selected to maintain the true phase data. Finally, the +1 (Science) in the Exponential Phase Factor is selected; the phase factor is set according to the formula listed in Numerical Recipes in C [6]. Then the OK button is selected to perform the FFT. The results are generated in two new windows: a graph and a worksheet window. The amplitude and phase information are plotted versus frequency in Hz in the graph window. The FFT worksheet contains the frequency data, the real and imaginary parts of the transformed data, the polar form of the transformed data and the power spectrum data.

The FFT mathematical description is shown as follows:

$$X[k] = \sum_{n=0}^{N-1} x[n] \exp(-i2\pi F_k n) \quad 5.15$$

with $F_k = \frac{k}{N}$, where FFT transforms $x[n]$ into $X[k]$. The input data set is $x[n]$ with index n in the range $0 \leq n \leq N-1$. It is easy to convert the index into “time” $t = n\tau$, where τ is the (time) interval, and $F_k = \frac{k}{N}$ into “frequency” $f_k = \frac{k}{N\tau}$.

5.3.3 “Origin” software for performing non-linear curve fitting

Curve fitting is important, as it will give the best curve fit to the graph obtained. Firstly, the Real and Imaginary part of the susceptibility (the results generated by the FFT from the previous section) are plotted against frequency in two different graphs. This is to ease the fitting procedure as the two graphs are of different shape hence two different fitting functions are defined.

The curve fitting is carried out by selecting Analysis: Non-linear Curve Fit (NLSF). This menu command would open the NLSF window to prepare the data and allowed the parameters for the calculations to be chosen. The advanced mode is selected to define a new function and initialise the parameters. The fitting menu bar includes five menus: Function, Action, Option and Scripts shown in figure 5.15.

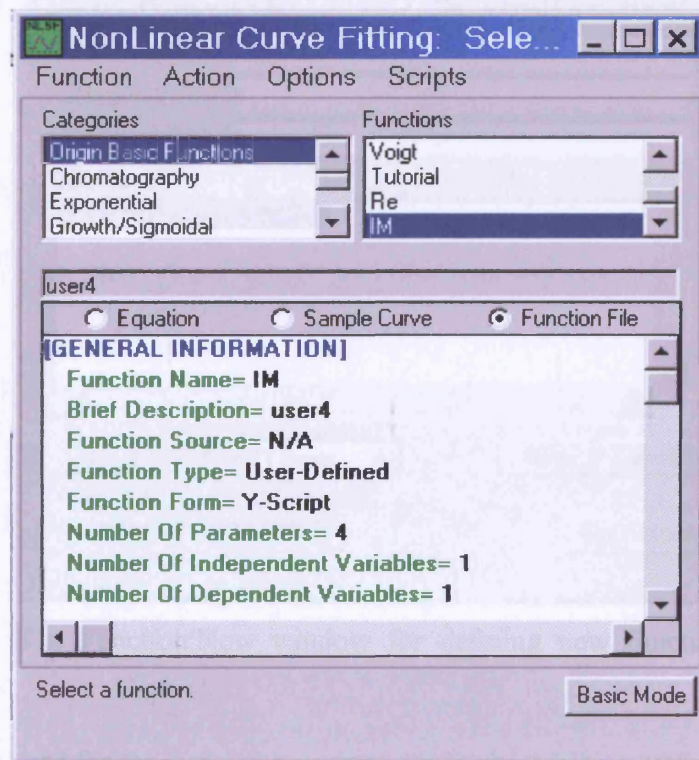


Figure 5.15: The NLSF window for performing non-linear curve fitting in “Origin” program.

The Function:New is selected. This menu command opens the Define New Function dialog box. The name of the new function is typed in the Name text box.

5.3.3.1 Relaxation Response

If the results exhibit a relaxation behaviour, then we would expect the loss peak to characterised by a power law frequency dependence above and below the peak frequency. The method of defining the Im function is explained here. The User Defined Param. Names check box is selected to enable arbitrary parameter names. A , x_p , b and d are typed in the Parameter Names text box, A is the amplitude factor, x_p is the absorption peak frequency factor, b and d are the frequency power exponents, see equation 5.16. By default x is typed in the Independent Var text box and y is typed in the Dependent Var text box as shown in figure 5.16.

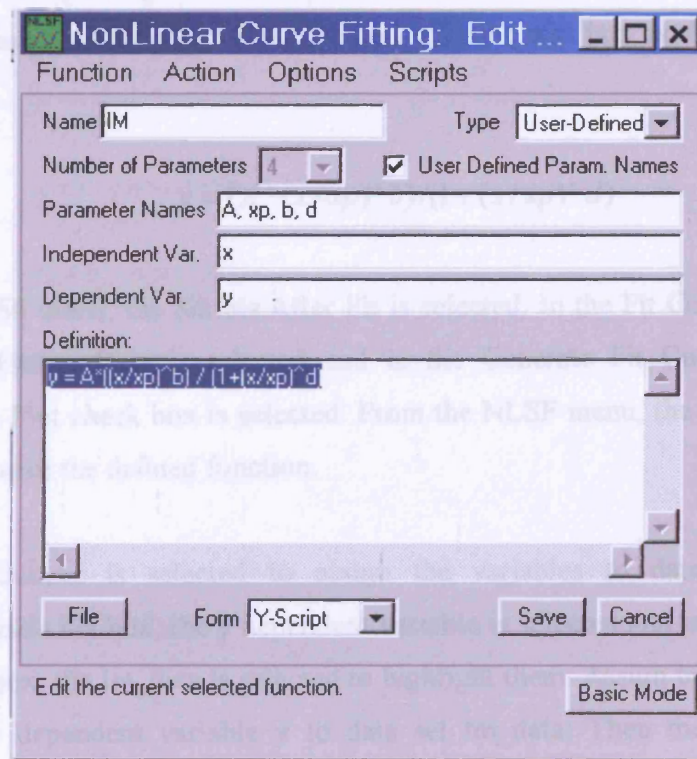


Figure 5.16: The Function:New window for defining new function in “Origin” program.

The equation used for the imaginary component is given in terms of y and x by

$$y = \frac{A \left(\frac{x}{x_p} \right)^b}{1 + \left(\frac{x}{x_p} \right)^d} \quad 5.16$$

for $x/x_p < 1$,

$$y \approx A \left(\frac{x}{x_p} \right)^b \quad 5.17$$

for $x/x_p > 1$,

$$y \approx A \left(\frac{x}{x_p} \right)^{b-d} \quad 5.18$$

The Y-Script is selected from the Form Drop-down List. Each dependent variable is defined in the scrip using the form “y = ...”, where y is the dependent variable. Then the required function is defined in the Definition edit box as shown in figure 5.16:

$$y = (A * (x/x_p)^b) / (1 + (x/x_p)^d) \quad 5.19$$

From the NLSF menu, the Scripts:After Fit is selected. In the Fit Curve group, the Same X as Fitting Data is selected and in the Generate Fit Curve, the Paste Parameters to Plot check box is selected. From the NLSF menu, the Function:Save is selected to save the defined function.

The Action:Dataset is selected to assign the variables to data sets. In the Variable:Datasets list box, the y dependent variable is selected and in the Available Datasets list box, the Im_data is selected to highlight them. Assign button is clicked to assign the dependent variable y to data set Im_data. Then the Action:Fit is selected and the parameters A , x_p , b and d are initialised. The Vary check boxes are selected to enable all the parameters to vary during fitting. Finally the 10 Iter button is selected to fit the data and Done button is selected to paste the parameter values to the graph.

The actual peak frequency (x_{peak}) and magnitude of the peak (y_{peak}) are dependent upon b and d . The expression for y_{peak} and x_{peak} are obtained as the calculation shown below:

$\frac{dy}{dx}$ of equation 5.16 gives

$$\frac{dy}{dx} = \frac{A}{[1 + (\frac{x}{x_p})^d]^2} \left[(1 + (\frac{x}{x_p})^d)b - d(\frac{x}{x_p})^d \right] \quad 5.20$$

when $\frac{dy}{dx} = 0$, the actual peak frequency, x_{peak} becomes

$$x_{peak} = x_p \left(\frac{b}{d-b} \right)^{1/d} \quad 5.21$$

Substitute this x_{peak} from equation 5.20 into equation 5.16 to obtain the actual magnitude of the peak. Hence

$$y_{peak} = A \frac{(d-b)}{d} \left(\frac{b}{d-b} \right)^{b/d} \quad 5.22$$

The parameters used to plot the graph in figure 5.17 are $x_p = 1.5 \times 10^{-14}$, $A = 1 \times 10^{12}$, $b = 1$ and $d = 2$. Hence by substituting the parameters into equation 5.21 and 5.22,

$$x_{peak} = 1.5 \times 10^{-14} \left(\frac{1}{2-1} \right)^{1/2} = 1.5 \times 10^{-14}$$

$$y_{peak} = 1 \times 10^{12} \frac{(2-1)}{2} \left(\frac{1}{2-1} \right)^{1/2} = 5 \times 10^{11}$$

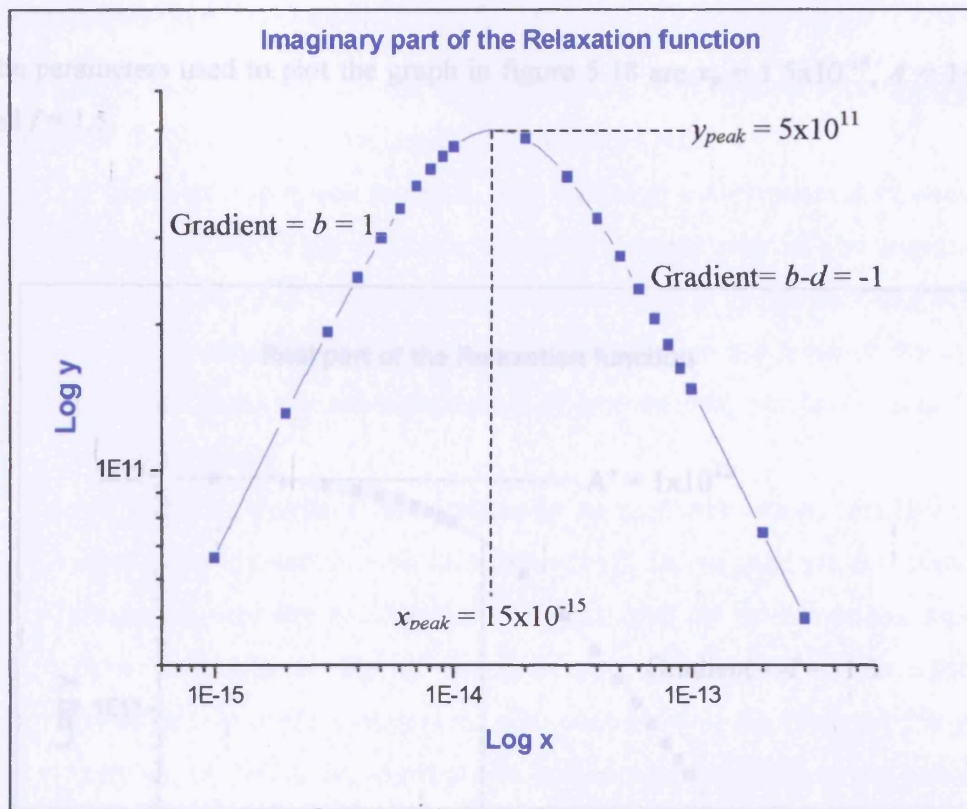


Figure 5.17: A diagram of the non-linear curve fitting for the Im function plotted in a log-log scale. A , x_p , b and d are the parameters used where A' is the amplitude factor, x_p is the absorption peak frequency factor, b and d are the frequency power exponents.

A similar technique is used to define the function for the real susceptibility. A' , x_p and f are the parameters used where A' is the saturation value of the curve, x_p is the peak frequency factor and f is the gradient for the curve. The expression used in term of y and x is

$$y = \frac{A'}{1 + \left(\frac{x}{x_p}\right)^f} \quad 5.23$$

for $x/x_p < 1$,

$$y \approx A' \quad 5.24$$

for $x/x_p > 1$,

$$y \approx A' \left(\frac{x}{x_p}\right)^{-f} \quad 5.25$$

The parameters used to plot the graph in figure 5.18 are $x_p = 1.5 \times 10^{-14}$, $A = 1 \times 10^{12}$ and $f = 1.5$.

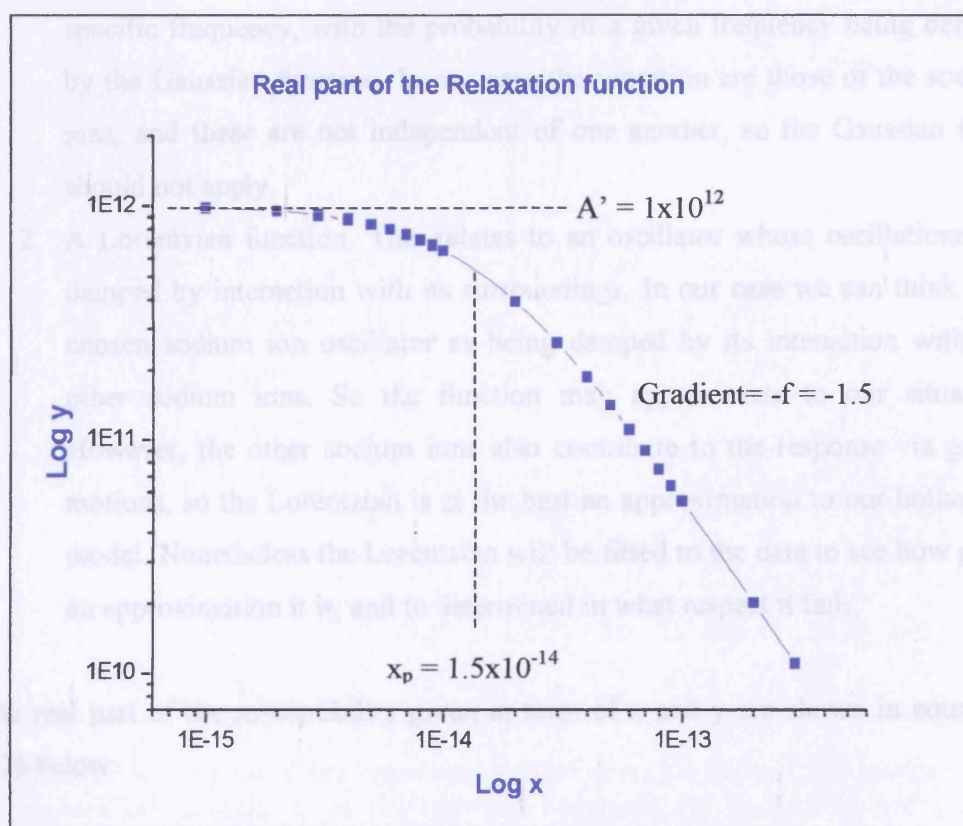


Figure 5.18: A diagram of the non-linear curve fitting for the Re function plotted in a log-log scale. A' , x_p and f are the parameters used for the saturation value of the curve, the peak frequency factor and the gradient for the curve respectively.

The imaginary part of the susceptibility given in term of x' and y are shown in equation 5.27 below.

$$y = \frac{2A}{w} \frac{x'}{x_p^2 - x'^2 + w^2} \quad (5.27)$$

A similar technique as described in section 5.3.3.1 is used to define the two non-fitting functions shown above. x_p , w and A' are the parameters used for the relaxation frequency, full width at 1/2 maximum and amplitude factor respectively.

5.3.3.2 Resonance absorption

If the results show a resonance character then we have to fit them to an appropriate expression. Two types of expressions are commonly used.

1. A Gaussian absorption function. This relates to a superposition of oscillator resonances with each oscillator vibrating independently of one another at a specific frequency, with the probability of a given frequency being defined by the Gaussian function. In our case the vibrations are those of the sodium ions, and these are not independent of one another, so the Gaussian form should not apply.
2. A Lorentzian function. This relates to an oscillator whose oscillations are damped by interaction with its surroundings. In our case we can think of a chosen sodium ion oscillator as being damped by its interaction with the other sodium ions. So the function may approximate to our situation. However, the other sodium ions also contribute to the response via group motions, so the Lorentzian is at the best an approximation to our hollandite model. Nonetheless the Lorentzian will be fitted to the data to see how good an approximation it is, and to determine in what respect it fails.

The real part of the susceptibility given in terms of x and y are shown in equation 5.26 below:

$$y = \frac{4A}{\pi} \frac{x_c - x}{4(x_c - x)^2 + w^2} \quad 5.26$$

The imaginary part of the susceptibility given in terms of x and y are shown in equation 5.27 below:

$$y = \frac{2A}{\pi} \frac{w}{4(x_c - x)^2 + w^2} \quad 5.27$$

A similar technique as described in section 5.3.3.1 is used to define the two new fitting functions shown above. x_c , w and A are the parameters used for the resonant frequency, full width at $\frac{1}{2}$ maximum and amplitude factor respectively.

Figure 5.19 below shows the diagram for the non-linear curve fitting for the real and imaginary part of the Lorentzian function. The parameters used is $x_c = 15$, $w = 8$ and $A = 250$.

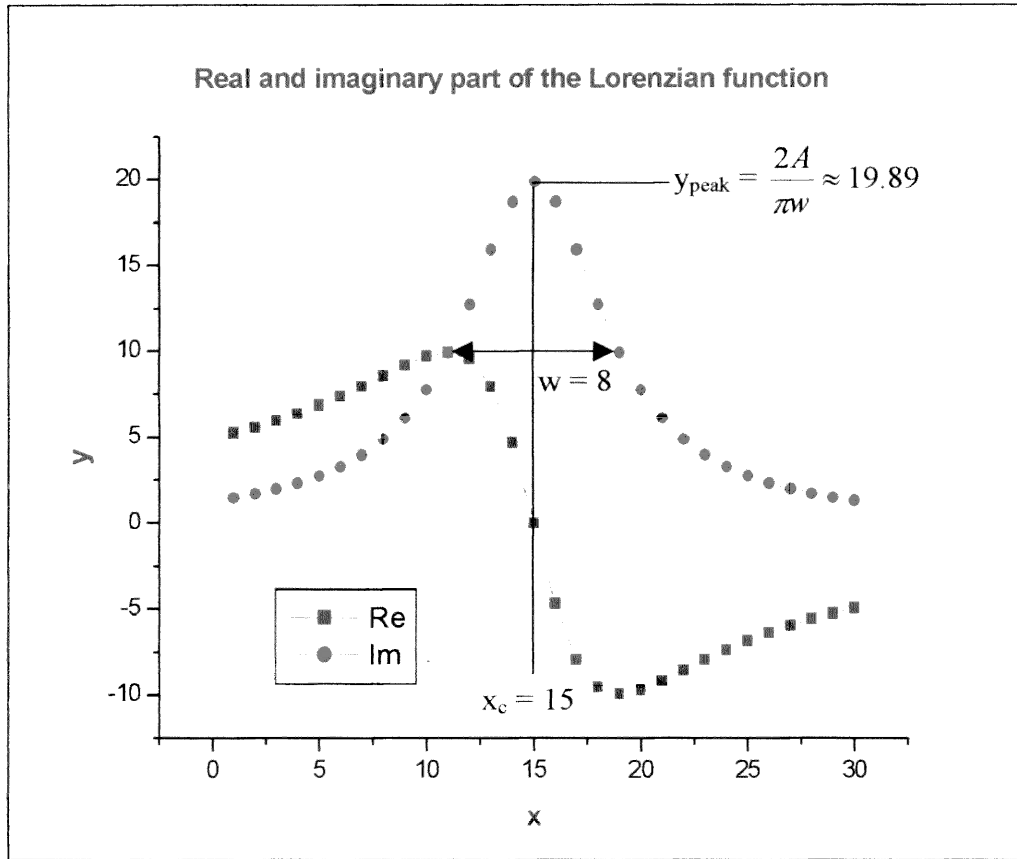


Figure 5.19: A diagram of the non-linear curve fitting for the real and imaginary of the Lorentzian function. x_c is the resonant frequency, w is the full width at $\frac{1}{2}$ maximum and A is the amplitude factor.

5.4 Two testing processes that are carried out

5.3.4 Only one tunnel ion is allowed to move

In this simulation only one sodium ion is allowed to move. There are total of 24 sodium ions in the tunnel; and the 9th sodium ion is selected to be the ion that is allowed to move. This would give the best approximation to a sodium ion in the body of the hollandite structure, as the sodium ion is one of the sodium ions in the middle of the tunnel. The rest of the sodium ions would remain static; this is the same as the ions in the lattice sites. This simulation should give the behaviour of a sodium ion that is trapped in a rigid cage formed by the lattice and the other sodium ions. A comparison with the data obtained when all the sodium ions are free to move will allow the effect of the liquid-like flexibility of the sodium ions to be move clearly demonstrated. The susceptibility is then obtained from the origin program. This simulation is carried out with initial conditions of temperature=297K, 100000 intervals, time step=10⁻¹⁵ s and electric field=743MV/m.

It would be expected that the sodium ion in this test would give a response in the vibration frequency, since the movement of that sodium ion is not affected by the movement of other ions.

5.3.5 Depolarisation

A constant DC electric field of 7.43GV/m is added at the start of simulation and is switched off at 5001th interval with the temperature set at 297K. The depolarisation was obtained and the continuous average of the depolarisation are calculated. Only the polarisation between 5001th and 100000th is plotted because the values in that range are the interesting results in which polarisation decays. The FFT is carried out as previously to give the frequency dependent susceptibility.

The purpose of doing this testing is that both the field being switched on and being switched off should show the same behaviour as long as the response to an electric field is linear [7]. This comparison could only be carried out for the simulation with the same temperature and applied dc field, which is 7.43GV/m for the applied field and the temperature being 297K.

6 RESULTS

6.1 Position and trajectories of movement for the sodium ions

6.1.1 Trajectories of movement for sodium ions in three-dimensions

C++ program has been used to perform the Molecular Dynamics (MD) simulation. There are total of five C++ programs as explained in section 4.3. The first program generates the new positions, new velocities and new forces of the sodium ions for each time interval. Figure 6.1 and figure 6.2 are the results generated for two different sodium ions, the 1st and the 15th sodium ion in the hollandite model respectively. The initial conditions were temperature=273K and time step= 10^{-15} s. The program was run for 100 000 intervals and this is the second 'run' mode shown in section 5.2.3.

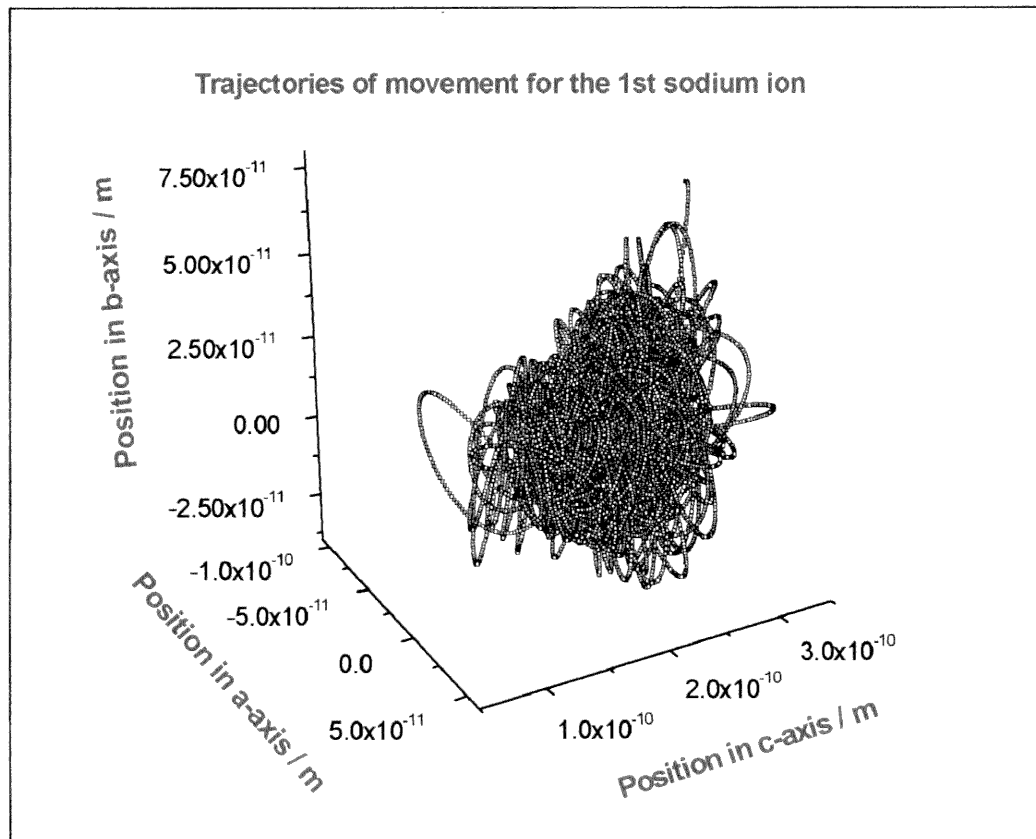


Figure 6.1: Trajectories of movement in three-dimensions of the 1st sodium ion (in the second 'run' mode) in the hollandite model.

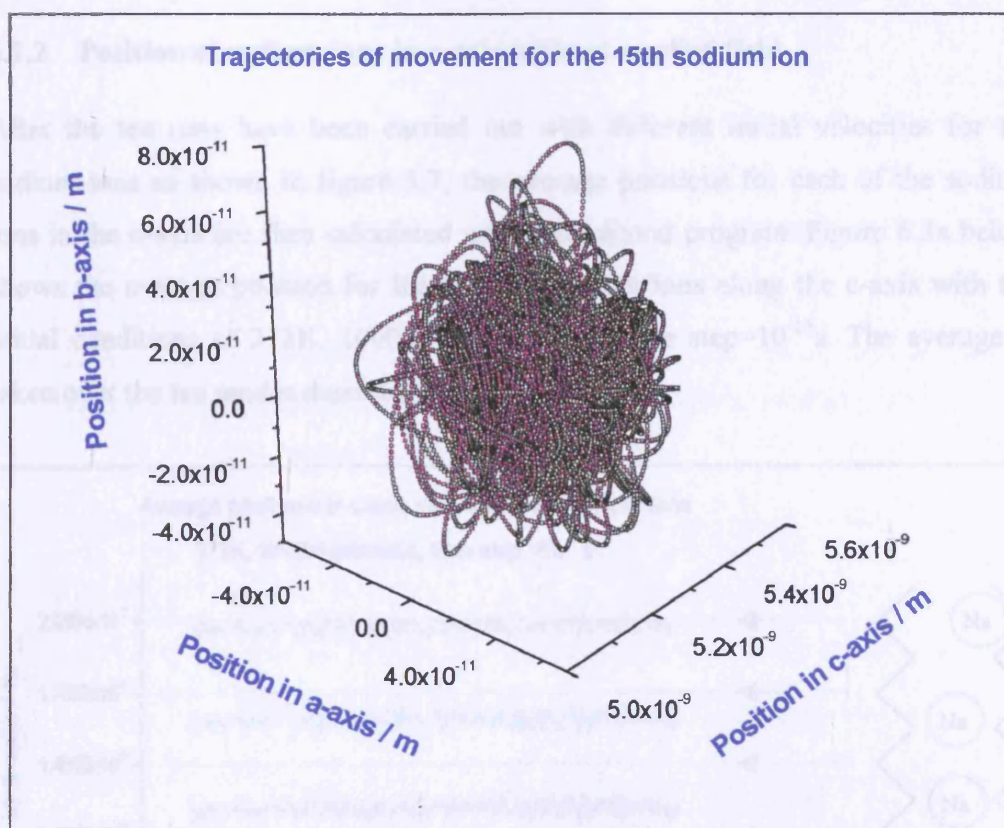


Figure 6.2: Trajectories of movement in three-dimensions of the 15th sodium ion (in the second 'run' mode) in the hollandite model.

From the figure 6.1 and 6.2 above, it is clearly shown that the sodium ions only vibrate around their equilibrium positions in the absence of electric fields. The vibration patterns for each of the sodium ions are different.

6.1.2 Position of sodium ions in c-axis without applied field

After the ten runs have been carried out with different initial velocities for the sodium ions as shown in figure 5.7, the average positions for each of the sodium ions in the c-axis are then calculated using the second program. Figure 6.3a below shows the average position for the first six sodium ions along the c-axis with the initial conditions of 273K, 100000 intervals and time step= 10^{-15} s. The average is taken over the ten modes describe in section 5.2.3.

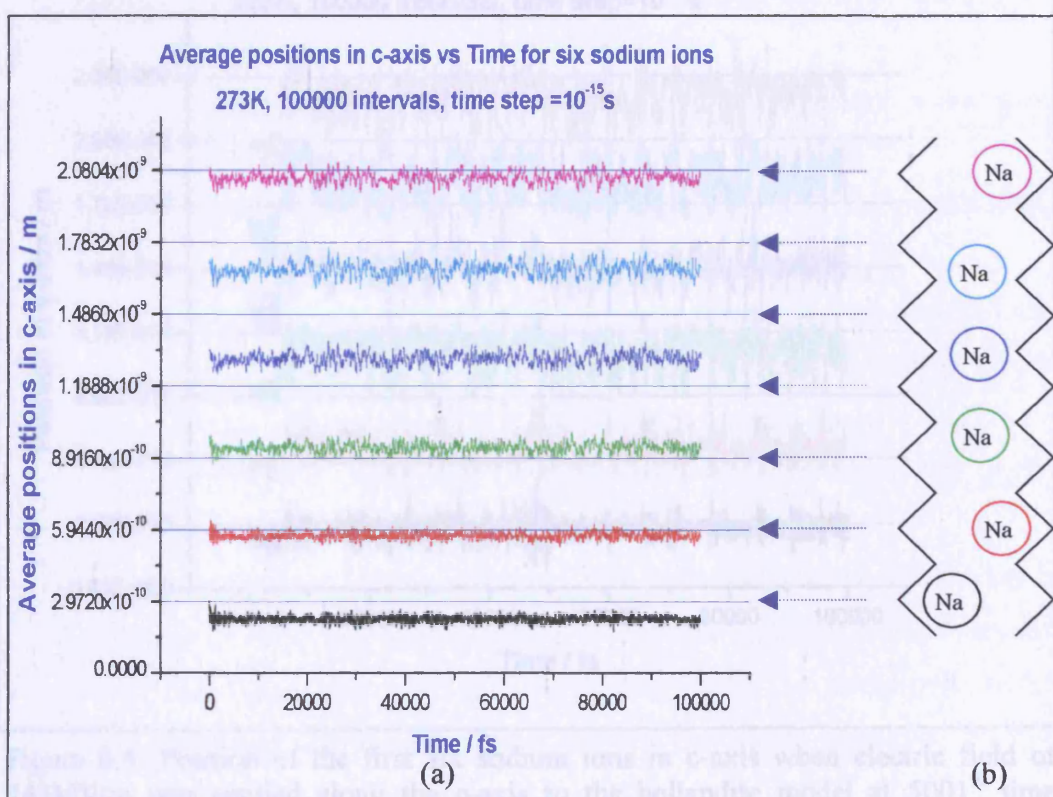


Figure 6.3: (a) The average position for the first six sodium ions in the c-axis (b) The arrangement for the first six sodium ions in the tunnel. The arrows show the alignment of the cavities in the tunnel and the graphs.

Figure 6.3a and 6.3b show the average positions of the first six sodium ions as a function of time and the positions of the first six sodium ions in the tunnel respectively. This gives a good comparison of the positions of the sodium ions throughout the 100000 intervals. The sodium ions only vibrate in their equilibrium positions depending upon where their equilibrium positions were. For example, the sixth sodium ion (pink) only vibrates around the cavity it belongs to.

6.1.3 Position of sodium ions in c-axis with applied field

In the third program, an electric field in the range of (7.43MV/m to 74.3GV/m) was applied along the c-axis to the hollandite model at the 5001th time intervals. The initial conditions for the results shown below were temperature=273K, time step= 10^{-15} s, 100 000 intervals and electric field=743MV/m.

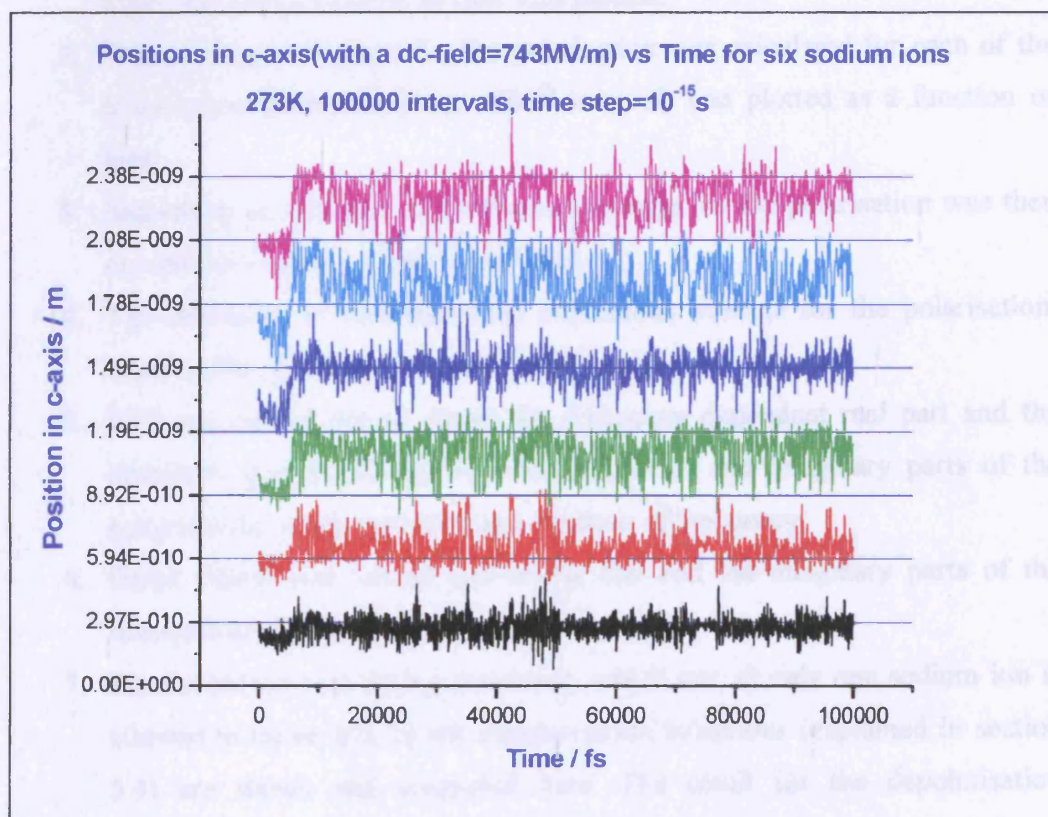


Figure 6.4: Position of the first six sodium ions in c-axis when electric field of 743MV/m was applied along the c-axis to the hollandite model at 5001th time interval.

Figure 6.4 shows the positions of the first six sodium ions as a function of time. Over the initial 5000 intervals, which was in the absence of the electric field, the sodium ions just vibrate around their equilibrium positions. Starting from 5001th intervals, the positions of the sodium ions seem to change dramatically. For example, the sixth sodium ion (pink) moved to the next cavity at some points and then back to the original cavity and then to the next cavity again.

6.2 Results obtained from the data analysis

Results from the data analysis are carried out as the procedures shown here with the “Origin” software.

1. The results of the polarisation are calculated by the fourth program for the specific temperatures and applied electric field. Then the graph of polarisation as a function of time was plotted.
2. The continuous average for the polarisation was calculated for each of the polarisation generated (from 5001th interval) and plotted as a function of time.
3. Smoothing of this plot of continuous average for the polarisation was then carried out to obtain a less ‘noisy’ plot.
4. The derivative of this smoothed continuous average for the polarisation, which is the polarisation current, was obtained.
5. FFT was carried out to obtain the frequency dependent real part and the imaginary part of the susceptibility. The real and imaginary parts of the susceptibility are then plotted as a function of frequency.
6. Graph fitting was carried out on the real and the imaginary parts of the susceptibility respectively.
7. Results for the two testing processes, which are: a) only one sodium ion is allowed to move and, b) the depolarisation behaviour (explained in section 5.4) are shown and compared here. The result for the depolarisation behaviour was also performed using the same procedures explained above.

In this section, only results with the initial conditions of temperature=273K, time step= 10^{-15} s, 100000 intervals and electric field=743MV/m are shown. The results for the other condition are summarised in table 6.1, and are discussed in chapter 7.

6.2.1 The polarisation

The polarisation in c-axis was calculated for a range of electric fields and temperatures.

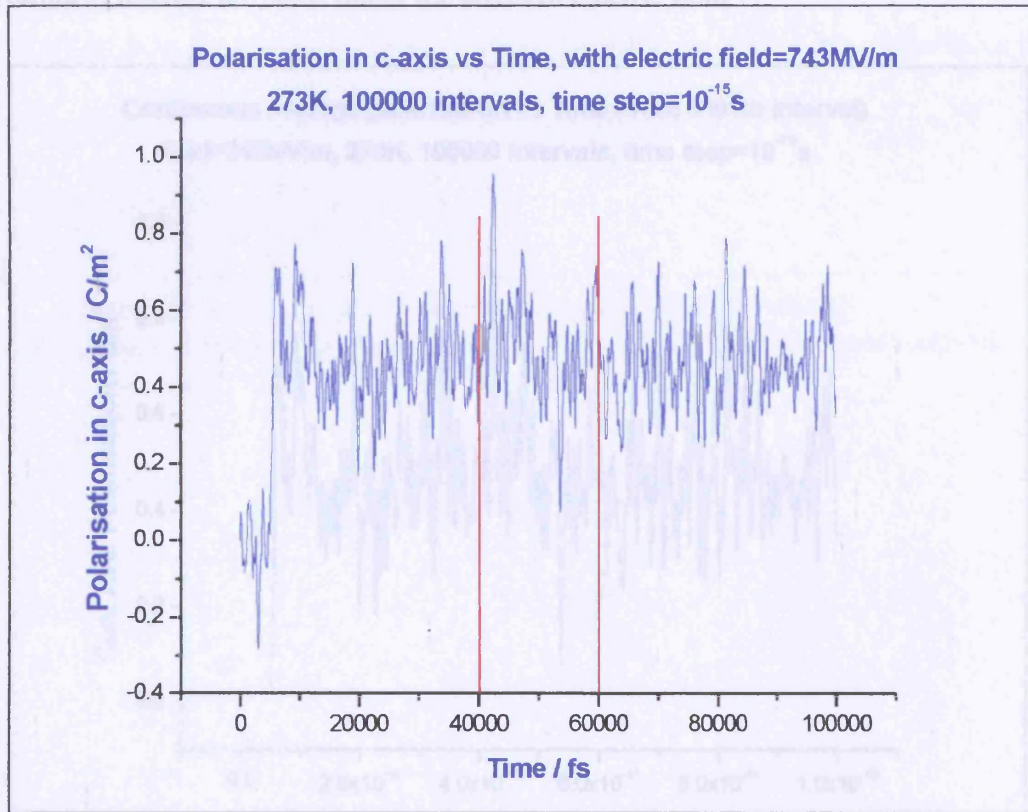


Figure 6.5: The polarisation in c-axis with an applied field of 743MV/m as a function of time.

Figure 6.4 shows the polarisation as a function of time. Over the initial 5000 intervals, the polarisation tends to fluctuate around zero polarisation. Once the electric field is applied at 5001th interval, the polarisation increases rapidly to around 0.7 C/m² and after that sudden increase, the polarisation remains at an average of that value for the rest of the time intervals. The results under different electric field are similar, but smaller field gives a smaller polarisation.

There are many details hidden in the graph, for example, the graph shows an oscillation with a period= 2×10^{-11} s, which is highlighted between the two red lines in figure 6.5.

6.2.2 The continuous average for the polarisation

A running average of the polarisation was taken over 100 intervals and only the results starting from 5001th intervals are taken into account. This is because the results of interest are those under the effect of electric field.

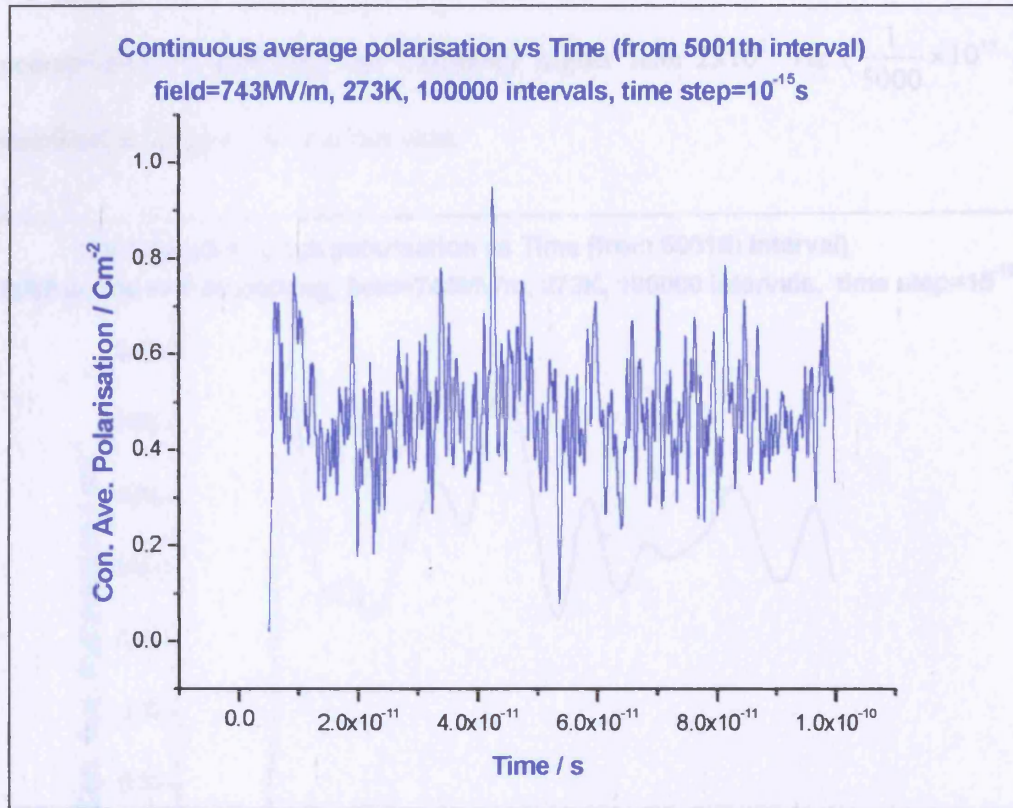


Figure 6.6: Continuous average for the polarisation with an applied field of 743MV/m as a function of time.

Figure 6.6 above gives the continuous average for the polarisation as a function of time. The plot obtained was not as noisy as the polarisation plot shown in figure 6.5, as the running average over 100 intervals eliminates vibration periods at 10⁻¹³ s and shorter.

6.2.3 The smoothing of the continuous average for the polarisation

From figure 6.6, it is clearly shown that the graph of the continuous average for the polarisation is very 'noisy'. Hence smoothing of the graph is necessary. 5000 points has been used as the number of data points considered to be smoothed at a time. FFT filter is the smoothing method, which had been used, and the smoothing is accomplished by removing the frequency higher than 2×10^{11} Hz ($\frac{1}{5000} \times 10^{15}$ as described in section 5.3.1) in our case.

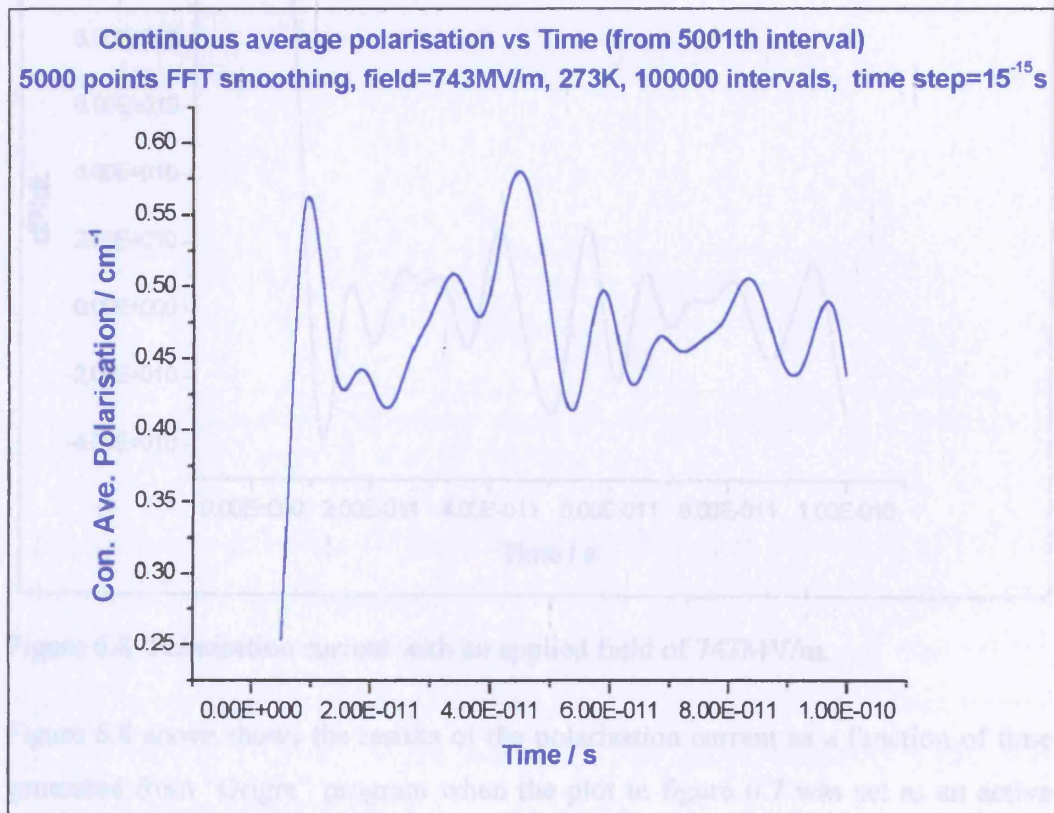


Figure 6.7: The smoothed plot for the continuous average for the polarisation with an applied field of 743MV/m as a function of time.

Figure 6.7 above shows the results of the continuous average for the polarisation after the smoothing process. The smoothing process eliminated a lot of the unwanted data.

6.2.4 The polarisation current

The polarisation current was obtained and plotted via a preset function in “origin” software. It is carried out by selecting the Analysis:Calculus:Differentiate and set the continuous average for polarisation plot as an active window.

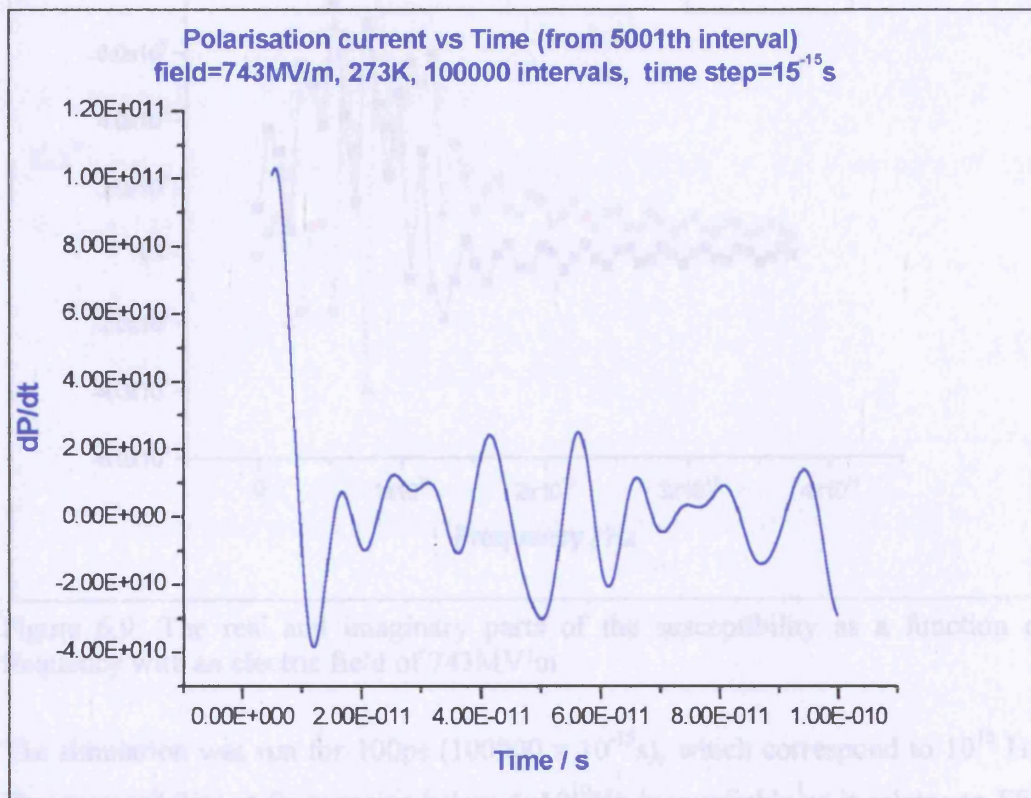


Figure 6.8: Polarisation current with an applied field of 743MV/m.

Figure 6.8 above shows the results of the polarisation current as a function of time generated from “Origin” program when the plot in figure 6.7 was set as an active window. This plot is important for obtaining the susceptibility via Fourier Transform.

6.2.5 Results of FFT generate from the “Origin” software

The real part of the susceptibility, $\chi'(f)$ and the imaginary part of the susceptibility, $\chi''(f)$ were then obtained by dividing the results generated from the FFT by the applied field and permittivity of free space. The $\chi'(f)$ and $\chi''(f)$ were then plotted as a function of frequency (obtained from the FFT) as shown in figure 6.9.

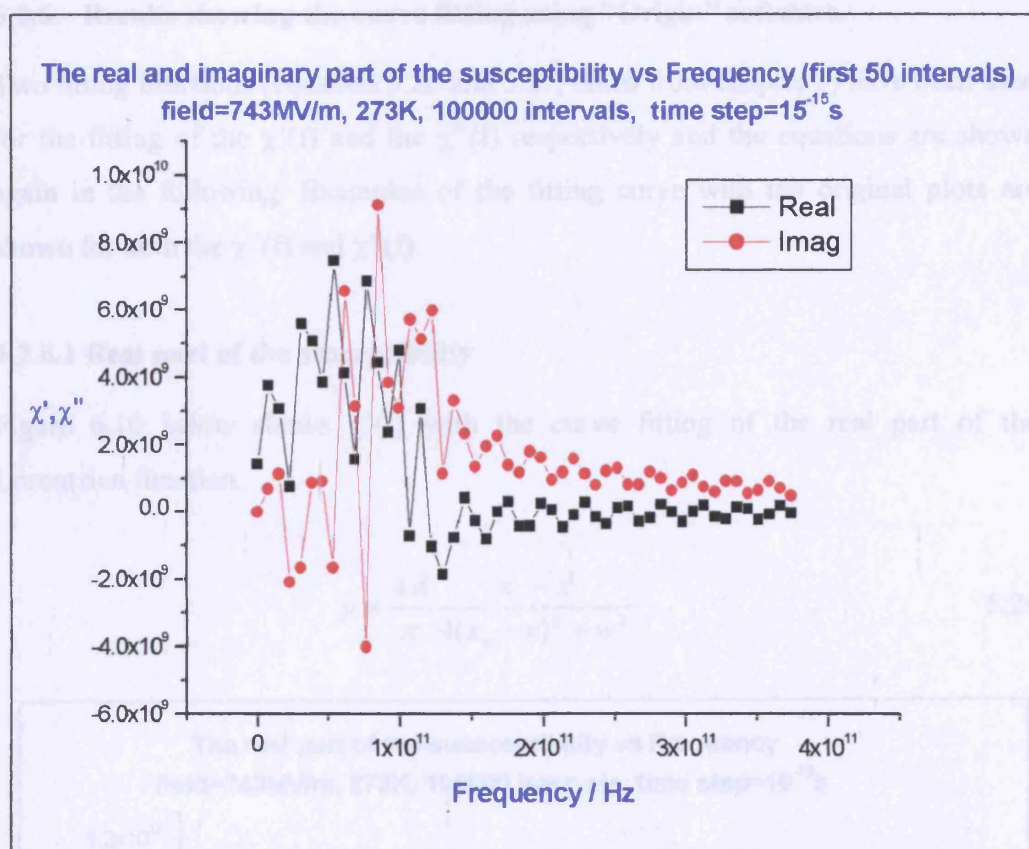


Figure 6.9: The real and imaginary parts of the susceptibility as a function of frequency with an electric field of 743MV/m.

The simulation was run for 100ps (100000×10^{-15} s), which correspond to 10^{10} Hz. The susceptibility at frequencies below 4×10^{10} Hz is unreliable as it relates to FFT extrapolations to regions, which are not consistent with the largest time (10^{-10} s) reached by the computation. At the higher frequency range, the smoothing process has removed the frequency higher than 2×10^{11} Hz; hence, frequency higher than 2×10^{11} Hz is similarly unreliable.

Figure 6.9 shows $\chi'(f)$ and $\chi''(f)$ as a function of frequency. $\chi'(f)$ goes to a positive value, then drop to a negative value and then starts to fluctuate around a smaller negative value. $\chi''(f)$ shows a peak at about 1×10^{11} Hz and the frequency of the peak lies about half way along the slope of the $\chi'(f)$. From the $\chi'(f)$, it is clearly shown that it is not a relaxation response; hence the curve fitting to the Lorentzian function which is the resonance response would have to be carried out.

6.2.6 Results showing the curve fitting using “Origin” software

Two fitting functions (equation 5.26 and 5.27, taken from chapter 5) have been used for the fitting of the $\chi'(f)$ and the $\chi''(f)$ respectively and the equations are shown again in the following. Examples of the fitting curve with the original plots are shown for both the $\chi''(f)$ and $\chi''(f)$.

6.2.6.1 Real part of the susceptibility

Figure 6.10 below shows $\chi'(f)$ with the curve fitting of the real part of the Lorentzian function.

$$y = \frac{4A}{\pi} \frac{x_c - x}{4(x_c - x)^2 + w^2} \quad 5.26$$

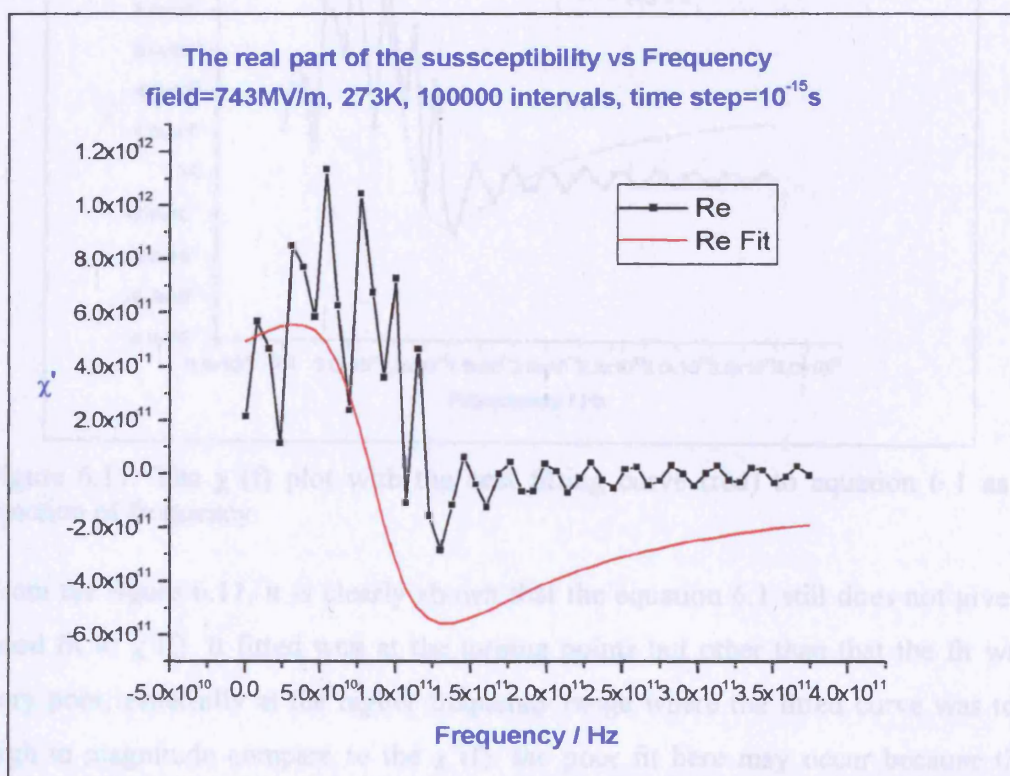


Figure 6.10: The $\chi'(f)$ plot with the best fitting curve (red) to equation 5.26 as a function of frequency.

The parameters obtained from the “Origin” program are $x_c = 8.6971 \times 10^{10}$ Hz, $w = 7.0597 \times 10^{10}$ and $A = 1.5142 \times 10^{23}$.

Figure 6.10 shows that equation 5.26 does not fit $\chi'(f)$ well. Although the shape of the fit is quite good the fitting graph is well below the results. A constant, y_0 has been introduced to the fitted function in equation 5.26 as shown below to see whether it would give a better fit.

$$y = y_0 + \frac{4A}{\pi} \frac{x_c - x}{4(x_c - x)^2 + w^2} \quad 6.1$$

The constant is added as if the responses in the higher frequencies are taken into account.

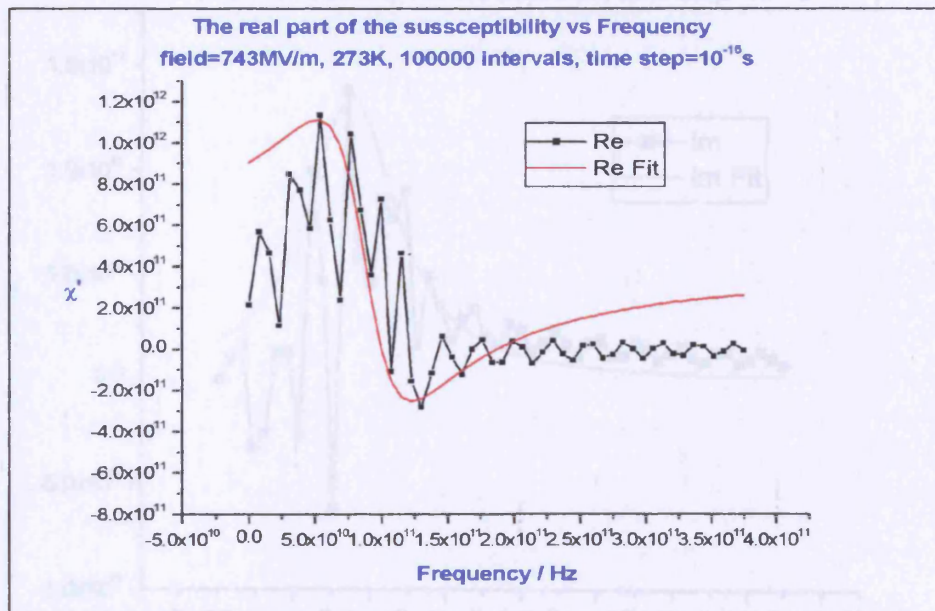


Figure 6.11: The $\chi'(f)$ plot with the best fitting curve (red) to equation 6.1 as a function of frequency.

From the figure 6.11, it is clearly shown that the equation 6.1 still does not give a good fit to $\chi'(f)$. It fitted well at the turning points but other than that the fit was very poor, especially at the higher frequency range where the fitted curve was too high in magnitude compare to the $\chi'(f)$. the poor fit here may occur because the response at these frequencies, that would give rise to y_0 , has been removed by the smoothing function.

The parameters obtained from the "Origin" program are $x_c = 8.6971 \times 10^{10}$ Hz, $w = 7.0597 \times 10^{10}$, $A = 1.5142 \times 10^{23}$ and $y_0 = 4.2944 \times 10^{11}$.

6.2.6.2 Imaginary part of the susceptibility

Figure 6.12 below shows $\chi''(f)$ with the graph fitting of the imaginary part of the Lorentzian function.

$$y = \frac{2A}{\pi} \frac{w}{4(x_c - x)^2 + w^2} \quad 5.27$$

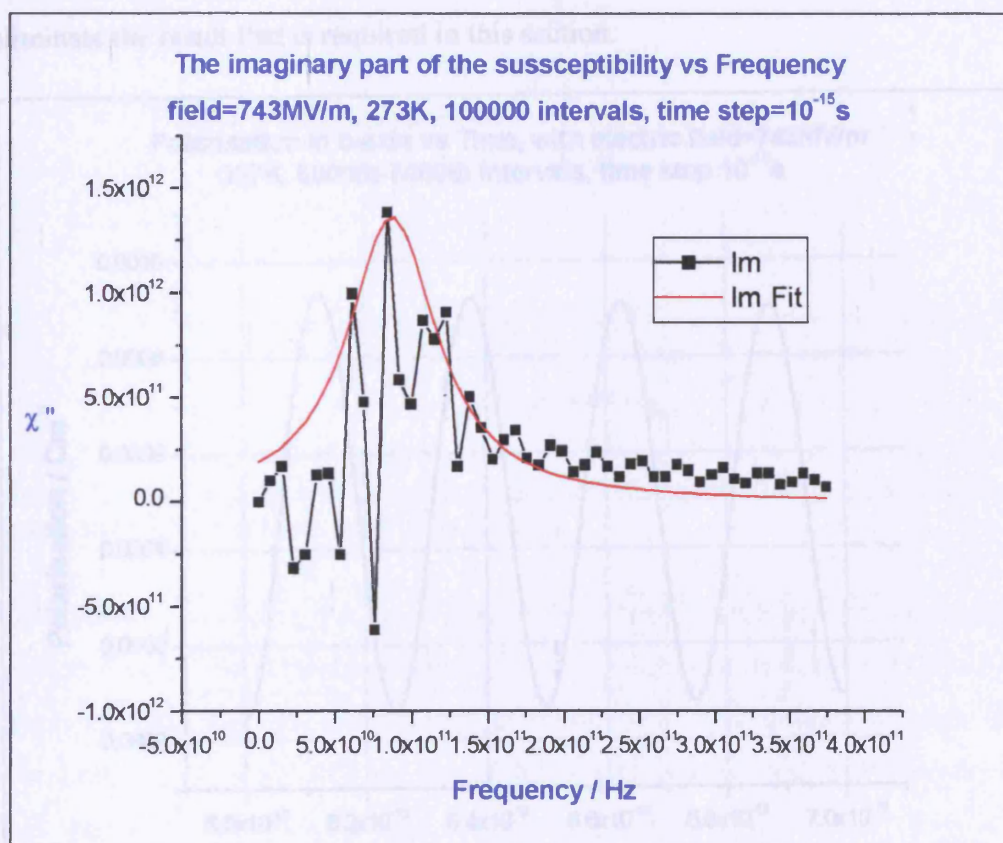


Figure 6.12: The $\chi''(f)$ plot with the best curve fitting (red) to equation 5.27 as a function of frequency.

From the figure 6.12, it is clearly shown that $\chi''(f)$ fitted equation 5.27 quite well in the frequencies above the peak frequency (resonance frequency). At the frequency below the resonance frequency, it has a steeper slope. Due to the symmetry of the Lorentzian function about x_c ; this is the best fit that can be fitted.

The parameters obtained from the "Origin" program are $x_c = 8.6971 \times 10^{10}$ Hz, $w = 7.0597 \times 10^{10}$, $A = 1.5142 \times 10^{23}$ and $y_0 = 0$.

6.3 Results for the two testing processes

6.3.1 Only one tunnel ion is allowed to move

The 9th sodium was selected to be the only sodium ion that was allowed to move in the hollandite model. The initial conditions were temperature=297K, 100000 intervals, time step= 10^{-15} s and electric field=743MV/m. The procedures in section 6.2 were carried out and the polarisation, polarisation current and FFT were obtained. Note that the continuous average was not obtained, as this would eliminate the result that is required in this section.

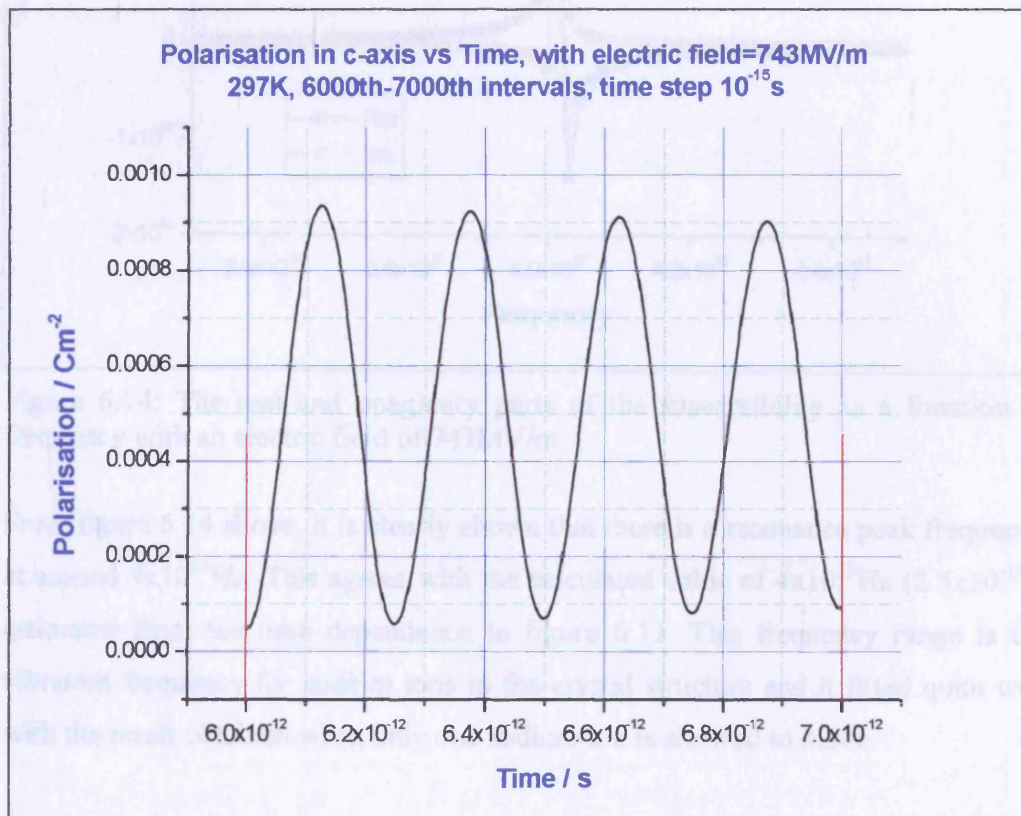


Figure 6.13: The polarisation in c-axis with an applied field of 743MV/m as a function of time.

Figure 6.13 above is just part of the polarisation plot (6000th-7000th intervals) with initial conditions of 297K, 743MV/m and time step= 10^{-15} s. The simulation was run for 100000 intervals, the polarisation obtained is the repetition of the plot shown in the figure above. There are four oscillations highlighted between the two red lines in the figure and the period of the oscillation is calculated as 2.5×10^{-13} s.

RESULTS

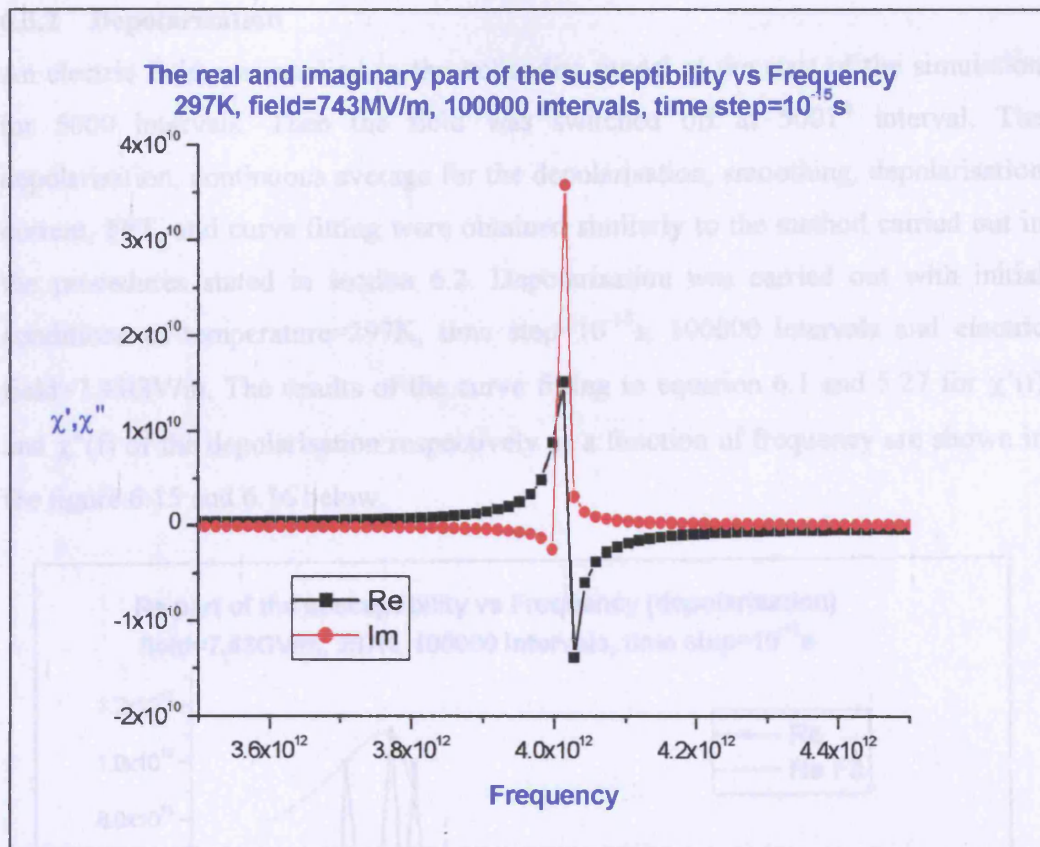


Figure 6.14: The real and imaginary parts of the susceptibility as a function of frequency with an electric field of 743MV/m.

From figure 6.14 above, it is clearly shown that there is a resonance peak frequency at around 4×10^{12} Hz. This agrees with the calculated value of 4×10^{12} Hz (2.5×10^{-13} s) estimated from the time dependence in figure 6.13. This frequency range is the vibration frequency for sodium ions in the crystal structure and it fitted quite well with the result obtained when only one sodium ion is allowed to move.

6.3.2 Depolarisation

An electric field was applied to the hollandite model at the start of the simulation for 5000 intervals. Then the field was switched off at 5001th interval. The depolarisation, continuous average for the depolarisation, smoothing, depolarisation current, FFT, and curve fitting were obtained similarly to the method carried out in the procedures stated in section 6.2. Depolarisation was carried out with initial conditions of temperature=297K, time step= 10^{-15} s, 100000 intervals and electric field=7.43GV/m. The results of the curve fitting to equation 6.1 and 5.27 for $\chi'(f)$ and $\chi''(f)$ of the depolarisation respectively as a function of frequency are shown in the figure 6.15 and 6.16 below.

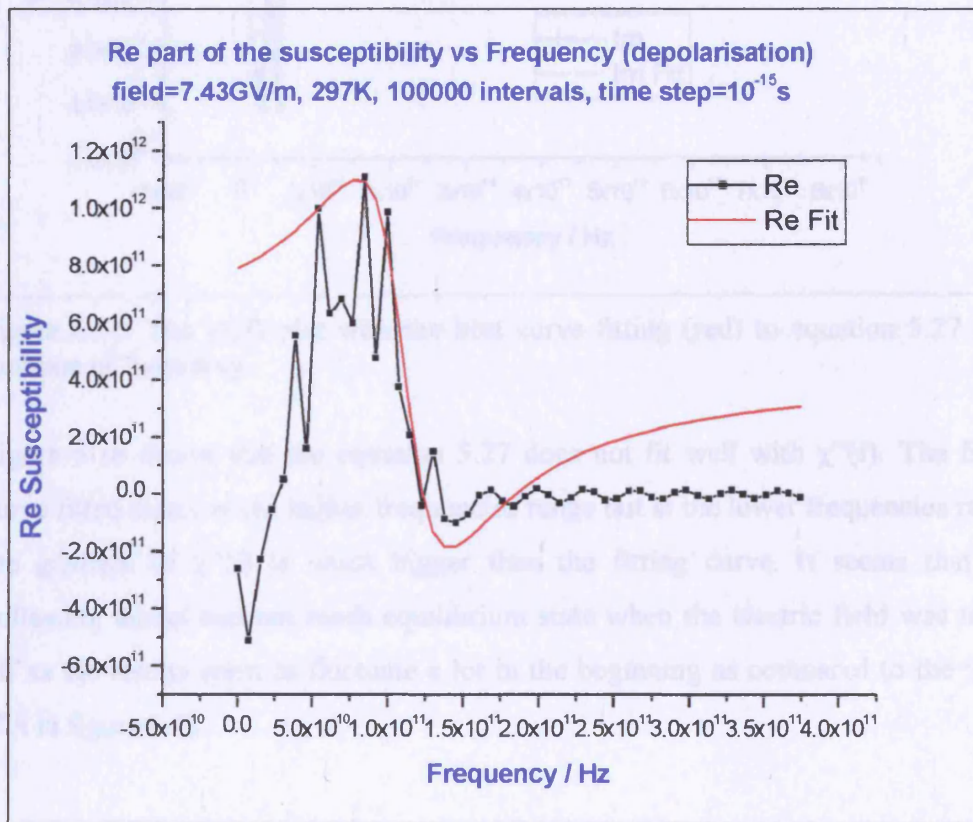


Figure 6.15: The $\chi'(f)$ plot with the best fitting curve (red) to equation 6.1 as a function of frequency.

From figure 6.15, it is clearly shown that the equation 6.1 does not fit well to $\chi'(f)$ at all. For resonance response, the magnitude for the lower frequencies range should not be lower than the magnitude in the higher frequencies range.

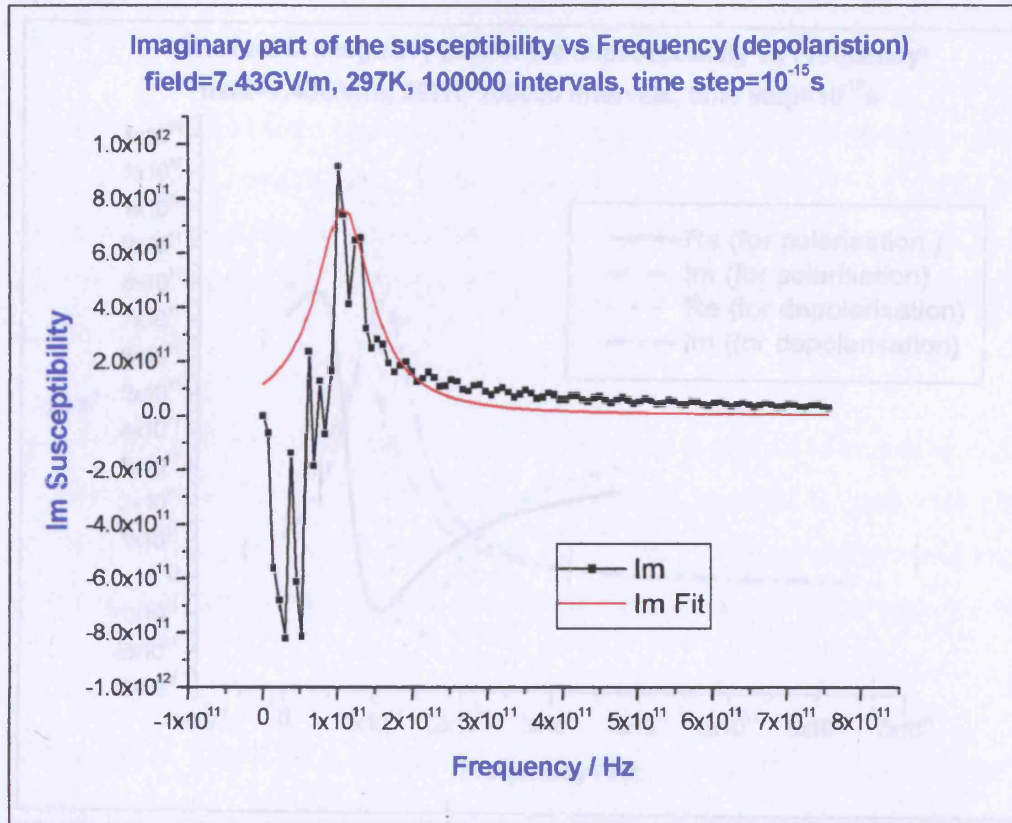


Figure 6.16: The $\chi''(f)$ plot with the best curve fitting (red) to equation 5.27 as a function of frequency.

Figure 6.16 shows that the equation 5.27 does not fit well with $\chi''(f)$. The fitted curve fitted nicely at the higher frequencies range but at the lower frequencies range, the gradient of $\chi''(f)$ is much bigger than the fitting curve. It seems that the hollandite model had not reach equilibrium state when the electric field was taken off as the results seem to fluctuate a lot in the beginning as compared to the $\chi''(f)$ plot in figure 6.12.

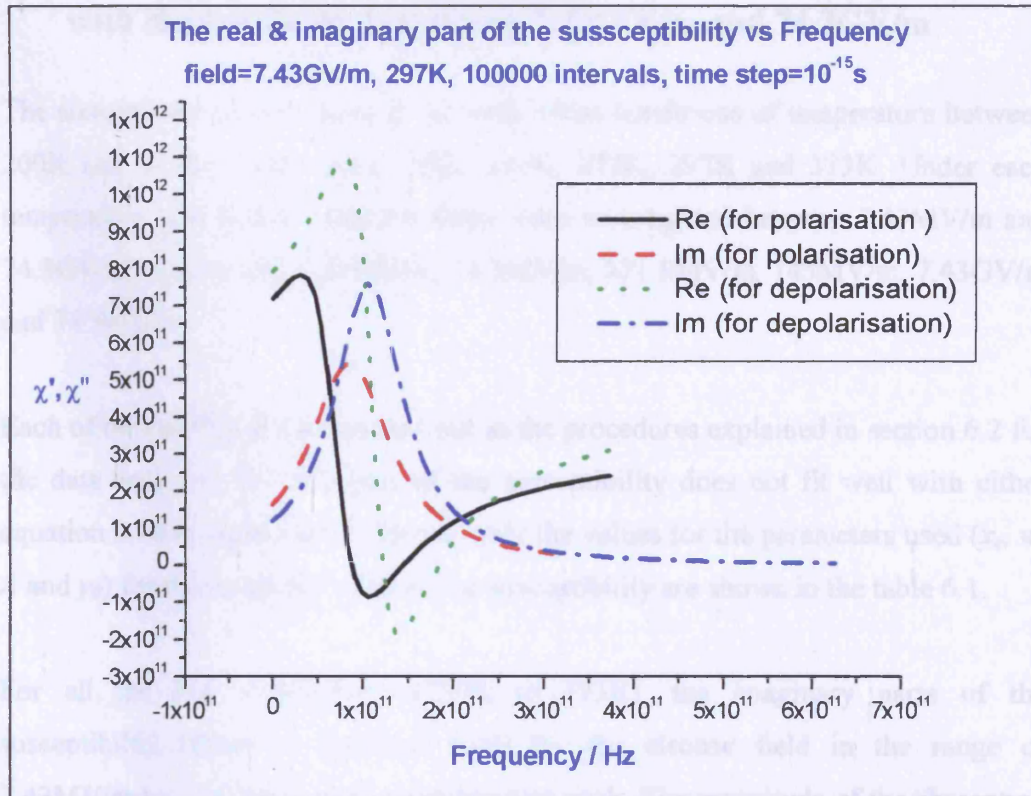


Figure 6.17: The results of the curve fitting to equation 6.1 and 5.27 for both the $\chi'(f)$ and the $\chi''(f)$ of polarisation and the depolarisation respectively with an electric field of 7.43GV/m.

From the figure 6.17 above, the $\chi'(f)$ and the $\chi''(f)$ for the polarisation and the depolarisation were different although they should be identical for a linear response. Both the magnitude of the $\chi'(f)$ and $\chi''(f)$ for the depolarisation are bigger than the $\chi'(f)$ and $\chi''(f)$ of the polarisation. The resonance frequency of $\chi''(f)$ for the polarisation is lower compared to the resonance frequency of $\chi''(f)$ for the depolarisation.

6.4 The results obtained at the temperature of 200K to 373K and with electric fields in between 7.43MV/m and 74.3GV/m

The simulation had been carried out with initial conditions of temperature between 200K and 373K, which were 200K, 250K, 273K, 297K and 373K. Under each temperature, six different electric fields were investigated between 7.43MV/m and 74.3GV/m, which were 7.43MV/m, 74.3MV/m, 371.5MV/m, 743MV/m, 7.43GV/m and 74.3GV/m.

Each of the result was then carried out as the procedures explained in section 6.2 for the data analysis. The real part of the susceptibility does not fit well with either equation 5.26 or equation 6.1. Hence, only the values for the parameters used (x_c , w , A and y_0) for the imaginary parts of the susceptibility are shown in the table 6.1.

For all the five temperature (200K to 373K), the imaginary parts of the susceptibility (fitted to equation 5.26) for the electric field in the range of 7.43MV/m to 7.43GV/m show an absorption peak. The magnitude of the absorption peak differs with temperature and electric field. At an electric field of 74.3GV/m the polarisation was found to oscillate between two values. The time period can be determined from the polarisation plot. An example of the polarisation plot at 273K is given in figure 6.18.

The “X” in the table 6.1 indicates that no fitting values were obtained for that particular temperature and electric field.

<i>Temperature</i>	<i>Field</i>	x_c / Hz	w	A
200K	7.43MV/m	4.9725×10^{10}	9.5740×10^{10}	1.2542×10^{25}
	74.3MV/m	7.6060×10^{10}	7.6709×10^{10}	1.4691×10^{24}
	371.5MV/m	8.2752×10^{10}	8.1569×10^{10}	3.1800×10^{23}
	743MV/m	6.0352×10^{10}	1.4819×10^{11}	3.0551×10^{23}
	7.43GV/m	6.8566×10^{10}	1.6000×10^{11}	1.6091×10^{23}
	74.3GV/m	X	X	X
250K	7.43MV/m	6.8981×10^{10}	6.0862×10^{10}	1.5521×10^{25}
	74.3MV/m	7.7697×10^{10}	4.5186×10^{10}	1.5553×10^{24}
	371.5MV/m	7.2492×10^{10}	1.2669×10^{11}	5.1734×10^{23}
	743MV/m	9.0780×10^{10}	1.3829×10^{11}	3.1967×10^{23}
	7.43GV/m	6.2830×10^{10}	2.6115×10^{11}	2.2998×10^{23}
	74.3GV/m	X	X	X
273K	7.43MV/m	8.0000×10^{10}	8.5186×10^{10}	1.0223×10^{25}
	74.3MV/m	6.8439×10^{10}	5.0805×10^{10}	8.7585×10^{23}
	371.5MV/m	2.6842×10^{10}	1.5083×10^{11}	5.9509×10^{23}
	743MV/m	8.6971×10^{10}	7.0597×10^{10}	1.5142×10^{23}
	7.43GV/m	7.7340×10^{10}	1.1147×10^{11}	1.3679×10^{23}
	74.3GV/m	X	X	X
297K	7.43MV/m	4.9078×10^{10}	6.2072×10^{10}	7.0296×10^{24}
	74.3MV/m	8.3584×10^{10}	8.0137×10^{10}	1.7449×10^{24}
	371.5MV/m	4.4657×10^{10}	1.0050×10^{11}	4.5638×10^{23}
	743MV/m	8.8021×10^{10}	8.5461×10^{10}	1.3662×10^{23}
	7.43GV/m	7.8825×10^{10}	1.2695×10^{11}	1.2511×10^{23}
	74.3GV/m	X	X	X
373K	7.43MV/m	3.1715×10^{10}	2.0310×10^{11}	3.7451×10^{25}
	74.3MV/m	7.5239×10^{10}	8.1134×10^{10}	1.9478×10^{24}
	371.5MV/m	6.5725×10^{10}	9.5740×10^{10}	5.4199×10^{23}
	743MV/m	7.9450×10^{10}	1.3905×10^{11}	2.8229×10^{23}
	7.43GV/m	8.2974×10^{10}	8.7608×10^{10}	1.4814×10^{23}
	74.3GV/m	X	X	X

Table 6.1: The values for the parameters used (x_c , w and A) for the curve fitting for the imaginary part of the susceptibility.

The $\chi''(f)$ plot with the best curve fitting (red) to equation 5.27 as a function of frequency for all the conditions are shown in Appendix A3.

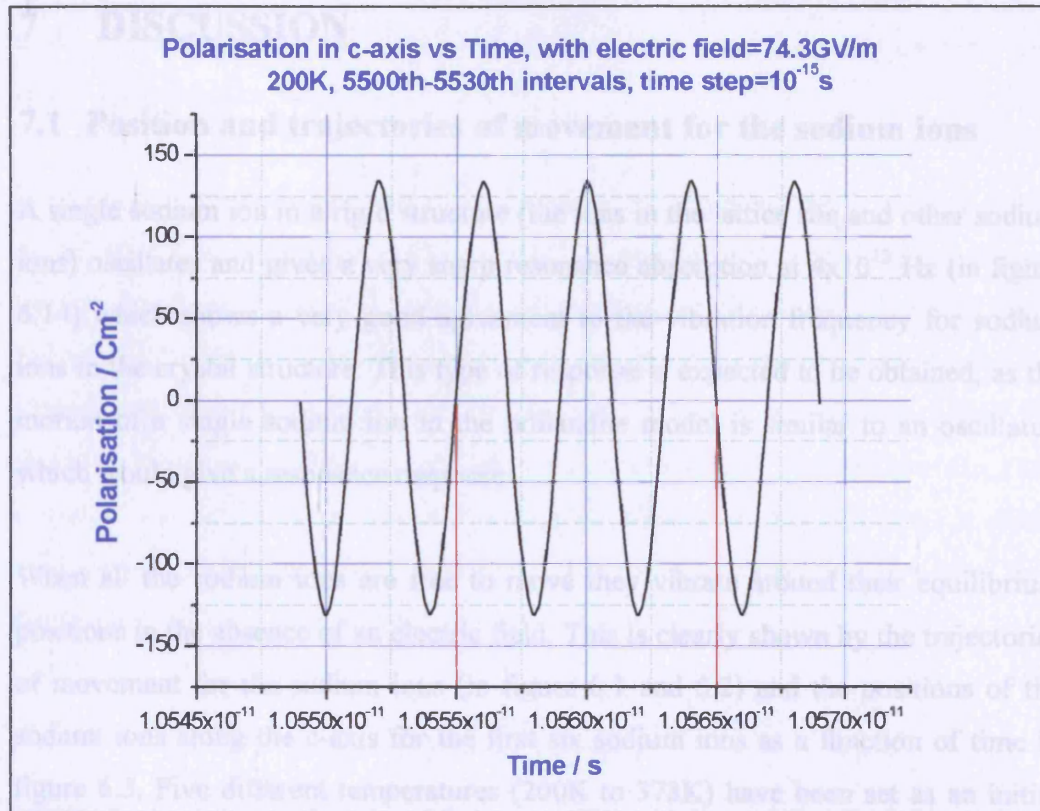


Figure 6.18: The polarisation in c-axis (5500th-5530th intervals) with an applied field of 74.3GV/m and at temperature=200K.

Figure 6.18 above is just part of the polarisation plot (5500th-5530th intervals) with initial conditions of 200K, 74.3MV/m and time step= 10^{-15} s. The polarisation plot of 100000 intervals is the replication of the plot shown above. There are two and a half oscillations highlighted between the two red lines in figure above and the period of the oscillation is 4×10^{-15} s. The time step for the simulation is 10^{-15} s, and the period of the oscillation is four times of the time step. Therefore, at high electric field, all the sodium ions were driven by this force field to move as a group and it shows a single frequency vibration.

7 DISCUSSION

7.1 Position and trajectories of movement for the sodium ions

A single sodium ion in a rigid structure (the ions in the lattice site and other sodium ions) oscillates and gives a very sharp resonance absorption at 4×10^{12} Hz (in figure 6.14) which shows a very good agreement to the vibration frequency for sodium ions in the crystal structure. This type of response is expected to be obtained, as the motion of a single sodium ion in the hollandite model is similar to an oscillator, which would give a resonance response.

When all the sodium ions are free to move they vibrate around their equilibrium positions in the absence of an electric field. This is clearly shown by the trajectories of movement for the sodium ions (in figure 6.1 and 6.2) and the positions of the sodium ions along the c-axis for the first six sodium ions as a function of time in figure 6.3. Five different temperatures (200K to 373K) have been set as an initial condition but even at the highest temperature 373K, the sodium ions still have not gained enough energy to leave the equilibrium positions for the next available sites. A comparison of the average position for the first and second sodium ions at 200K and 373K is shown in the figure 7.1 below:

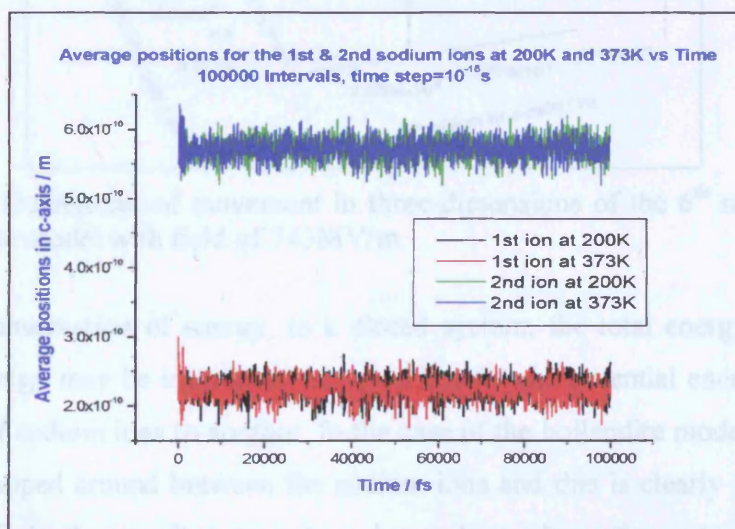


Figure 7.1: A comparison of the average positions along c-axis for the first and second sodium ions at 200K and 373K as a function of time.

At 373K, the sodium ions have more energy as the fluctuations are bigger compared to the average positions at 200K, but the sodium ions still do not have enough energy to go into the next available site.

The next part of the research was to introduce the electric field to the hollandite model. The field was applied from 5001th interval to 100000th interval; it was clearly shown in figure 6.4 that the fluctuations of the sodium ions increase dramatically at 5001th interval. This is due to the extra energy obtained by the sodium ions from the applied field. In figure 6.4, take the sixth sodium (pink) for example; it gained enough energy from the applied field to hop into the next available site, which is the next cavity. It then vibrates in this new site for about 2000 intervals until it gained enough energy to hop back to the original cavity. This can be seen in figure 7.2 below.

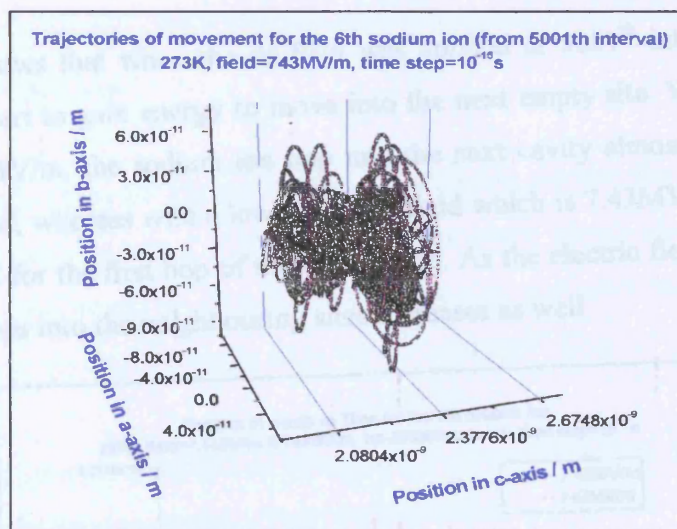


Figure 7.2: Trajectories of movement in three-dimensions of the 6th sodium ion in the hollandite model with field of 743MV/m.

From the conservation of energy, in a closed system; the total energy is constant although energy may be transferred between kinetic and potential energy and from one group of sodium ions to another. In the case of the hollandite model, the energy is being swapped around between the sodium ions and this is clearly shown in the figure 7.3. Only three sodium ions have been shown here, the rest of the sodium ions would behave in a similar way.

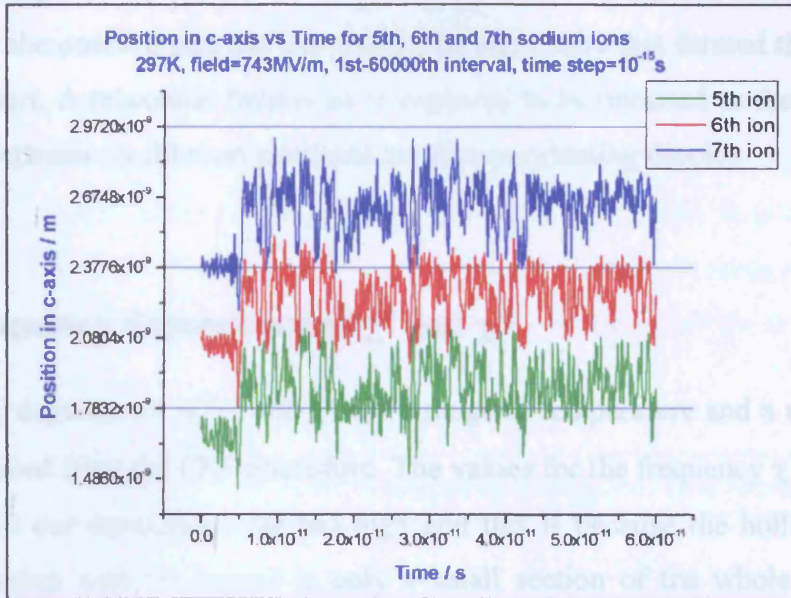


Figure 7.3: A comparison of the position in c-axis for the 5th, 6th and 7th sodium ions with field of 743MV/m. The blue line represents the cavity.

Figure 7.4 shows that when the dc-field was applied at 5001th interval, the sixth sodium ion start to gain energy to move into the next empty site. With the applied field of 743MV/m, the sodium ion hop into the next cavity almost as soon as the field is applied, whereas with a lower applied field which is 7.43MV/m, about 9×10^{-12} s is needed for the first hop of the sodium ion. As the electric field increases, the number of hops into the neighbouring sites increases as well.

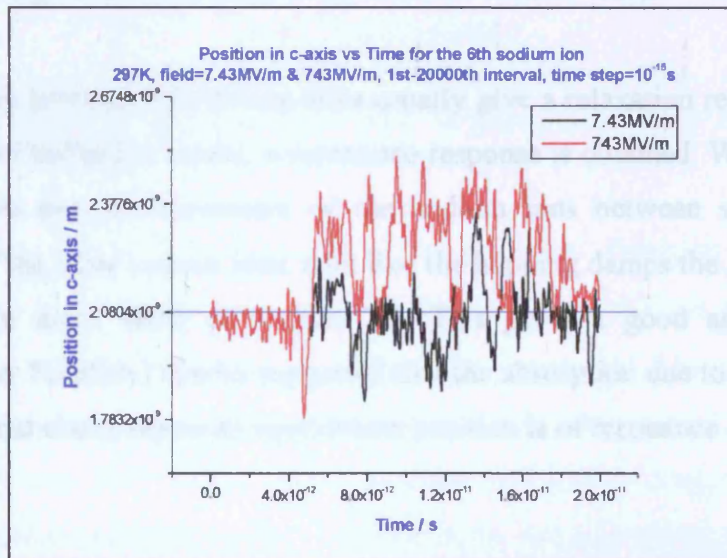


Figure 7.4: A comparison of the position in c-axis for the 6th sodium ion with field of 7.43MV/m and 743MV/m. The blue line represents the cavity.

This movement of the sodium ion is like a dipole moving around, as the sodium ion represents the positive part and the ions at the lattice site that formed the cage is the negative part. A relaxation behaviour is expected to be obtained as the sodium ions hopping between equilibrium positions are like re-orienting dipoles.

7.2 Frequency dependence of χ' and χ''

Frequency dependence of χ' and χ'' for a range of temperature and a range of field were obtained from the FFT procedure. The values for the frequency $\chi'(f)$ and $\chi''(f)$ obtained in our simulations are too high and this is because the hollandite model used (1 tunnel with 60 layers) is only a small section of the whole crystal. If a bigger model had been considered, the average displacement of the ions would be much smaller because the movement of the sodium ions are affected by the sodium ions in the other tunnels, and a smaller polarisation and smaller value of $\chi'(f)$ and $\chi''(f)$ would be obtained.

From the $\chi'(f)$ obtained (figure 6.10); it is clearly shown that $\chi'(f)$ is not a relaxation response as part of $\chi'(f)$ gives negative values. Hence the results obtained for $\chi'(f)$ and $\chi''(f)$ would be more likely to relate to a resonance response. The peak frequency for $\chi''(f)$ is in the range of $(2.7 \times 10^{10} - 8.8 \times 10^{10} \text{ Hz})$.

Ions hopping between equilibrium sites usually give a relaxation response, whereas in the case of hollandite model, a resonance response is obtained. What seems to be happening is that the movement of the sodium ions between sites change the vibration of the other sodium ions, a bit like the hopping damps the libration. This is explained in more detail in section 7.6. This gives a good agreement to the prediction by Fröhlich [1] who suggested that the absorption due to displacement of charges bound elastically to an equilibrium position is of resonance character.

In order to fit $\chi'(f)$ an additional y_0 term had been added as shown in equation 6.1. y_0 relates to the isolated higher frequency oscillations which had been removed by the smoothing process. Figure 7.5 below shows the real and imaginary parts of the susceptibility with a smoothing level of 2000 (that is 2000 points have been used as the number of data points considered to be smoothed at a time). It is clearly shown that higher frequency oscillations occur as additional resonance absorption has been observed. The lowest resonance absorption was at the same position as in the results shown in figure 6.9.

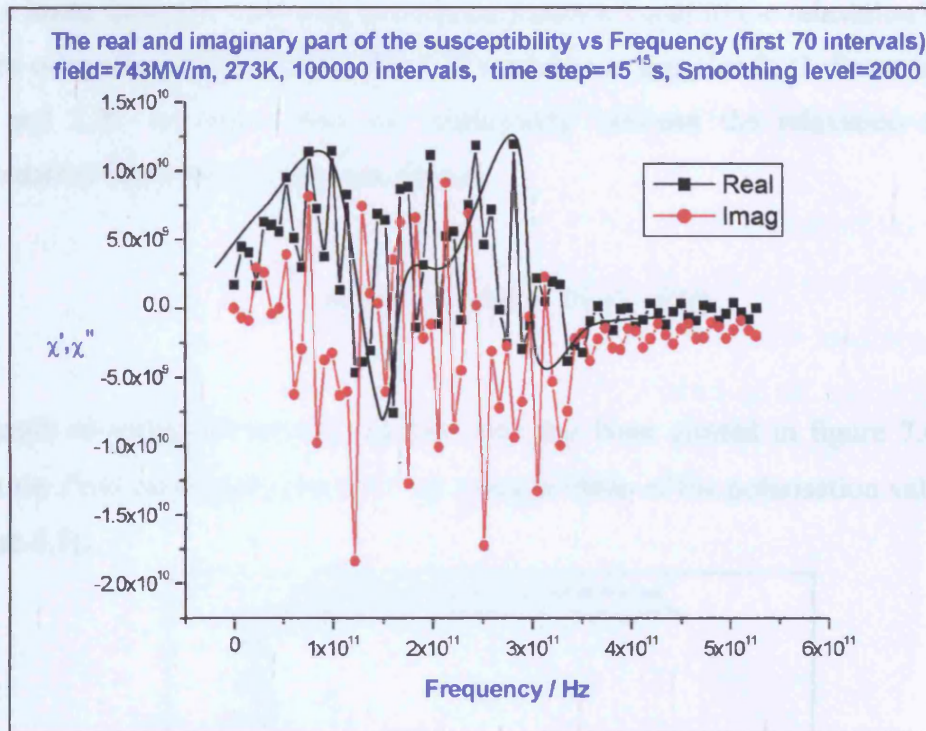


Figure 7.5: The real and imaginary parts of the susceptibility as a function of frequency with an electric field of 743MV/m.

Lorentzian function does not fit both $\chi'(f)$ and $\chi''(f)$ well. Equation 5.27 does not fit $\chi''(f)$ well as it gives a symmetrical peak curve whereas $\chi''(f)$ is not symmetrical. $\chi''(f)$ shows a steeper gradient at frequencies below the resonance absorption compared to the fitted curve (equation 5.27). Similarly, equation 5.26 would not fit $\chi'(f)$ as equation 5.26 would give a symmetrical plot in magnitude where the maximum and the minimum points have the same value in magnitude but different sign. This is understandable as the Lorentzian function is generated when a single oscillator is damped by the surroundings whereas in the hollandite model the

movement of the sodium ions between sites depend on the other sodium ions. The hopping of any of the sodium ions would damp the libration of the rest of the sodium ions. Hence, there is no specific frequency, which can be considered as a resonance. However, the Lorentzian function has been used because there is no general non-linear frequency dependent expression available and we have to try to find some ways of expressing the results.

7.3 Correlation function

For a linear dielectric response, correlation function equal to the relaxation function of the orientational polarisation (for $t > 0$) as shown in equation 2.23. From equations 2.9 and 2.25, we can obtain the relationship between the relaxation function (correlation function) and the polarisation:

$$\varphi(t) = \int_t^{\infty} \phi(t) dt \approx P(\infty) - P(t) \quad 7.1$$

A graph of relaxation function against time has been plotted in figure 7.6 below with the $P(\infty)$ estimated to be 0.47 (an average value of the polarisation value from figure 6.7).

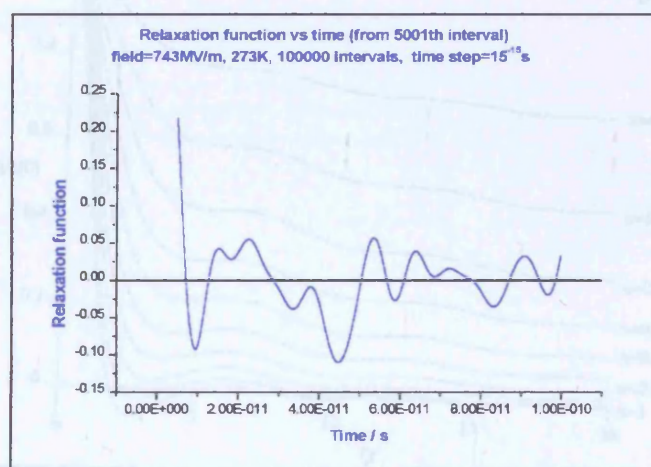


Figure 7.6: Relaxation function plotted against time with the $P(\infty)$ estimated to be 0.47.

Böttcher [2] shows a plot of dipole correlation function (fig 7.2 of [2]) for freely rotating symmetric-top molecule and if the hollandite model has a linear response, the two plots should give a similar shape. For a freely rotating symmetric-top

molecule, the correlation function initially would give a sharp decrease from positive to negative then gradually increase to above zero. This occurs for the particular case of free rotating symmetric tops because the rotation cannot randomise the component of the dipole moment that lies along the symmetry axis. The relaxation function plotted above does not give the shape similar to the correlation function of the freely rotating symmetric-top molecule. Instead it approaches zero as the time becomes large as expected for free rotation in all directions, even though the dipole formed by the sodium ion and its counter charge is a little like a rotating top. The reason is that we have restricted our calculation of the polarisation to its component along the tunnel axis. The reorientation of a component perpendicular to this axis will not be shown up in the calculation.

The plot of dP/dt shown in figure 6.8 is close in form to that of the theoretical expression for the response function $\phi(t)$ calculated for the cluster model $n \approx 1$, (see figure 1a of [3]). Unlike the symmetric top model, the cluster model does predict that $\phi(t) \rightarrow 0, t \rightarrow \infty$. The cluster model therefore appears to be the closest to our results.

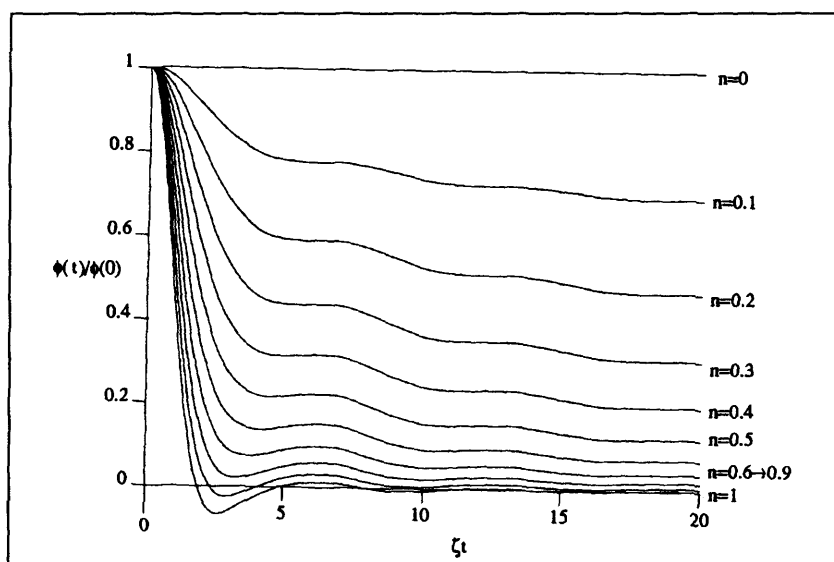


Figure 7.7: The response function $\phi(t)/\phi(0)$ as a function of ξt (Adapted with permission from Dissado, Figure 1(a), Ref [3].)

In our simulation, the reason for not using dipole correlation function in our simulation is because high fields have been applied and a non-linear response is expected to obtain.

7.4 Temperature dependence

Simulation has been carried out for a range of electric field between 7.43MV/m and 7.43GV/m and temperature between 200K and 373K. Peak frequency, which is also the resonance frequency and the resonance peak height, has been plotted as a function of temperature for a range of electric field in figure 7.8 and 7.9.

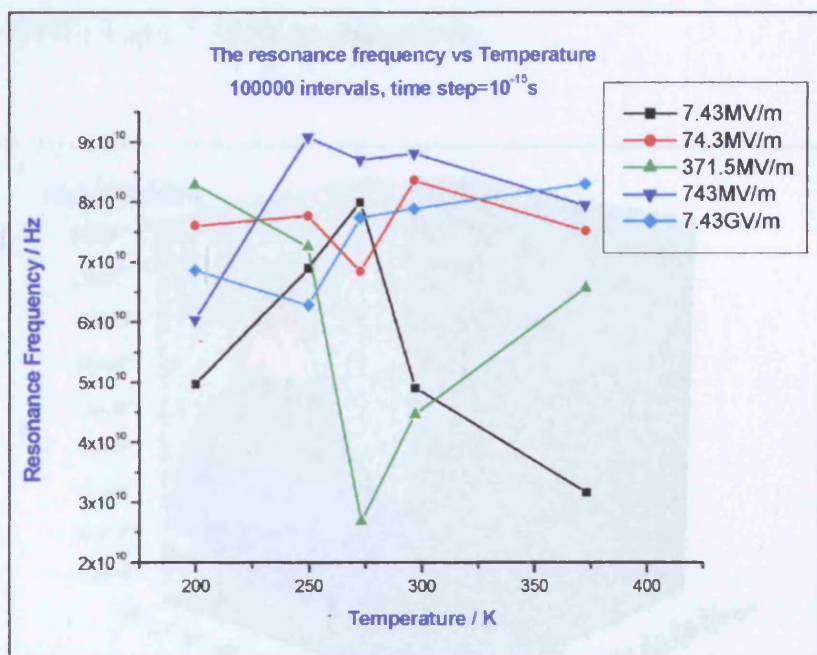


Figure 7.8: The resonance frequency as a function of temperature for a range of electric field (7.43MV/m – 7.43GV/m).

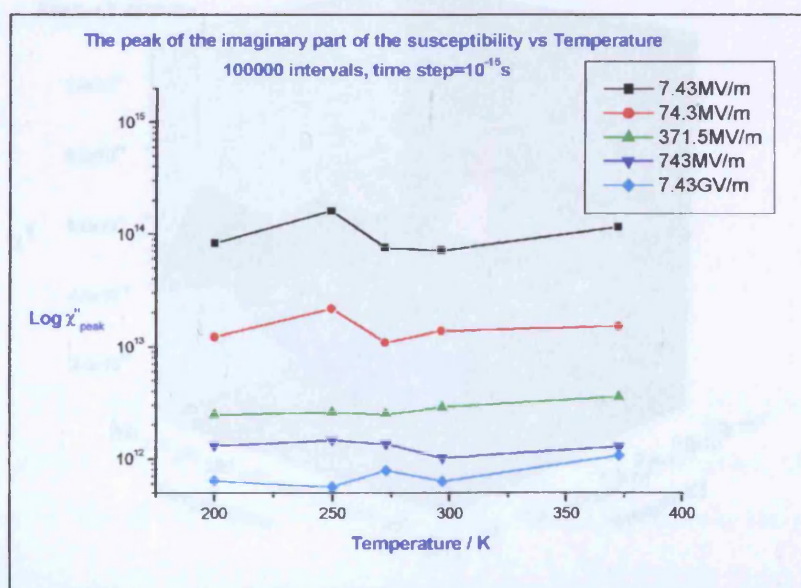


Figure 7.9: The peak of the imaginary part of the susceptibility as a function of temperature for a range of electric field (7.43MV/m – 7.43GV/m).

From figure 7.8, the resonance frequency is independent of temperature for all the different electric field applied and from figure 7.9, the resonance peak height does not change much as the temperature increases.

Figure 7.10 shows two “three dimensional” plots of the imaginary part of the susceptibility, $\chi''(f, T)$ as a function of temperature and frequency, with electric fields of 7.43MV/m and 7.43GV/m respectively.

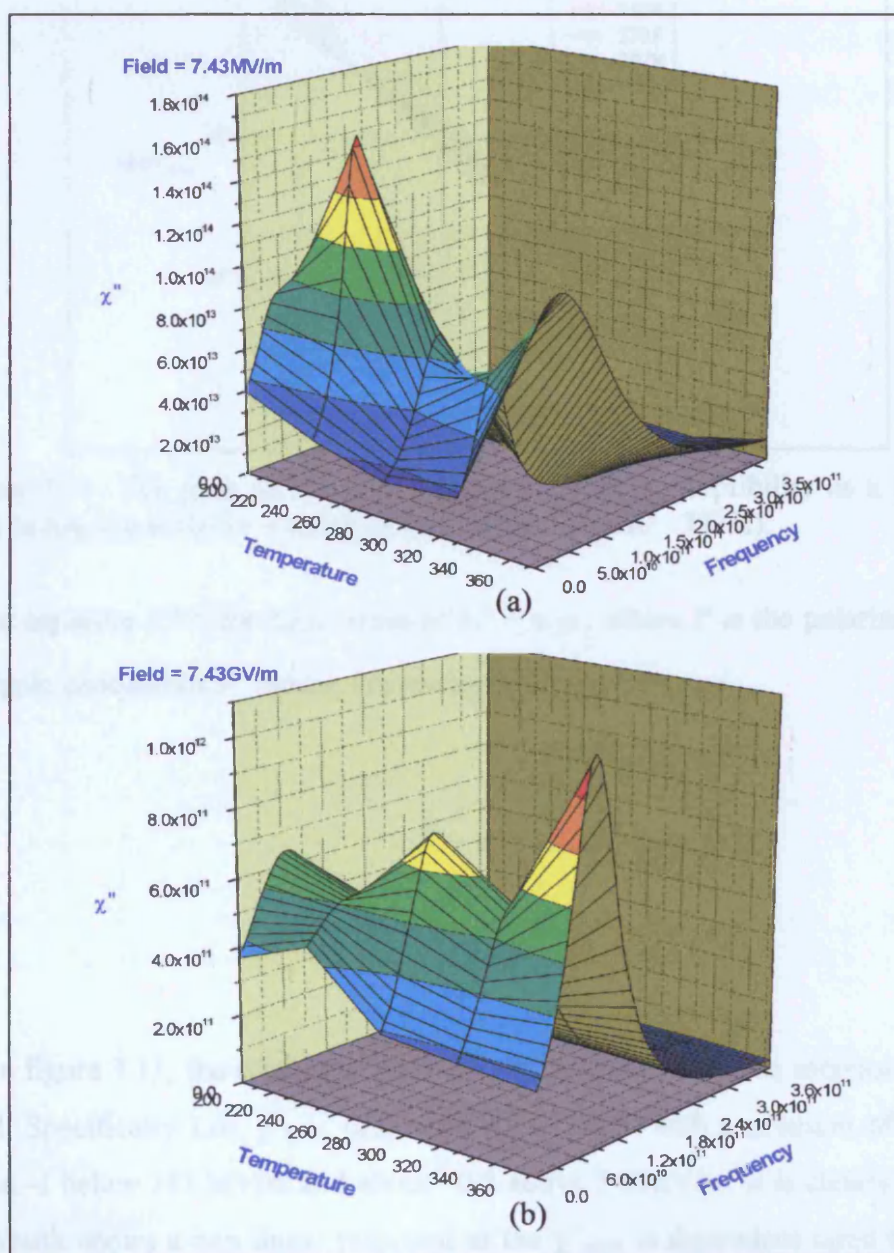


Figure 7.10: The imaginary part of the susceptibility as a function of temperature and frequency (a) field of 7.43MV/m (b) field of 7.43GV/m

7.5 Non-linear response

The field dependence of χ''_{peak} has been plotted. χ''_{peak} was plotted against electric field in a log-log scale for a range of temperature (200K – 373K) shown in figure 7.11 below.

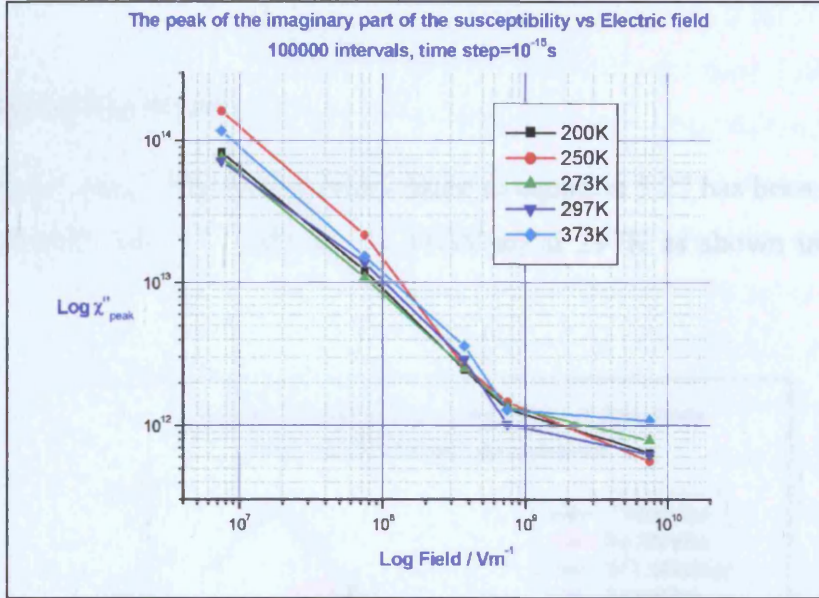


Figure 7.11: The peak of the imaginary part of the susceptibility as a function of field in log-log scale for a range of temperature (200K – 373K).

From equation 2.36, for large value of E , $P = \mu$, where P is the polarisation and μ is dipole concentration. Hence, the susceptibility, χ becomes

$$\chi = \frac{P}{E} = \frac{\mu}{E}$$

and

$$\text{Log } \chi = \text{Log } \mu - \text{Log } E \quad 7.2$$

From figure 7.11, the resonance peak height decreases with the increase of electric field. Specifically $\text{Log } \chi''_{\text{peak}}$ decreases with $\text{Log } E$ with a gradient of magnitude about -1 below 743 MV/m and about -0.2 above 743MV/m. It is clearly shown that the result shows a non-linear response as the χ''_{peak} is dependent upon the field, E . At field below 743MV/m χ''_{peak} is proportional to $1/E$ and this fitted very well to equation 7.2 as χ'' and χ have the same dependence upon field. This part of the field

range behaves as predicted by Langevin function in the high field region as shown in section 2.1.5. Fields above 743MV/m show a gradient of -0.2 and this was not predicted by Langevin function. At a field of 74.3GV/m, which is not shown in the figure 7.11 a group oscillation is found, which is also not predicted by Langevin function. This is discussed in more detail in section 7.7.

7.6 Poley absorption

The imaginary part of the susceptibility fitted to equation 5.27 has been plotted for a range of electric field (7.43MV/m – 7.43GV/m) at 297K as shown in figure 7.12 below.

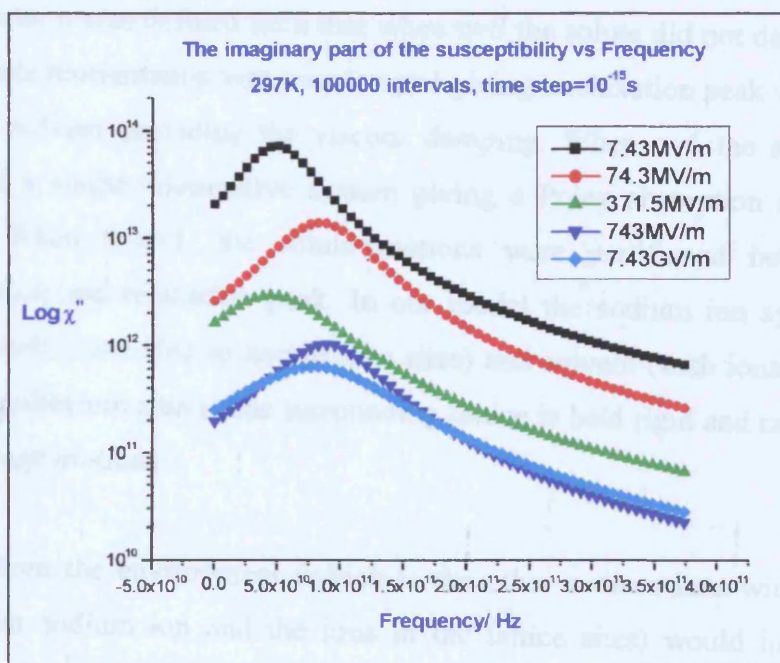


Figure 7.12: The imaginary part of the susceptibility fitted to equation 5.27 has been plotted for a range of electric field (7.43MV/m – 7.43GV/m) at 297K.

When the applied field get higher, χ'' becomes smaller and from section 7.1, more switches between sites are obtained. This indicates that the higher the field, the less ions are involved in libration and more in damping. The hopping of the sodium ions damp the libration of other sodium ions similar to the friction between the disc and annulus damps the libration in the Itinerant Oscillator (IO) model [4]. This IO model does not explain the process that happen in the hollandite model well enough

as the IO model is a harmonic model and does not take the effect of molecular translations upon the potentials and forces controlling the motion [3], a factor that molecular dynamics have shown to be important. The periodic potential model [5, 6] is also not a good approximation for the same reason.

On the other hand, the process in the hollandite model has a good agreement with the cluster model shown by Dissado [3], where the cluster model takes into account the translations of the dipole. The displacements (translations) of the solute molecule was affected by the positions of its surrounding solvent molecules (solvent cage) and vice versa to bring the group (cluster) into an equilibrium configuration. This will cause the deformation of the solvent cage so that reorientations of the solute dipole will also involve reorganisation of the solvent cage deformations. A parameter n was defined such that when $n=0$ the solute did not deform the cage and its dipole reorientation was overdamped giving a relaxation peak with the vibrations of the solvent providing the viscous damping. When $n=1$ the solute and solvent formed a single cooperative system giving a Poley absorption and no relaxation peak. When $0 < n < 1$, the solute motions were partitioned between the Poley absorption and relaxation peak. In our model the sodium ion system forms both solute (with ions able to hop to new sites) and solvent (with ions vibrating around their equilibrium sites). The surrounding lattice is held rigid and cannot be involved in the cage motions.

Force from the environment (which is the other sodium ions with respect to that particular sodium ion and the ions in the lattice sites) would initially cause the librations of the sodium ions and then the sodium ions themselves would produce a force acting on each other, and the displacement of each sodium ion would be adjusted according to the new equilibrium configuration at each interval, and hence translations changing the potentials occurs on top of the librations. The cluster model would suggest that since all sodium ions motions act cooperatively the parameter $n \approx 1$ and there would be a Poley peak with either a weak relaxation peak or none at all. Although the simulations have not been carried through to times longer than $\sim 10^{-10}$ s, this seems to be what is happening, as the ion motions include

both hopping and vibration and give just a damped resonance without any evidence of a relaxation peak.

At 297K, the resonance frequency is in the range of about $4.5 \times 10^{10} - 8.8 \times 10^{10}$ Hz for a range of electric field (7.43MV/m – 7.43GV/m). Poley [7] predicted that there is a significant power absorption in dipolar liquids at the ambient temperature in the $1.2 - 70 \text{ cm}^{-1}$ ($3.6 \times 10^{10} - 2.1 \times 10^{12}$ Hz) region and Davies [8] named the broad peak as ‘Poley absorption’. The absorption peaks obtained for the hollandite model lie at the lower end of Poley’s prediction range. This absorption is due to the libration of the sodium ions confined to the host structure undergoing displacement under the effect of electric field. The absorption calculated below the resonance frequency of a single sodium ion, which defines the edge of the quantum region. They correspond to coupled displacements of the sodium ions. It would be reasonable to assume that our calculated absorption corresponds to what would be the Poley absorption for this material.

A similar process happens in the ice clathrate shown by Johari [9], where an absorption peak was seen in the far-infrared region (7.5×10^{11} and 1.14×10^{12} Hz) and was contributed by the rotational oscillation of the tetrahydrofuran molecule, while confined to the cages of the ice clathrate crystal.

From figure 7.8, the resonance frequency is independent of temperature for all the different electric field applied. This is different from the deduction made by Johari [9] on the ice clathrate crystal and Nousekova et al [10] on the model of restricted rotator where the resonance frequency decreases with the increase in temperature due to the increase of the libration magnitude. From figure 7.9, the resonance peak height does not change much as the temperature increase. This is also different from the deduction made by both Johari [9] and Nousekova [10]. Johari reported that the resonance peak height increases with the increase in temperature whereas Nousekova said that the resonance peak height decreases with the increase in temperature. In the hollandite model, the system does not behave in a simple harmonic motion; hence, the resonance frequency and the resonance peak height may not be affected by temperature. The second reason might due to the non-linear response exhibited

by the hollandite model and this is yet to be investigated. For example, the high field susceptibility of equation 7.2 is temperature independent, whereas the linear susceptibility from the Langevin function, equation 2.35 is inversely proportional to temperature.

7.7 Group oscillation at very high field

From figure 6.18, it is clearly shown that at high electric field, which is 74.3GV/m for the hollandite model, all the sodium ions were driven by this force field to move as a group and show a single frequency vibration. The period of the oscillation is 4×10^{-15} s. This is similar to the plasma oscillation, where a gas of charges move in collective modes of vibration and Coulomb interaction being the long-range force, is capable of causing this to happen.

In the case of the hollandite model, with a smaller field, the sodium ion would just hop between empty sites next to the original site where it belongs. As the field becomes too big, the sodium ions would have enough energy to move to the empty sites located furthest away. Figure 7.13 shows an example of three sodium ions in a tunnel. When the applied field is small, the sodium ions will hop between the available empty sites next to them. The only available site for Ion1 is the one on its right, whereas Ion2 and Ion3 will have two available sites to go to and this depends on the direction of the force acting on that particular sodium ion at that moment. When the applied field is too high, this additional force will force all the sodium ions to move to the furthest available sites as shown in figure 7.13c. The reflective boundary condition at the two ends of the tunnel cause the sodium ions to vibrate between the two ends and this coherent group oscillation was generated.

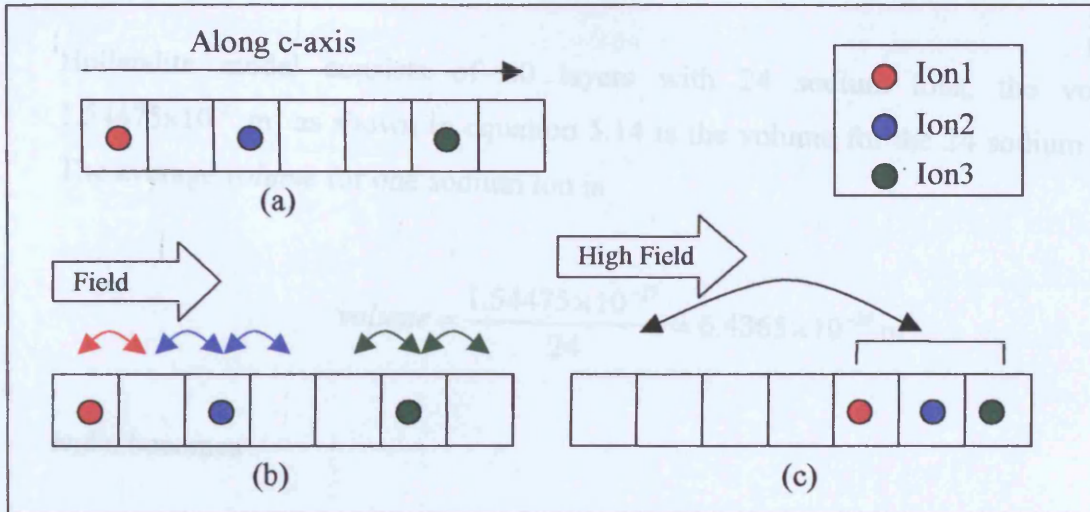


Figure 7.13: The position on three sodium ions along c-axis (a) without electric field (b) with low electric field (c) with high electric field. The square denotes the available sites for the sodium ions to move to.

The oscillatory motion of frequency is 2.5×10^{14} Hz and this falls into the infrared frequency region. With a longer tunnel, higher electric field would be needed to give coherent group oscillation, as higher force is required to push all the sodium ions to a further distance. When all the sodium ions move to one end of the tunnel under the high field, it is just like dipoles being force to align in one direction and a non-linear response occurred.

The plasma oscillation frequency is given in equation 7.3 below [11]

$$\omega_p = 2\pi f_p = \sqrt{\frac{ne^2}{m_{Na}\epsilon_0}} \quad 7.3$$

where m_{Na} is the mass for the sodium ion, which is 3.81361×10^{-26} kg (Appendix A2), e is the electron charge, ϵ_0 is the permittivity of free space and n is the concentration of sodium ions (number of sodium ions in a volume of 1m^3). The calculation of n is shown as follow:

Hollandite model consists of 60 layers with 24 sodium ions, the volume $1.54475 \times 10^{-27} \text{ m}^3$ as shown in equation 5.14 is the volume for the 24 sodium ions. The average *volume* for one sodium ion is

$$\text{volume} = \frac{1.54475 \times 10^{-27}}{24} = 6.4365 \times 10^{-29} \text{ m}^3 \quad 7.4$$

and n becomes

$$n = 1/\text{volume} = 1.5536 \times 10^{28} \text{ m}^{-3} \quad 7.5$$

Substituting equations 7.4 and 7.5 into equation 7.3. f_p obtained is $5.469 \times 10^{12} \text{ Hz}$. The estimated plasma frequency is much lower ($\sim 1/46$) of the group oscillation frequency, but is ten times higher than the frequency of χ''_{peak} calculated for lower field.

7.8 Very short pulse excitation

Figure 6.17 shows the comparison of $\chi'(f)$ and $\chi''(f)$ for the polarisation and depolarisation at 297K with an electric field of 7.43GV/m. It is clearly shown that the susceptibility plots for the polarisation and the depolarisation are not identical. The reason for this is that, in the depolarisation testing process, the initial short period of polarisation, about 5ps (5000 intervals $\times 10^{-15}\text{s}$) has not allowed the longer period collective modes of the many-body system of sodium ions to develop. Consequently, they do not show up in the depolarisation and the resonance frequency moves to higher values as shown in figure 6.17. The best way to obtain the depolarisation is to let the system reach equilibrium for the first 5000 intervals, and then field is applied at 5001th interval until the 100000th interval and switched off the field at 100001th interval and leave for another 100000 intervals. The polarisation obtained from 5001th interval to 100000th interval and the depolarisation obtained from 100001th interval should give identical results.

The $\chi'(f)$ and $\chi''(f)$ shown in figure 6.15 and 6.16 respectively would be more likely to show the results given under the effect of high electric pulse for 5ps rather than showing the depolarisation effect. From the curve fitting for $\chi'(f)$ and $\chi''(f)$ shown in figure 6.15 and 6.16, it is clearly shown that the equation 6.1 and 5.27 do not fit well to $\chi'(f)$ and $\chi''(f)$. $\chi'(f)$ shows a sharper resonance effect. $\chi''(f)$ gives a higher peak and the full width at $\frac{1}{2}$ maximum (9.1027×10^{10}) is smaller than the full width at $\frac{1}{2}$ maximum (1.2695×10^{11}) for the polarisation of a step-field under the same conditions.

8 CONCLUSIONS AND FURTHER WORK

It has been shown that our hollandite model gives a good approximation to the dielectric response of polar liquids in the far-infrared frequency region. Some conclusions have been made as follow:

- The susceptibility shows an absorption peak $\chi''(f)_{\text{peak}}$ in the frequency region between 4.5×10^{10} and 8.8×10^{10} Hz at 297K. This fitted very well with Poley's prediction of an absorption typically observed in polar liquids in the $1.2 - 70 \text{ cm}^{-1}$ ($3.6 \times 10^{10} - 2.1 \times 10^{12}$ Hz) region at room temperature.
- The frequency dependence χ' and χ'' obtained show resonance behaviour and this is due to the movement of the sodium ions between sites change the vibration of the other sodium ions This gives a good agreement to the prediction by Fröhlich who suggested that the absorption due to displacement of charges bound elastically to an equilibrium position is of resonance character.
- The absorption peak was associated with cooperative motions of the sodium ions as suggested by the cluster model. The itinerant oscillator model does not allow for such many-body motions.
- When the applied field get higher, χ'' becomes smaller and, more switches between sites are obtained. This indicates that the higher the field, the less ions are involved in libration and more in damping. The hopping of the sodium ions damps the libration of other sodium ions.
- $\chi''(f)$ is electric field dependent. χ''_{peak} shows a non-linear response as χ''_{peak} is proportional to $1/E$ below field of 743MV/m and this fitted well with the prediction of Langevin function in high field region. At fields above 7.43GV/m, $\chi''(f)$ is still field dependent but with a smaller gradient. This was not predicted by Langevin function.
- The resonance frequency and the resonance peak height are independent of temperature at the high fields of the simulation. This contrasts with the experimental data and theoretical predictions for low fields.

- At very high field, which is 74.3GV/m in our simulation, all the sodium ions were driven by this force field to move as a group and it shows a single frequency vibration.

Further Work

In order to further the investigations, some recommendations have been shown as follow:

- A hollandite model that consists of more tunnels should be constructed, as this will give a better approximation to a real system. The values for the frequency dependence χ' and χ'' obtained in our simulations are too high. If a bigger model had been taken into account, the average displacement of the ions would be much smaller and this will give rise to a smaller polarisation and smaller value of $\chi'(f)$ and $\chi''(f)$.
- More runs have to be carried out, about 100 different runs would be good enough and the average over all the runs is then used for the calculation of the polarisation.
- Simulations could be run for a longer period, say 1000 000 intervals with the same time step of 10^{-15} s (1×10^{-9} s). With this longer time scale, we would expect to see any relaxation response in the lower frequency range.
- Vibrating lattice is used instead of a rigid lattice approximation, as this again would give a better approximation of the actual system. The change in height of the potential barrier due to displacement of ions in the lattice sites would be clearly shown.
- It would be quite interesting to see the response of the pulse excitation under high field by varying the temperatures and fields.
- Calculations could be carried out with one sodium ion replaced by a heavier ion, e.g. potassium. This would be more like a solute-solvent system, with the potassium ion forming the solute. This system could be used to check the predictions of the cluster model.
- Different boundary conditions could be used, such as periodical boundary conditions.

- Results could be analysed in time domain as some of the information might be lost in transforming the results into frequency domain.
- Perform a check on the effect of the lengthening the tube on the values of the susceptibility.

REFERENCES

Chapter 1

1. S. R. Elliott, "The Physics and Chemistry of solids", J. Wiley, Chichester, UK, pp186-187, 1998
2. M. Dixon, M. J. Gillan, "Computer Simulation in Solids", Springer-Verlag, Berlin, Germany, v166, pp275, 1982
3. A. R. West, "Basic Solid State Chemistry", Wiley, Chichester, UK, 1988
4. Y. Michiue, M. Watanabe, "Molecular dynamics simulation of sodium ions in one-dimensional tunnel structure of hollandite-type", Journal Physics Chemistry Solids, v57, pp547-551, 1996
5. Y. Michiue, M. Watanabe, "X-ray analysis of sodium ion distribution in the one-dimensional tunnel of priderite", Solid State Ionics, v79, pp116-119, 1995
6. Y. Michiue, M. Watanabe, "Na_x(Ti_{8-x}Cr_x)O₁₆, priderite with sodium ions in the tunnel-structural study for stability and Na ion transport", Journal of Solid State v116, pp296-299, 1995
7. A. Byström, A. M. Byström, "The Crystal of hollandite, the related manganese oxide minerals, and α MnO₂", Acta Crystallographica, v3, pp146-154, 1950
8. J. S. Dryden, A. D. Wadsley, "The structure and dielectric properties of compounds with the formula Ba_x(Ti_{8-x}Mg_x)O₁₆", Transaction Faraday Soc., v54, 1958
9. R. W. Cheary, J. S. Dryden, "Dielectric relaxation in hollandite and rutile", Philosophical Magazine B, v64, pp709-722, 1991
10. J. Singer, H. E. Kautz, W. L. Fielder, J. S. Fordyce, "Fast ion transport in solids", ed. W. van Gool, Amsterdam, Holland, pp653-663, 1973
11. A. Yoshikado, T. Ohachi, I Taniguchi, Y. Onoda, M. Watanabe, Y. Fujiki, "AC ionic conductivity of hollandite type compounds from 100 Hz to 37.0 GHz", Solid State of Ionics, v7, pp335-344, 1982
12. A. K. Jonscher, "Dielectric relaxation in solids", Chelsea Dielectric Press Ltd, London, UK, 1983

REFERENCES

13. Y. Michiue, M. Watanabe, "Atomistic simulation study of K-hollandite: Ionic and dynamics of the linearly disordered solid", *Physical Review B*, v59, n17, pp11298-11302, 1999
14. R. M. Hill, L. A. Dissado, "The Temperature-dependence of relaxation process", *Journal of Physics C: Solid State Physics*, v15, n25, pp5171-5193, 1982
15. L. A. Dissado, J. M. Alison, "The relationship between the Poley absorption and fractional power law relaxation in the cluster model", *Journal of Molecular Liquids*, v56, pp295-316, 1993
16. J. Ph. Poley, "Microwave Dispersion of some Polar liquids", *Journal Applied. Science*, v4, pp337-387, 1955
17. M Davies, in: N. E. Hill, W. E. Vaughan, A. H. Price, M. Davies. "Dielectric properties and molecular behaviour", van Nostrand and Reinhold, London, UK, pp306, 1969
18. G. P. Johari, "Molecular inertial effects in liquids: Poley absorption, collision-induced absorption, low frequency Raman spectrum and Boson peaks", *Journal of Non-Crystalline Solids*, v307-310, pp114-127, 2002
19. G. W. Chantry, "Dielectric Measurements in the submillimeter region and a suggested interpretation of the Poley absorption", *IEEE Transactions on Microwave Theory and Technique*, vMTT-25, n6, pp496-501, 1977
20. J. M. Haile, "Molecular Dynamics Simulation, Elementary Methods", John Wiley & Son Inc., Canada, 1992
21. ¹ M. Karpus, G. A. Petsko, "Molecular dynamics simulations in biology", *Nature*, v347, pp631-639, 1990
22. A. Rahman, "Particle motions in superionic conductors", *J. Chem. Phys*, v65, pp4845-4848, 1976
23. M. J. Gilan, "Computer simulation of fast ion conductors", *Solid State Ionics*, v9&10, pp755-764, 1983
24. J. V. L. Beckers, "Ionic conductions in Na⁺- β -alumina studied by molecular dynamics simulation", Ed: K. J. van der Bent, S.W. de Leeuw, *Solid State Ionics*, v133, pp217-231, 2000
25. A. N. Cormack, C. R. A. Catlow, A. S. Nowick, "Theoretical studies of off-center Sc³⁺ impurities in CeO₂", *J.Phys. Chem Solids*, v50, pp177-181, 1989

Chapter 2

1. Duncan Q.M. Craig, "Dielectric Analysis of Pharmaceutical Systems", Taylor & Francis Ltd, London, UK, 1995
2. R. Kubo, "Statistical-mechanical theory of irreversible processes 1. General theory and simple application to magnetic and conduction problem", Journal of the Physics Society of Japan, v12, n6, pp570-586, 1957
3. C. J. F. Böttcher, "Theory of Electric Polarization, volume 1 Dielectrics in static fields", Elsevier Science Publishers B. V., Amsterdam, Netherlands, 1993
4. J. M Thiébaud, A. Weisbecker, C. Ginet, "Dielectric saturation of liquid mixtures by taking into account the molecular anisotropy", Comptes Rendus des Seances de l'Academie des Sciences, Serie C: Sciences Chimique, v267, pp661, 1968
5. P. Debye, "Polar Molecules", Dover, NY, US, 1945
6. K. S. Cole, R. H. Cole, "Dispersion and absorption in dielectric alternating current characteristics", J. Chem. Phys, v9, pp341-351, 1941
7. D. W. Davidson, R. H. Cole, "Dielectric relaxation in Glycerol, Propylene and n-Propanol," J. Chem. Phys., v19, n12, pp1480-1490, 1951
8. A. K. Jonscher, "Dielectric relaxation in solids", Chelsea Dielectric Press Ltd, London, UK, 1983
9. L. A. Dissado, R. M. Hill, "Non-exponential decay in dielectrics and dynamics of correlated systems", Nature, v279, pp685-689, 1979
10. D. K. Das-Gupta, P. C. N. Scarpa, "Modelling of Dielectric Relaxation Spectra of Polymers in the Condensed Phase", IEEE Electrical Insulation Magazine, v15, pp23-32, 1999
11. L. A. Dissado, R. M. Hill, "A cluster approach to the structure of imperfect materials and their relaxation spectroscopy", Proc. Roy Soc London, v390, pp131-180, 1983
12. J. Ph. Poley, "Microwave Dispersion of some Polar liquids", Journal of Applied Science, v4, pp337-387, 1955
13. M Davies, in: N. E. Hill, W. E. Vaughan, A. H. Price, M. Davies. "Dielectric properties and molecular behaviour", van Nostrand and Reinhold, London, UK, pp306, 1969

REFERENCES

14. H. Fröhlich, "Theory of Dielectrics, 2nd edition", Clarendon Press, Oxford, UK, pp131, 1958
15. L. A. Dissado, J. M. Alison, "The relationship between the Poley absorption and fractional power law relaxation in the cluster model", *Journal of Molecular Liquids*, v56, pp295-316, 1993
16. G. P. Johari, "Molecular inertial effects in liquids: Poley absorption, collision-induced absorption, low frequency Raman spectrum and Boson peaks", *Journal of Non-Crystalline Solids*, v307-310, pp114-127, 2002
17. G. W. Chantry, "Dielectric Measurements in the submillimeter region and a suggested interpretation of the Poley absorption", *IEEE Transactions on Microwave Theory and Technique*, vMTT-25, n6, 1977
18. T. A. Novskova, A. M. Kukebaev, V. I. Gaiduk, "One parameter model of dielectric relaxation in polar liquids", *Institute of Radio Engineering and Electronics, Academy of Sciences of USSR*, v29, n1, pp41-54, 1986
19. J. K. Vij and F. Hufnagel, in "Advances in Chemical Physics: Dynamical processes in Condensed Matter", Ed. M. W. Evans, (J. Wiley and Sons, NY, 1985) LXIII, pp775
20. E. Praestgaard, and N. G. van Kampen, "A model for rotational relaxation and resonance", *Mol. Phys*, v43, pp33-45, 1981
21. W. T. Coffey, P. M. Corcoran and M. W. Evans, "On the Role of Inertial Effects and Dipole-Dipole Coupling in the Theory of the Debye and Far-Infrared Absorption of Polar Fluids", *Proc. Roy. Soc*, vA410, pp61-88, 1987
22. M. W. Evans, "Advances in Chemical Physics", Ed. I. Prigogine, S. A. Rice, (J. Wiley and Sons, NY, 1992), LXXXI, pp361
23. A. K. Jonscher, "Review article, Dielectric relaxation in solids", *Journal. of Physics D:Applied Physics*, v32, R57-R70, 1999
24. L. A. Dissado, J. C. Fothergill, "Electrical Degradation and Breakdown in Polymers", Peter Peregrinus, London, UK, 1988
25. F. Henn, S. Devautour, L. Maati, J. C. Giuntini, H. Schaefer, J. V. Zanchetta, J. Vanderschueren, "Dielectric relaxation in ionic solids: experimental evidences", *Solis State Ionics*, v136-137, pp1335-1343, 2000

Chapter 3

1. LMGP-Suite Suite of Programs for the interpretation of X-ray Experiments, by Jean laugier and Bernard Bochu, ENSP/Laboratoire des Matériaux et du Génie Physique, BP 46. 38042 Saint Martin d'Hères, France. WWW: <http://www.inpg.fr/LMGP> and <http://www.ccp14.ac.uk/tutorial/lmgp/>
2. J. M. Haile, "Molecular Dynamics Simulation, Elementary Methods", John Wiley & Son Inc., Canada, 1992
3. B. H. Flowers, E. Mendoza, "Properties of matter", Wiley, Chichester U.K., 1970
4. A. R. West, "Basic Solid State Chemistry", Wiley, Chichester U.K., pp54, 1988
5. Y. Michiue, M. Watanabe, "Molecular dynamics simulation of sodium ions in one-dimensional tunnel structure of hollandite-type", J. Phys. Chem. Solids, 57, pp547-551, 1996
6. J. S. Dryden, A. D. Wadsley, "The structure and dielectric properties of compounds with the formula $\text{Ba}_x(\text{Ti}_{8-x}\text{Mg}_x)\text{O}_{16}$ ", Transaction Faraday Society, v54, 1574-1580, 1958
7. Y. Michiue, M. Watanabe, "Molecular dynamics simulation of sodium ions in one-dimensional tunnel structure of hollandite-type", Journal Physics Chemistry Solids, v57, pp547-551, 1996
8. Y. Michiue, M. Watanabe, "X-ray analysis of sodium ion distribution in the one-dimensional tunnel of priderite", Solid State Ionics, v79, pp116-119, 1995
9. Y. Michiue, M. Watanabe, S. Yoshikado, "High-temperature X-ray study for a single crystal of the hollandite-like one-dimensional ionic conductor, $\text{Na}_x\text{Cr}_x\text{Ti}_{8-x}\text{O}_{16}$ ($x=1.7$)", Solid State Ionics, v136-137, pp939-943, 2000

Chapter 4

1. Michael J. Pont, "Software Engineering with C++ and CASE Tools", Addison Wesley, Wokingham, U.K., 1996
2. <http://www.cs.sunysb.edu/~skiena/214/lectures/lect13/lect13.html>, 1997
3. Matlab The Language of Technical Computing, The MathWorks, Inc Natick, US, 1996
4. <http://www.originlab.com/www/products/origin/index.asp>, 1992-2003
5. J. M. Haile, "Molecular Dynamics Simulation, Elementary Methods", John Wiley & Son Inc., New York, US 1992
6. <http://www.engr.iupui.edu/~reid/eet114/lab3.pdf>, 2003

Chapter 5

1. J. H. Weiner, "Classical and quantum rate theories for solids", Physical Review, V169, N3, pp570-577, 1968
2. LMGP-Suite Suite of Programs for the interpretation of X-ray Experiments, by Jean laugier and Bernard Bochu, ENSP/Laboratoire des Matériaux et du Génie Physique, BP 46. 38042 Saint Martin d'Hères, France. WWW: <http://www.inpg.fr/LMGP> and <http://www.ccpl4.ac.uk/tutorial/lmgp/>
3. Y. Michiue, M.Watanabe, "X-ray analysis of sodium ion distribution in the one-dimensional tunnel of priderite", Solid State Ionics, v79, pp116-119, 1995
4. W. J. Duffin, "Electricity and Magnetism, 4th edition", McGraw Hill Book Company, London, UK, pp282-304, 1990
5. D. Shutin, K. Witrissal, "Signal Processing and speech Communication Laboratory, handout", V21, pp1-10, 2002 and
6. <http://spsc.inw.tugraz.at/courses/dsplab/dft1/dft1.pdf>
7. W. H. William, "Numerical Recipes in C: the art of scientific computing, 2nd edition", Cambridge University Press, Cambridge UK, pp503, 1992
8. A. K. Jonscher, "Dielectric relaxation in solids", Chelsea Dielectric Press Ltd, London, UK, 1983

Chapter 7

1. H. Fröhlich, "Theory of Dielectrics, 2nd edition", Clarendon Press, Oxford, UK, pp131, 1958
2. C. J. F. Böttcher, "Theory of Electric Polarization, volume2 Dielectrics in time-dependent fields", Elsevier Science Publishers B. V., Amsterdam, Netherlands, 3rd impression, 1996
3. L. A. Dissado, J. M. Alison, "The relationship between the Poley absorption and fractional power law relaxation in the cluster model", Journal of Molecular Liquids, v56, pp295-316, 1993
4. W. T. Coffey, P. M. Corcoran and M. W. Evans, "On the Role of Inertial Effects and Dipole-Dipole Coupling in the Theory of the Debye and Far-Infrared Absorption of Polar Fluids", Proc. Roy. Soc, vA410, pp61-88, 1987
5. J. K. Vij and F. Hufnagel, in "Advances in Chemical Physics: Dynamical processes in Condensed Matter", Ed. M. W. Evans, J. Wiley and Sons, NY, 1985 LXIII, pp775
6. E. Praestgaard, and N. G. van Kampen, "A model for rotational relaxation and resonance", Mol. Phys, v43, pp33-45, 1981
7. J. Ph. Poley, "Microwave Dispersion of some Polar liquids", Journal of Applied Science, v4, pp337-387, 1955
8. M Davies, in: N. E. Hill, W. E. Vaughan, A. H. Price, M. Davies. "Dielectric properties and molecular behaviour", van Nostrand and Reinhold, London, UK, pp306, 1969
9. G. P. Johari, "Molecular inertial effects in liquids: Poley absorption, collision-induced absorption, low frequency Raman spectrum and Boson peaks", Journal of Non-Crystalline Solids, v307-310, pp114-127, 2002
10. T. A. Novskova, A. M. Kukebaev, V. I. Gaiduk, "One parameter model of dielectric relaxation in polar liquids", Institute of Radio Engineering and Electronics, Academy of Sciences of USSR, v29, n1, pp41-54, 1986
11. J. M. Ziman, "Electron and Phonons. The theory of transport phenomena in solids", Ed. N. F. Mott, E.C. Ballard, D. M. Wilkinson, Clarendon Press, Oxford, UK, pp161-162, 1960

Appendix

A1 Positions for the titanium ions and the oxygen ions

The positions for the titanium ions and the oxygen ions in a and b-axis. The hollandite model is the repetition of the two layers shown in the figure below. The sodium ion is placed in the middle of the hollandite model just to indicate its existence and it is not at the exact position, as the exact position will depend on the position of the chromium ion, which is not shown here.

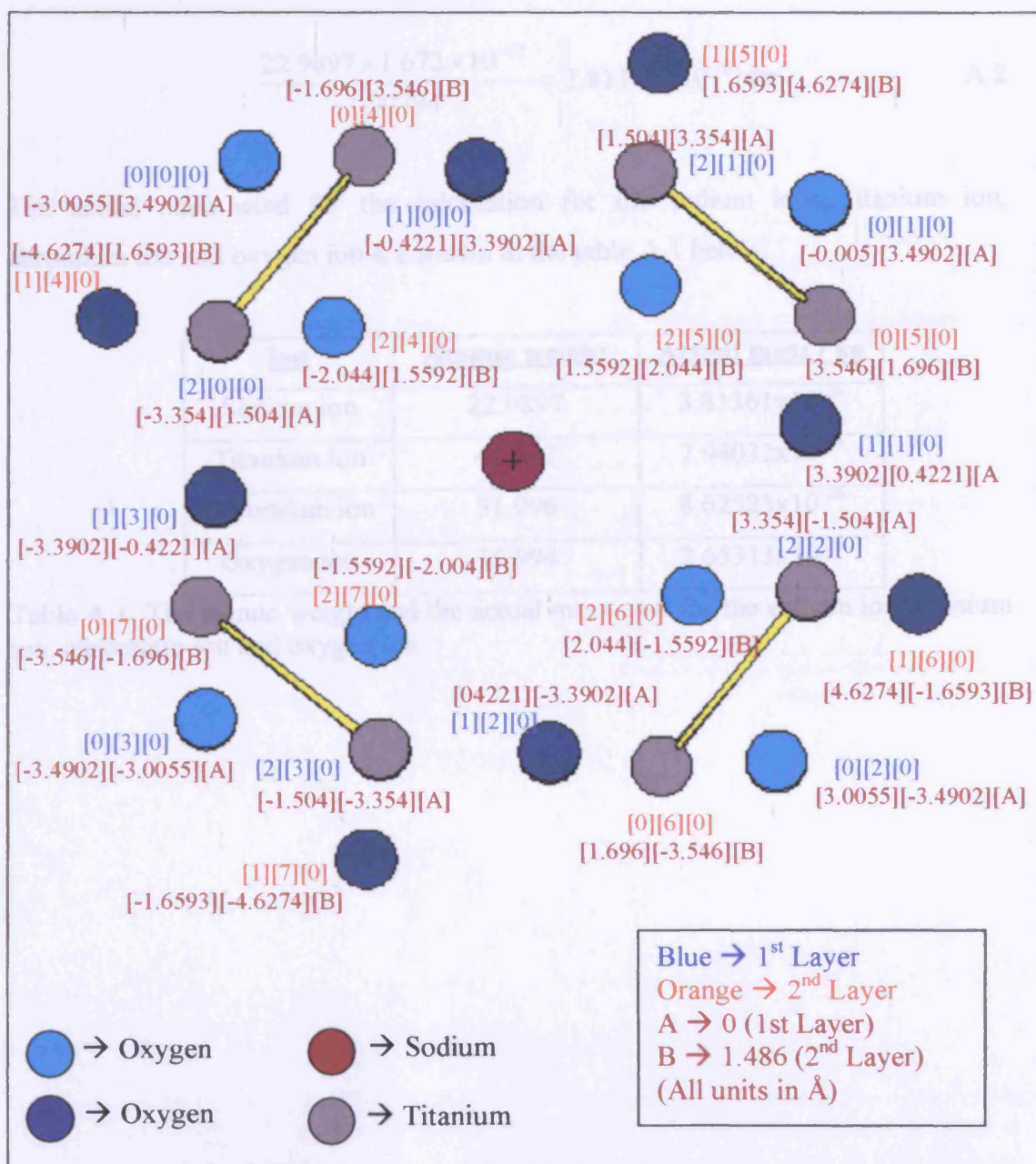


Figure A1: The positions for the titanium ions and the oxygen ions in a and b-axis.

A2 Calculation of the actual mass for the ions

The mass used in the calculation is the actual mass of the ions; the equation used is shown below:

$$\frac{\text{atomic weight of } N\text{th ion} \times \text{mass of proton}}{\text{atomic weight of Hydrogen}} \quad \text{A.1}$$

For example, the mass of the sodium ion used is

$$\frac{22.9897 \times 1.672 \times 10^{-27}}{1.00794} = 3.81361 \times 10^{-26} \text{ kg} \quad \text{A.2}$$

The actual mass used for the calculation for the sodium ions, titanium ion, chromium ion and oxygen ion are shown in the table A.1 below:

<u>Ion</u>	<u>Atomic weight</u>	<u>Actual mass / kg</u>
Sodium ion	22.9897	3.81361×10^{-26}
Titanium ion	47.867	7.94032×10^{-26}
Chromium ion	51.996	8.62525×10^{-26}
Oxygen ion	15.994	2.65313×10^{-26}

Table A.1: The atomic weight and the actual mass used for the sodium ion, titanium ion, chromium ion and oxygen ion.

A3 Results for the curve fitting in the electric field range between 7.43MV/m and 74.3GV/m and at temperature range between 200K and 373K

Figures below shows $\chi''(f)$ with the graph fitting of the imaginary part of the Lorentzian function (equation 5.27).

At temperature 200K

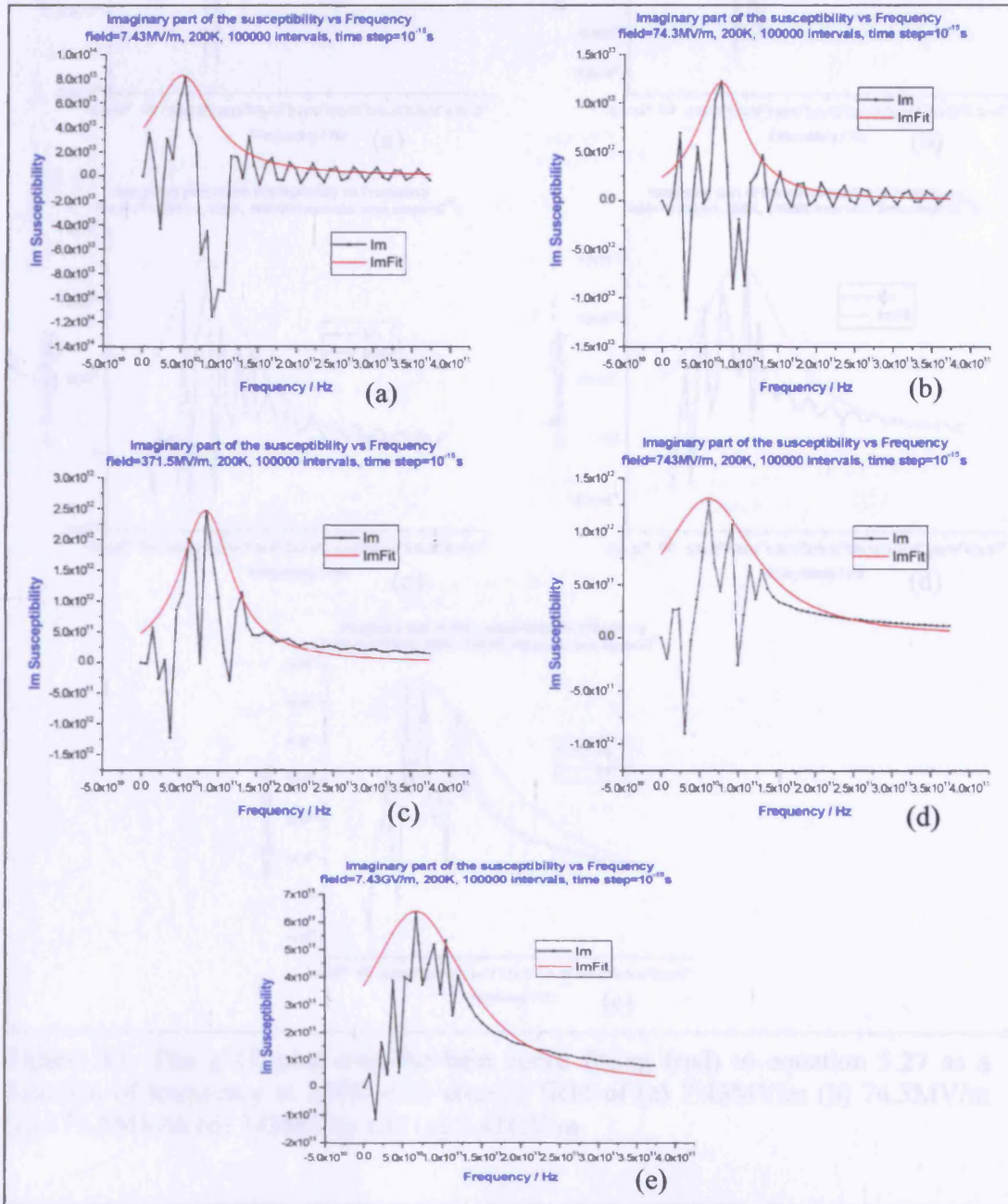


Figure A2: The $\chi''(f)$ plot with the best curve fitting (red) to equation 5.27 as a function of frequency at 200K with electric field of (a) 7.43MV/m (b) 74.3MV/m (c) 371.5MV/m (d) 743MV/m and (e) 7.43GV/m

At temperature 250K

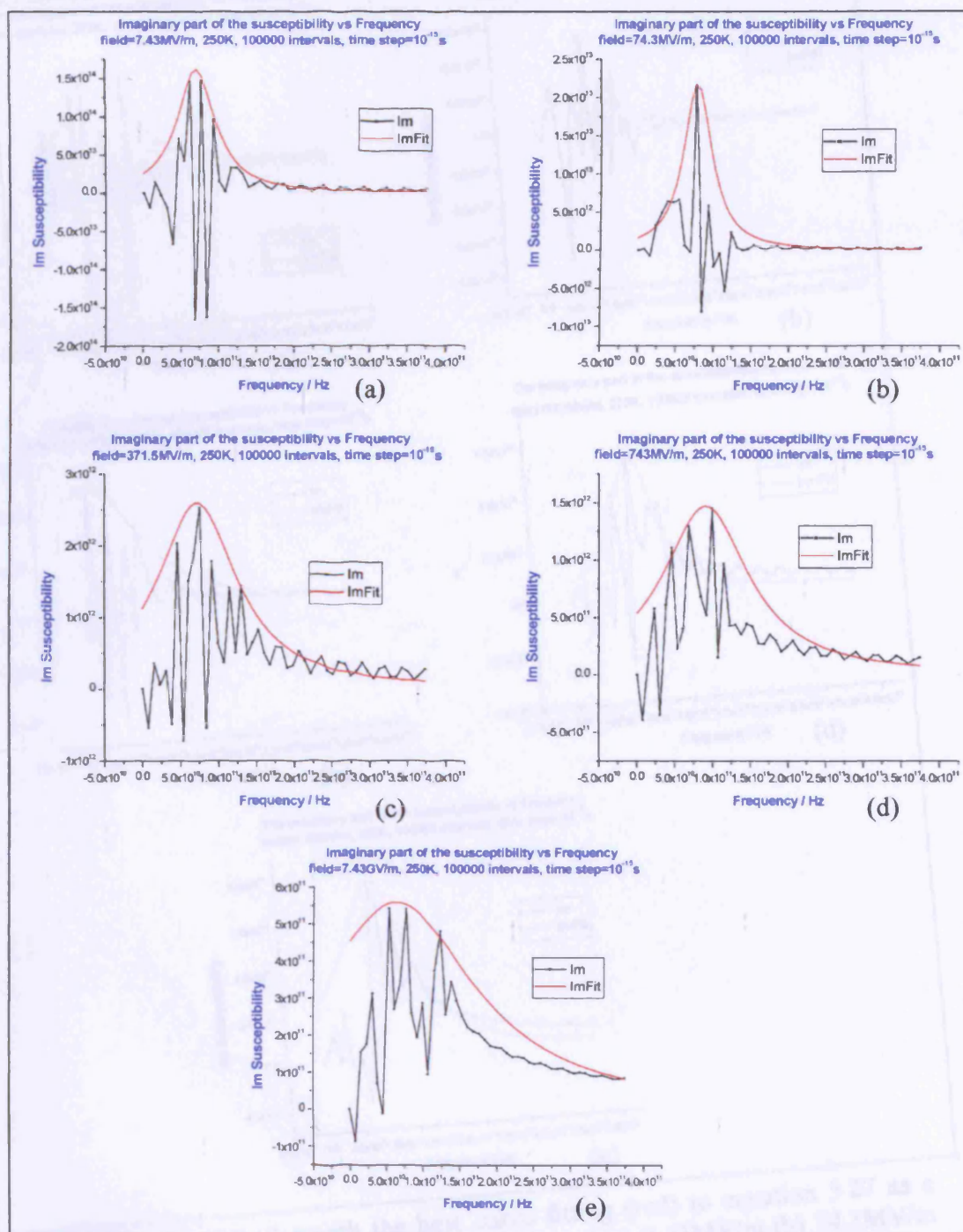


Figure A3: The $\chi''(f)$ plot with the best curve fitting (red) to equation 5.27 as a function of frequency at 250K with electric field of (a) 7.43MV/m (b) 74.3MV/m (c) 371.5MV/m (d) 743MV/m and (e) 7.43GV/m

At temperature 273K

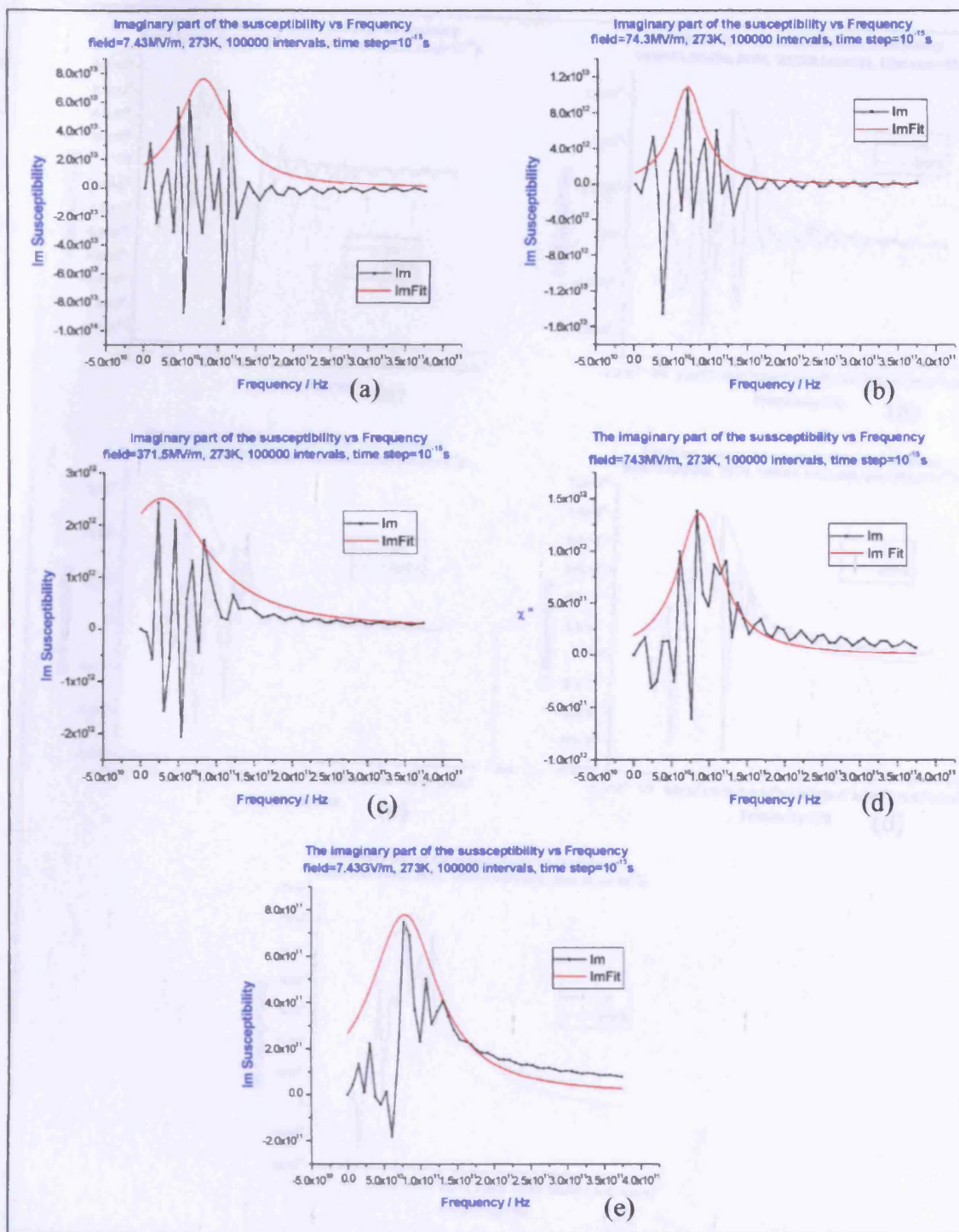


Figure A4: The $\chi''(f)$ plot with the best curve fitting (red) to equation 5.27 as a function of frequency at 273K with electric field of (a) 7.43MV/m (b) 74.3MV/m (c) 371.5MV/m (d) 743MV/m and (e) 7.43GV/m

At temperature 297K

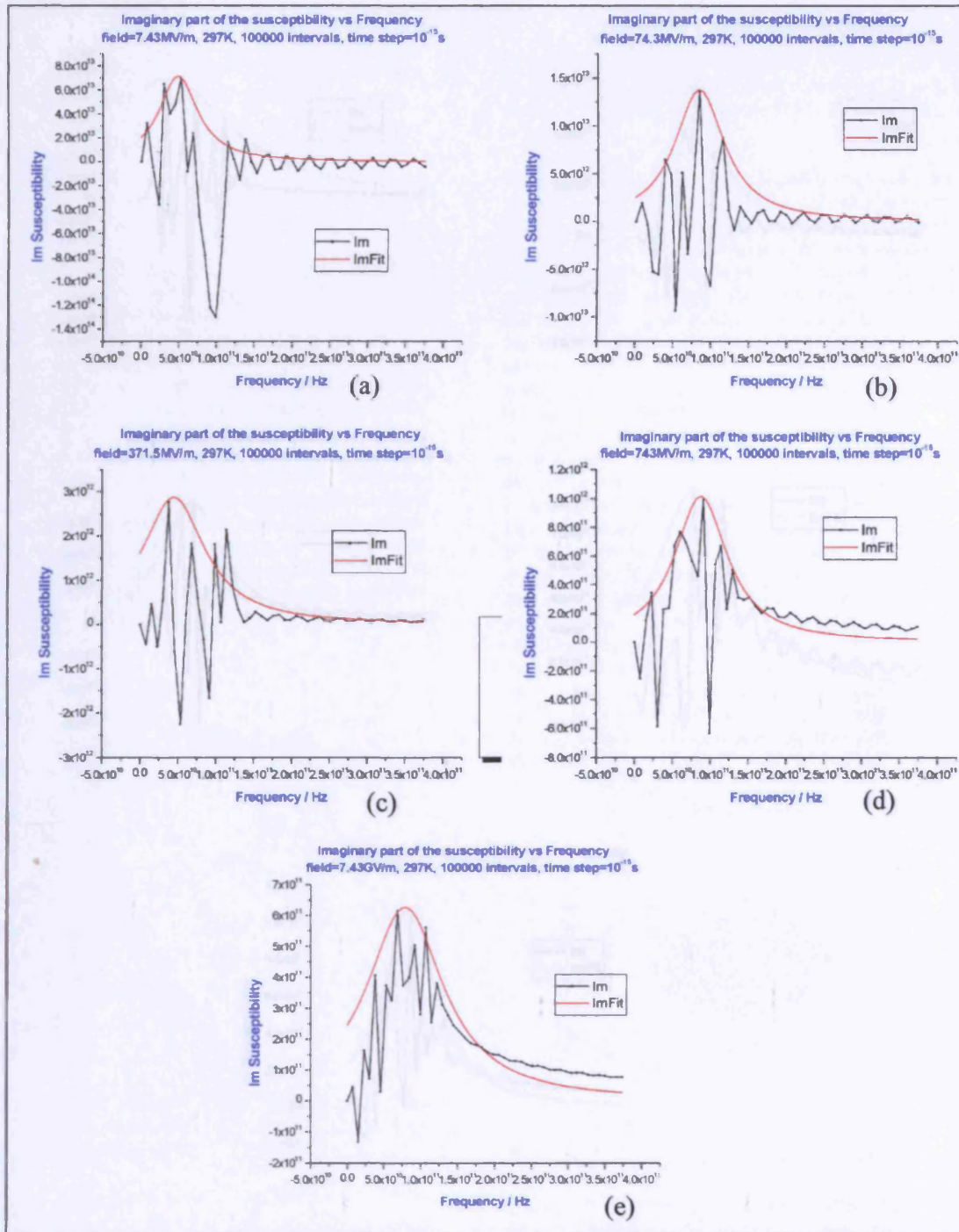


Figure A5: The $\chi''(f)$ plot with the best curve fitting (red) to equation 5.27 as a function of frequency at 297K with electric field of (a) 7.43MV/m (b) 74.3MV/m (c) 371.5MV/m (d) 743MV/m and (e) 7.43GV/m

At temperature 373K

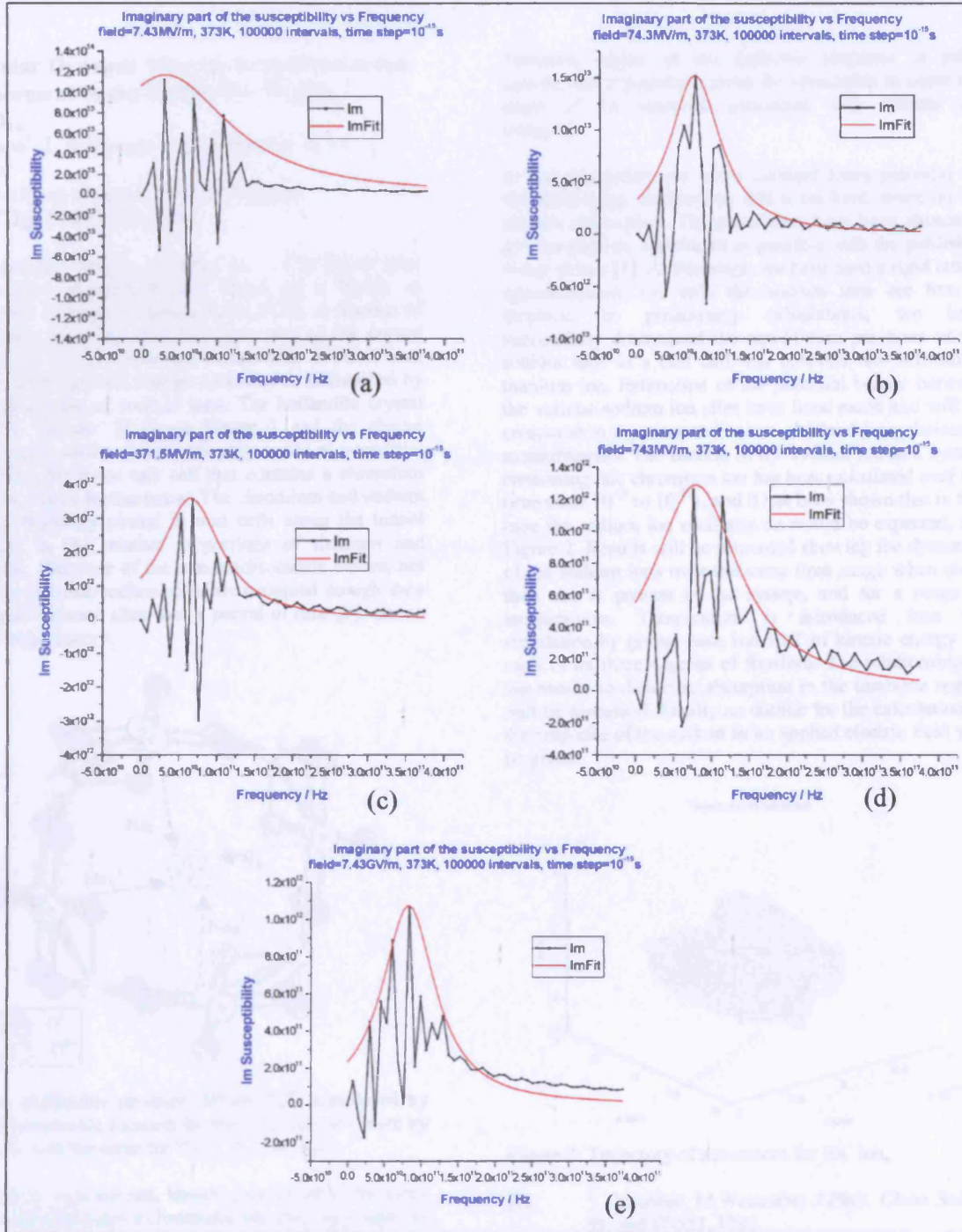


Figure A6: The $\chi''(f)$ plot with the best curve fitting (red) to equation 5.27 as a function of frequency at 373K with electric field of (a) 7.43MV/m (b) 74.3MV/m (c) 371.5MV/m (d) 743MV/m and (e) 7.43GV/m

Molecular Dynamic Simulation of Sodium Ion Displacement in the Hollandite $\text{Na}_x(\text{Ti}_{8-x}\text{Cr}_x)\text{O}_{16}$

K L Khoo¹, L A Dissado¹, J C Fothergill¹ & I J Youngs²

¹ University of Leicester, United Kingdom

² QINETIQ, United Kingdom

The hollandite $\text{Na}_x(\text{Ti}_{8-x}\text{Cr}_x)\text{O}_{16}$, ($x = 1.7$) [1] is non-stoichiometric material that is based on a family of compounds of general formula $\text{A}_x\text{M}_{4-x}\text{N}_y\text{O}_8$. A fraction of the 4-valent titanium ions that form part of the crystal structure of the hollandite are replaced by 3-valent ions such as chromium and charge neutrality is maintained by an equal number of sodium ions. The hollandite crystal possesses 'tunnels' [1,2] see Figure 1 and the charge compensating sodium ions preferably reside at interstitial sites within the same unit cell that contains a chromium ion [1] as shown by the arrow. The chromium and sodium ions are randomly placed in unit cells along the tunnel according to the relative proportions of titanium and chromium. Because of the non-stoichiometric nature, not all of the possible sodium sites are occupied though they may move between sites over a period of time [3], due to their thermal energy.

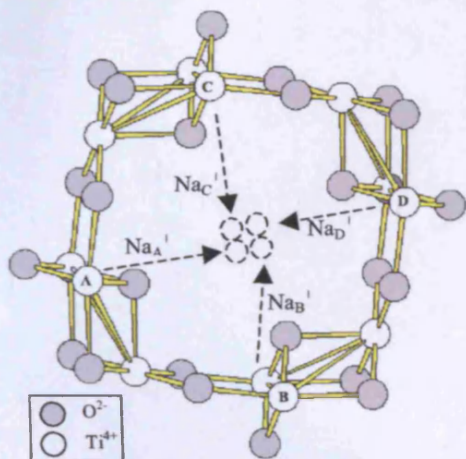


Figure 1: Hollandite structure (When Ti_A^{4+} is replaced by Cr^{3+} , the preferable location for the Na_A^+ ions is shown by the arrow, it is the same for Ti_B^{4+} , Ti_A^{4+} & Ti_D^{4+})

The sodium ions are not, however restricted to the same unit cell that contains a chromium ion, they may move to neighbouring cells if the site is unoccupied. Electrostatic interactions between the sodium ions along the tunnel lead to a fluctuating potential environment for the motion of the sodium ions. In some senses, therefore, they resemble a liquid, particularly at high temperatures [4]. In the presence of an ac electric field the sodium ion motion will give a polarisation contribution at high frequencies and a dc current as the frequency approaches zero. Our intention in this work is to use a molecular dynamics type of simulation to investigate whether or not the many body interaction between the sodium ions is sufficient to give the Pooley absorption [5] sometimes observed in the

Terahertz region of the dielectric response of polar liquids, and if possible extend the simulation to cover the onset of the response connected with sodium ion transport.

In our simulation, we use a Lennard-Jones potential for the short-range interactions and a coulomb potential for ion-ion interactions. The parameters have been chosen to give as good an agreement as possible with the published 6-exp values [1]. At this stage, we have used a rigid lattice approximation, i.e. only the sodium ions are free to displace. In preliminary calculations, we have successfully determined the equilibrium positions of the sodium ions in a unit cell that contains one substituted titanium ion. Estimation of the potential barrier between the various sodium ion sites have been made and will be compared to experimental values obtained from dielectric measurements. The motion of the sodium ion in a system containing one chromium ion has been calculated over the time scale 10^{-15} to 10^{-12} s, and it has been shown that in this case the sodium ion oscillates as would be expected, see Figure 2. Results will be presented showing the dynamics of the sodium ions over the same time range when more than one is present in the system, and for a range of temperatures. Temperature is introduced into the simulation by giving each ion $\frac{1}{2}kT$ of kinetic energy for each of its three degrees of freedom. The relationship of the results to dielectric absorption in the terahertz region will be discussed. Finally an outline for the calculation of the response of the system to an applied electric field will be given.

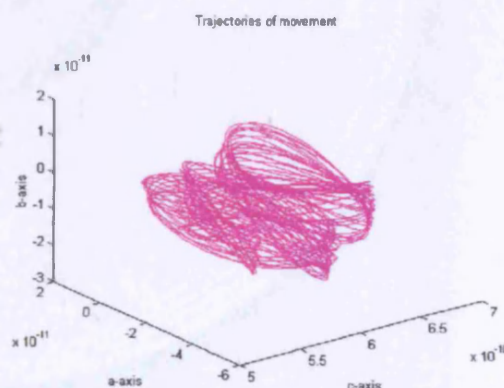


Figure 2: Trajectory of movement for Na^+ ion,

- [1] Y. Michiue, M. Watanabe, *J. Phys. Chem Solids*, **57**, pp547-551, 1996
- [2] Y. Michiue, M. Watanabe, *Solid State Ionics*, **79**, pp116-119, 1995
- [3] Y. Michiue, M. Watanabe, *J. Solid State Chem.*, **116**, pp296-299, 1995
- [4] M. L. Wolf, J. K. Walker, C. R. A. Catlow, *Solid State Ionics*, **13**, pp33-38, 1984
- [5] L. A. Dissado, J. M. Alison, *Journal of Molecular Liquids*, **56**, pp295-316, 1993